

Deep Learning Methods for Partial Differential Equations and Related Parameter Identification Problems

Derick Nganyu Tanyu^{†‡*}, Jianfeng Ning^{†‡}, Tom Freudenberger[†], Nick Heilenkötter[†],
Andreas Rademacher[†], Uwe Iben[§], and Peter Maass[†]

[†]Centre for Industrial Mathematics (ZeTeM), University of Bremen, Germany

[†]School of Mathematics and Statistics, Wuhan University, China

[§]Robert Bosch GmbH, Germany

[‡]Both authors contributed equally

*Corresponding author: derick@uni-bremen.de

May 17, 2023

Abstract

Recent years have witnessed a growth in mathematics for deep learning—which seeks a deeper understanding of the concepts of deep learning with mathematics and explores how to make it more robust—and deep learning for mathematics, where deep learning algorithms are used to solve problems in mathematics. The latter has popularised the field of scientific machine learning where deep learning is applied to problems in scientific computing. Specifically, more and more neural network architectures have been developed to solve specific classes of partial differential equations (PDEs). Such methods exploit properties that are inherent to PDEs and thus solve the PDEs better than standard feed-forward neural networks, recurrent neural networks, or convolutional neural networks. This has had a great impact in the area of mathematical modeling where parametric PDEs are widely used to model most natural and physical processes arising in science and engineering. In this work, we review such methods as well as their extensions for parametric studies and for solving the related inverse problems. We equally proceed to show their relevance in some industrial applications.

1 Motivation

Arguably, partial differential equations (PDEs) provide the most widely used models for a large variety of problems in natural sciences, engineering and industry. The ever-increasing complexity of these models such as digital twins for high-tech industrial applications requires the most efficient solvers.

These models follow the full life cycle of products from classical simulation and optimisation during the development phase to process monitoring and control during production. Such models typically rely on accurate calibration of critical parameters, which might be scalar parameters or even distributed spatial-time varying parameter functions. The calibration process itself requires multiple runs of the model and increases the need for efficient solvers even more.

Not surprisingly, data-driven concepts and in particular neural network approaches have been studied extensively over the last few years as they have the potential to overcome three major obstacles in PDE simulations: First of all, no mathematical-physical model is ever complete, however, even the finest detail or tricky non-linearity is contained in a sufficient data set; secondly, the parameters to be determined most often are not arbitrary but follow an unknown, application specific distribution, which can be recovered and exploited from training data; thirdly, as already mentioned, the complexity of PDE-based modelling has reached a level such that conventional and most widely used methods such as finite elements or finite

difference do require computational times beyond reasonable limits, while neural network concepts after training are most efficient.

This is matched by our own experience over the last few years, where an increasing number of our industrial and engineering collaboration partners started to experiment with deep learning (DL) concepts based on neural networks for PDE problems. However, they as much as we were overwhelmed by the somewhat confusing variety of different DL concepts for these tasks. These span from general approaches for large classes of problems to very specifically tailored approaches for individual equations. The present paper is based on our endeavour to provide an unbiased overview of the most common general approaches and to provide limited, but scientifically based guidance on how to select appropriate methods. We are well aware of the many extension of the mentioned methods and the exploding body of literature dealing with such problems, and we readily apologise to those scientists, whose research we neglected to include. To be more precise, we are considering second-order partial differential equations defined in a bounded domain $\Omega \subset \mathbb{R}^d$, which depend on a parameter function λ :

$$\mathcal{N}(u, \nabla u, \Delta u, u_t; \lambda) = 0 \quad (1)$$

$$\lambda : \Omega \rightarrow \mathbb{R} \quad (2)$$

In this general notation, \mathcal{N} encodes the differential equation as well as boundary conditions. We always assume, that the parameter-to-state operator F , which maps a given parameter λ to the solution of the PDE, is well-posed. I.e. we assume a function space setting such that the solution u of the PDE is unique and depends continuously on the parameter λ . We will consider three related classes of problems:

Level 1: Forward problem: solving a single PDE: given λ , compute $u = F(\lambda)$

Level 2: Parametric studies: given many parameters, $\lambda \in \{\lambda_1, \dots, \lambda_N\}$, compute corresponding u 's

Level 3: Parameter identification (inverse problem): given a measured u^δ or its values Pu^δ under a measurement operator P , determine a corresponding λ , e.g. solve $F(\lambda) \sim u^\delta$.

Our main target is the third class of problems, i.e. inverse problems stated as parameter identification problems for PDEs. These problems are typically non-linear and ill-posed, even if the differential equation is linear and the forward operator is well-posed. Nevertheless, we start with the first problem and review the most common DL approaches for solving the forward problem. We then discuss their potential for parametric studies and parameter identification problems. As an underlying motivation for using DL concepts in this setting, we assume that an evaluation of the forward operator F by classical methods, e.g. finite difference schemes or finite elements, is computationally expensive and not suitable for large-scale parametric studies.

We have two remarks for clarifying the scope of the present survey. First of all, parameter identification problems are inverse problems and can be attacked by well-established general regularisation schemes for operator equations. For a recent overview of such data-driven concepts for inverse problems and their regularisation properties, see e.g. [5]. However, these concepts, e.g. unrolled iteration schemes, typically involve an evaluation of the forward operator or its adjoint. This will not lead to efficient schemes in our framework, where the evaluation of F is assumed to be too costly for large-scale parametric studies. We will remark shortly on that in our section on the state of the art. Hence, in the present paper, we only consider DL concepts, where the forward operator itself, i.e. the parameter-to-state operator, or its inverse are replaced by a neural network. Secondly, there exists a growing number of highly optimised DL concepts for very specific PDE problems e.g. for coupled physics systems, molecular dynamics, or complex fluid dynamic problems. These approaches do have a limited potential for transfer to other problems, and we will not address these concepts. We will rather focus on general classes of DL concepts that apply to a larger variety of PDE-based problems. However, we will highlight some of those successful but specialised approaches in the section on the state of the art. All the codes and dataset used for the numerical experiment will equally be made available online on GitHub (see also Section A.2)

1.1 Classical methods for solving PDEs numerically

Let us first comment on the main competitors for data-driven concepts, namely the classical and well-established concepts of finite difference (FDM), finite element (FEM), boundary element Method (BEM), finite volume (FVM) or particle methods.

The so-called finite difference method (FDM) is based on the replacement of the occurring derivatives by difference quotients. In this process, the function values of the solution are approximated at individual discrete grid points. The result is a so-called grid function. We refer, e.g., to [145] for a more detailed description. The great advantage of the FDM is its straightforward realisation. However, its extension to more complex problems is limited and rather unrealistic smoothness assumptions are necessary for its analysis.

The finite element method (FEM) overcomes the mentioned disadvantages of FDM methods to a large extent. In contrast to the FDM, it is based on the weak formulation of the PDE under consideration and searches for the discrete solution over a finite-dimensional subspace of the underlying function space, see [15] for more details. Especially in connection with adaptive and domain decomposition methods, it shows its full potential. An interesting variant is discontinuous Galerkin (dG) methods, in which the smoothness assumptions for the discrete solution, which stems from the weak formulation of the PDE, are only enforced by penalty terms.

The boundary element method (BEM) follows a different idea. In this concept, the PDE is transformed into a boundary integral equation, which, however, is only possible in special cases. This reduces the dimension of the problem. The boundary integral equation is then discretised by means of FEM, for example. However, the resulting system of equations is dense and its numerical solution is often tricky and numerically very elaborate. Nevertheless, the BEM offers great advantages for exterior space problems in which an unbounded area is considered. We refer for instance to [59] for more information.

The Finite Volume Method (FVM) brings together ideas from the FEM and the FDM and combines them with arbitrary control volumes, see e.g. [100]. The FVM is particularly well suited for the discretisation of hyperbolic equations and convection-dominated problems. However, its theoretical analysis is not yet that advanced.

Another approach are particle methods or discrete element methods (DEM), see e.g. [19], which are based on a completely different approach. Here, individual particles and their interaction with each other are considered. By using different approaches to describe the interaction, different materials and processes can be simulated. They thus achieve very good accuracy in many applications, e.g. in the simulation of sand, which is difficult to simulate with the other methods.

The mentioned concepts are well-established for solving PDE-based forward problems and all of them have been adapted to inverse problems, in particular in the context tasks of optimal control or numerical parameter identification. They lead to accurate results in this context. However, two main difficulties have to be mentioned: Firstly and as said already in the previous section, solving these inverse problems requires solving the forward problem multiple times, which leads to unacceptable overall computing times at least for large problems. Furthermore, the optimisation algorithms for solving the above-mentioned parameter identification tasks require the first and, if possible, also the second derivative with respect to the unknown parameters. At first, it is often unclear whether the mentioned derivatives exist at all. In addition, their calculation is algorithmically very complex and time-consuming, especially for time-dependent problems. We refer, for example, to [151] for a detailed discussion.

In summary, the classical methods are well-researched and reliable and should be used whenever possible within the given restrictions of data and computer power. Hence, we once again stress, that the present paper refers to potential applications where solving the forward problem multiple times is simply too costly.

1.2 Deep learning for PDE solvers and scope of this survey

The main purpose of this section is to list the DL methods considered in this present survey. In the subsequent sections, we will then analyse their potential for parametric studies and inverse problems.

As already mentioned, mesh-based methods for solving PDEs such as finite element methods, finite difference methods, and finite volume methods, are the dominant techniques for obtaining numerical solutions of PDEs. When implementing these methods, the computational domain of interest should be first discretised using a set of mesh points and the solution is then approximated at the chosen grid points. The solutions are usually obtained from a finite linear space by solving a linear or non-linear system of equations. The classical methods are very stable and efficient for low-dimensional problems and regular geometries. They have been well understood in terms of existence, stability and error estimate, and we can usually achieve the desired accuracy by increasing the resolution of the discretisation. In addition to the more general remarks above, the

classical methods have several additional drawbacks and limitations. Firstly, the curse of dimensionality has limited the use of mesh-based methods, since the number of discretisation points will increase exponentially with the dimension, and there is no straightforward way to discretise irregular domains in high-dimensional spaces. Secondly, traditional methods are designed to model one specific instance of the PDE system, not the parameter-to-state operator. Thus, for any given new instance of the PDE system, the problem has to be solved again. Thirdly, the numerical solution is only computed at the mesh points and evaluation of the solution at any other point requires interpolation or some other reconstruction method. Fourthly, classical methods require the knowledge of the underlying analytic system of differential equations, but sometimes the exact physics is unknown. Lastly, solving inverse problems by classical problems is often prohibitively expensive and requires complex formulations, repeated computation of forward problems, new algorithms and elaborate computer coding.

Deep learning methods have shown great power in addressing the above difficulties. Since there are many different deep learning methods for PDEs, and each method has its particular properties, we will discuss them one by one. We should add, that the theoretical investigation of deep learning concepts for PDEs, beyond more or less direct applications of the universal approximation theorem, is still scarce. This is in contrast to the classical PDE theory, where there exists an exhaustive literature on the analytic properties of different types of PDEs. The theoretical characterisation of PDEs, as well as the type of theoretical background needed for proving solvability and uniqueness, differentiates between linear and non-linear elliptic, parabolic or hyperbolic equations in terms of the given boundary conditions. Analytic tools are different for these different classes, hence it is somewhat surprising that DL concepts for PDEs hardly ever use this classical classification but rather use a classification based on whether or not the PDE (no matter which type of PDE) is known, which type of data is given for training and which type of network architecture as well as which loss function for training is used.

We follow this data-driven classification scheme. Our first level of characterisation is based on the input and output structure of the network. A first class of networks takes x or (t, x) as input and outputs a one- or low-dimensional scalar value or vector $u_\Theta(\cdot)$. During training the weights Θ of the network are optimised such that $u_\Theta(\cdot) = \hat{u}(\cdot)$ is an approximation to the solution u of the PDE at the specified point x or (t, x) , i.e. a regression problem for the function $u_\Theta \approx u$ is solved. These networks aim at a function approximation. Otherwise, one aims at an operator approximation for the parameter-to-state map and uses networks which take a parameter function, either in discretised form or as a vector of precomputed feature values, as input and outputs the full solution function u . The solution u again is delivered either in discrete form or as a related feature vector, that can be turned into a proper function representation in a post-processing step. The general idea of these two characterisations is summarised in the following Figures 1-2:

- Function evaluation, neural network $u_\Theta(t, x) \approx u(t, x)$ based on the PINN concept, [137]

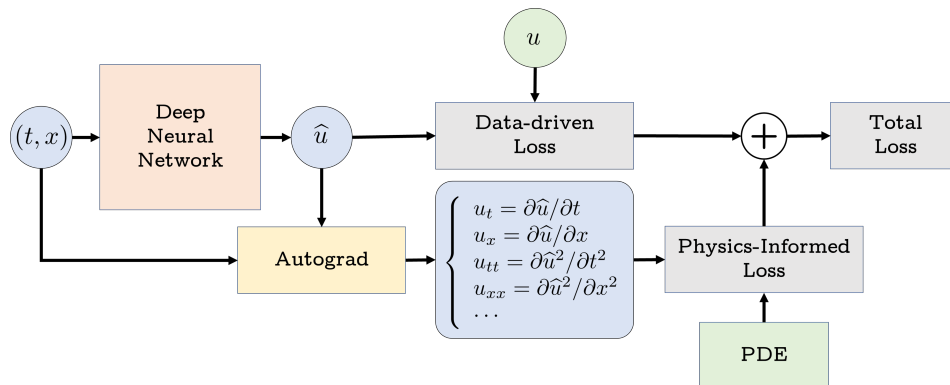


Figure 1: A network with a low input dimension for (t, x) , which outputs a scalar or low-dimensional $\hat{u}(t, x) = u_\Theta(t, x)$. Hence, the neural network is trained to be a function approximation of the solution $\hat{u}(t, x) \approx u(t, x)$. During training, automatic differentiation by backpropagation is used to compute all necessary derivatives for checking, whether the PDE is satisfied. In addition, the loss function typically sums up over several values of (t, x) and their corresponding function points. After training, the Deep Neural Network is then used and \hat{u} can be evaluated at arbitrary points (t, x) .

- Operator evaluation, neural network $\Phi_{\Theta}(\lambda)$ following the PCANN concept [12]

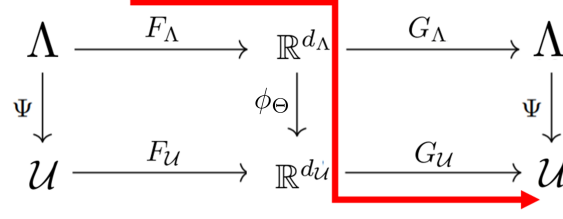


Figure 2: A typical setup for an operator approximation scheme. Here an order reduction model (see [141, 24, 11] for an overview of reduction models) in combination with a neural network is employed. First, the parameter $\lambda \in \Lambda$ is reduced to a feature vector in $\mathbb{R}^{d_{\Lambda}}$ by determining its scalar products with a pre-computed reduced basis, i.e. $c_k = \langle \lambda, b_k \rangle$ (which in case of an orthonormal system is equivalent to $\lambda \sim \sum c_k b_k \in \Lambda$). Only the feature vectors are mapped by the neural network $\phi_{\Theta} : \mathbb{R}^{d_{\Lambda}} \ni c \mapsto \tilde{c} \in \mathbb{R}^{d_{\mathcal{U}}}$. The output features \tilde{c} are then used to determine an expansion of the sought-for solution $\hat{u} = \sum_{\ell} \tilde{c}_{\ell} \tilde{b}_{\ell}$ in terms of a basis $\{\tilde{b}_{\ell}\}$ in the solution space. In this way, we then approximate the parameter to solution function $\Psi : \Lambda \ni \lambda \mapsto u \in \mathcal{U}$ by $\Phi_{\Theta} = G_{\mathcal{U}} \circ \phi_{\Theta} \circ F_{\Lambda}$ as indicated by the red arrow. F_{Λ} and $F_{\mathcal{U}}$ are encoder functions (PCA maps) in the parameter and solution spaces respectively, while G_{Λ} and $G_{\mathcal{U}}$ are their respective decoder functions. (see 5.1 and [12]).

Networks	PDE usage	Data usage	Neural Network approximation	discretisation		Reference
				Parameter	Solution	
Deep Ritz	yes	no	function	no	no	[165, 107]
PINN	yes	no	function	no	no	[137]
WAN	yes	no	function	no	no	[167, 6]
PCANN	no	many	operator	free grids	free grids	[12]
FNO	no	many	operator	free grids	free grids	[102]
UFNO	no	many	operator	free grids	free grids	[159]
MWT	no	many	operator	free grids	free grids	[58]
DeepONet	no	many	operator	fixed	no	[113]
PINO	yes	if needed	operator	free grids	free grids	[105]
PI-DeepONet	yes	if needed	operator	fixed	no	[156]

Table 1: The list of DL concepts considered in this survey is based on a pre-selection mirroring our own interest in inverse problems. Hence, concepts for operator approximation are preferred. In their original papers, most of these concepts were designed for Level 1 problems only. Hence, we need to specify in later sections how to extend them for Level 2 or Level 3 problems. Also, we will later refine the features characterising the different methods in terms of limitations, e.g. which PDE equations are most suitable and which are not.

Typical examples of DL concepts aiming for a function approximation are Deep Ritz method [165, 107], Physics-Informed Neural Network (PINN) [137], Deep Galerkin Method (DGM) [144], Weak Adversarial Networks [167], and Deep Splitting Approximation methods [9]. In all these concepts, information of the underlying physics must be used when training the neural network, i.e. the PDE must be known analytically. These concepts are usually mesh-independent and accurate, while they require knowledge of the governing laws of the PDEs, and the optimisation problem needs to be solved for every new instance. This is similar to classical methods.

Examples for the second type, i.e. methods aiming at an operator approximation, include Model reduction neural network (PCANN) [12], Deep Operator Network (DeepONet) [113] and its extensions [156, 48], Fourier neural operator (FNO) [102] and its physics-informed extension–Physics Informed Neural Operator (PINO) [105], Graph Kernel Network [103, 104], Bayesian deep convolutional encoder-decoder networks [170], Wavelet Neural Operators [150], Multiwavelet based operator (MWT) [58] and many more. These operator methods usually learn the neural network with some paired input-output (parameter-solution) observations with or

without the knowledge of the physical system (using the physics information could sometimes alleviate the need for much data as in the case of PINO and PI-DeepONet) as highlighted in Table 1. Thus, the neural network only needs to be trained once, and a new parameter identification task can be directly solved by a forward pass of the network. Some of these deep learning methods still need to discretise the domain of interest, and the solutions are sought in a finite linear space [170]. A recently published paper [29] aims at comparing some of these operator approximation concepts for solving various PDEs. The primary criterion for comparison in this well-written paper is the cost-to-accuracy curve. Accordingly, the authors compare results obtained with different network sizes. However, their comparison includes the basic methods PCANN, DeepONet and FNO which in our tests did not yield the best results. Also, the numerical test stays in a range - when compared with FEM methods - of rather large approximation errors. This matches our experience, it is hard to get to high precision for forward solvers with DL concepts. Anyway, our focus is on inverse problems, which are not covered in the mentioned paper.

In terms of the involved computational load, the computational cost of classical methods for solving linear PDEs is mainly determined by the need to solve a large linear system. For deep learning methods, it is the training process (optimisation) of the neural network. As a general rule of thumb, for low dimensional problems with regular geometries, classical methods are in general more powerful and efficient than deep learning methods. Ignoring rounding errors, the main error of the classical methods arises from the step size of the discretisation. There exists a trade-off on the resolution: coarse grids are fast but less accurate; fine grids are more accurate but slower. On the other hand, for DL approaches one usually has to carefully choose the neural network, optimisation method and hyperparameters in consideration of the underlying differential equation. Additionally, the error of deep learning methods is usually difficult to estimate and consists of several factors. The accuracy can be characterised by dividing the total error into three main types: approximation, optimisation, and generalisation errors. More specifically, the approximation error measures the smallest difference between the neural networks and the underlying function or operator, which we aim to approximate. This error is influenced by the size and architecture of the neural networks. The optimisation error arises from the non-convexity property of the loss function and the limited number of iterations used for its minimisation. Stochastic Gradient Descent is an efficient algorithm for escaping local minima and reducing the optimisation error, nevertheless, in real-life applications, we never achieve a global minimum. The generalisation error refers to how the trained networks perform on unseen data and is mainly affected by the amount of training data, the modelling information of the PDEs, and the architecture of the neural networks.

The selection of DL-based PDE solvers which are further investigated in this survey is based on our endeavour to cover a most complete range of different concepts. Hence we included the basic concepts of learned DL solvers as well as some recent improvements of these.

A more detailed description of these approaches, their algorithmic implementation and their analytical properties will be given in the subsequent sections. There we will also highlight, how these methods, which were typically designed as PDE-forward solvers can be extended to parameter identification problems.

1.3 Some remarks on concepts not covered in this survey

In this section, we want to highlight those directions of research, which are not covered in this survey.

First of all, there exist several specialised and powerful DL concepts for complex but specific PDEs. Research on neural networks for such specialised cases of PDEs as well as related parametric studies and inverse problems is exploding and it is impossible to give an exhaustive list of references. Hence, we only want to highlight areas of research, which have reached a certain level of maturity in terms of experimental success as well as mathematical rigor. Again, this selection is based on personal preferences and we apologise to those, who quite rightly might want to see their own work included.

A particularly successful area for DL applications are coupled-physics systems, which lead to some of the most complex inverse problems. Typically, those inverse problems cannot be solved by standard concepts, neither in the classical analytical regularisation setting nor in data-driven frameworks. Hence, such problems, e.g. opto-acoustic tomography, require specialised concepts, which typically integrate domain-specific expert knowledge or at least partially draw their motivation from analytic reconstruction formulae, see e.g. [26, 148, 66, 4]. While we are at it, we also mention successes of DL methods in other sub-fields of tomography such as electrical impedance tomography [64, 69], diffuse optical tomography [126] and computed tomography

[99, 98, 98]. Another class of papers do take numerical schemes for PDEs as a starting point for developing network architectures, see e.g. [60, 140]. In these papers, the different layers of a neural network are regarded as time stepping in a discretised scheme. In particular, this allows to specifically mimic and improve numerical schemes for parabolic equations, which e.g. are the basis for many imaging problems based on diffusion processes. Simulation of turbulent flows also is an area, where DL concepts have shown good success. We only list some papers, which in our opinion together with the cited literature therein allow an overview of this topic [153, 121, 34]. One should also mention the spectacular results on simulating molecular dynamics [83, 14] and many other fields of applications, where DL simulations lead to groundbreaking novel insights.

We also do not cover the topic of DL for stochastic PDEs and recent results, which we regard to be more on the side of PDE theory and simulation. Hence, we do not cover recent developments as e.g. described in [36, 17, 32].

Secondly, we want to remark on general regularisation schemes for inverse problems using a data-driven approach, which can be applied to but are not particularly tailored for PDE-based parameter identification problems. Typically these general data-driven regularisation schemes for parameter identification problems do need an evaluation of F or any form of its adjoints. For reference to this type of schemes we refer to [5] or to [1] for a recent paper, which embeds the learning of the network together with the parameter identification into a regularisation scheme. We would like to remark that unrolled iteration schemes such as LISTA or unrolled primal-dual, are somewhat hybrid methods and could be included in our survey. However, LISTA is predominately successful for linear forward operators A and it still needs the adjoint A^* for initialising the input of the network. One could extend such DL schemes, which are derived from classical regularisation theory, in such a way that the evaluation F or its adjoint would be done by training an embedded network for every operator evaluation. However, this leads to a rather complex training task and this extension is not part of the scope of the original papers for e.g. primal-dual, NETT or DeepPrior or similar [2, 101, 32].

2 Characterisation of DL concepts for PDEs

Having specified the restricted scope of the present survey, we will now list the concepts under consideration in the following sections. Before starting the introduction of the individual methods we include some general remarks on the characterisation of deep learning methods for PDEs. As already mentioned, the characterisation of DL concepts for solving PDEs differs considerably from the analytic characterisation of PDEs. They are mainly characterised in terms of the information needed for applying them. The two main classes of information are data and physical models, where 'physical models' refers to the mathematical formulation of the differential equations and their boundary conditions.

2.1 Data

Data-driven methods rely on the availability of sufficiently large data sets of good quality. The data provided can be sampled values of single or multiple solutions, where sampling can be done either on a predefined grid or with arbitrary sampling points. Some of the most advanced theoretical investigations do start from assuming a sampling in function space, which opens the path for incorporating functional analytical machinery in their analysis, see e.g. [12, 136, 1].

However, the volume of available data is usually rather scarce, e.g. useful experimental data is generally limited or even intractable for many practical scenarios and high-fidelity numerical simulations are often computationally expensive. Sometimes it is also a challenge to extract interpretable information and knowledge from the data deluge. Moreover, purely data-driven methods may fit observations very well, but predictions may be physically inconsistent or implausible. Theoretically, finite data can not fully and correctly determine a mapping which maps an infinite set to an infinite set. However, we can still see the success of data-driven methods, which is mainly due to two reasons: first of all the search for a solution or parameter typically follows a certain prior distribution, which we might be able to approximate well with few samples; and secondly most problems are continuous, which in connection with suitable regularisation schemes leads to good generalisation properties even for limited sets of training data, [137]

In addition to sampled data, there exists a wealth of domain-specific expert knowledge for most applications. This information may come in the form of observational, physical or mathematical understanding of the system under consideration. Integrating data and this prior knowledge can yield more interpretable machine

learning methods and can improve the accuracy and generalisation performances without large amounts of data.

In our context information from physics may come in different forms: most commonly, the system of partial differential equations as well as boundary conditions are specified. Otherwise, some energy functionals or a weak formulation may be given. Also, certain approaches [142] incorporate conservation laws in the network architecture. Whenever such information is used, the concept is typically called ‘physics informed’.

Different from data-driven methods, the physics information may uniquely determine the systems, however, only within the limitations of the chosen model. For example, given the PDE formula and some initial and boundary equations, the solution is uniquely determined if the system is well-posed. In other words, mathematical formulae may inherently contain all information of the physical systems, while data are just some observations and reflections of the physical systems and thus can not fully reveal the whole information of the systems.

The most common approach is to use this physics information in the loss function during the training of the network. Hence, the type of physics information determines the loss function.

2.2 Network training and application

Training the resulting networks typically leads to additional problems. This may require extensive hyperparameter search, data preprocessing or subtle parameter settings for controlling the convergence of the training scheme. We have listed the respective training concepts for each method in the Appendix A.

As pointed out in [84], specific to physics-informed learning, there are currently three pathways that can be followed separately or in tandem to accelerate training and enhance the generalisation of ML models by embedding physics in them. The first one is **observational biases** from observational data, which is the foundation of data-driven methods in machine learning. The second is **inductive biases** by designing special NN architectures that can automatically and exactly satisfy some properties and conditions. The most common example are convolutional NNs which can be designed to respect properties, such as symmetry, rotations and reflections. Other examples are Graph neural networks [103] which are adapted to graph-structured data. Another concept is based on Quadratic residual networks(QREs) [16], which increases the potential of the neural networks to model non-linearities by adding a quadratic residual term to the weighted sum of inputs before applying activation functions. They were shown to have good performance in learning high-frequency patterns. The invertible neural network [3] makes the inverse of the neural network well-defined. It has applications in inverse problems and generative models. Specific architectures can also be designed to satisfy the initial/boundary conditions. The last pathway is **learning biases**, where the physics constraints are imposed in a soft manner by appropriately penalising the loss function of conventional NN approximations. Representative examples include the Deep Ritz method and PINN.

We also want to comment on the arguably most important tools for physics-informed machine learning, namely automatic differentiation [8]. In principle, this general concept us to compute exactly the derivatives of the network output with respect to the input variables. Hence, we can incorporate weak or strong formulations of the underlying PDE conveniently. However, compared to conventional numerical gradients such as finite difference, the automatic differentiation method is usually slower and requires more memory.

Moreover, after training, the methods will again differ substantially in their scope of applicability. Methods might allow the sampling of a solution of a PDE at arbitrary points. In this case, the method is called meshfree, which is one of the most desirable properties of most DL concepts for PDEs. Another important property, in particular for Level 2 and Level 3 problems, is the computational load needed for applying the network to a different parameter of the PDEs. This is most efficient for most operator learning schemes but might require re-training or the computation of specific feature vectors.

In conclusion, different deep learning methods for PDEs are mainly different in terms of their neural network architecture and the particular choice of the loss function for training.

2.3 General DL concepts for PDE-based inverse problems

So far we have sketched two main approaches for solving PDEs (forward problems), namely function or operator approximation schemes. In the following sections, we will introduce these methods and their baseline

implementation in more detail. We will also include, whenever appropriate, the related concepts for the PDE-based inverse problems.

The extension of function approximations $u_\Theta(t, x)$ for solving inverse problems is not straightforward and differs from method to method. In contrast to that, the application of learned operator approximation schemes $\Phi_\Theta(\lambda)$ to inverse problems is always based on one of the two following concepts:

- The direct (or backward) method, where the network is trained with reversed input-output. In other words, the solution of the PDE is the input of a neural network which outputs the parameter function. This method is similar to the forward problem, but we learn the backward operator.
- Tikhonov Regularisation, for this case, the forward operator $\Phi_\Theta(\lambda)$ is trained as usual. For an inverse problem with given noisy data u^δ we then approximate a suitable parameter λ by minimising a Tikhonov functional with respect to λ

$$\|\Phi_\Theta(\lambda) - u^\delta\|^2 + \alpha R(\lambda) .$$

The choice of the penalty term R adds to the flexibility of the method and can encode further properties of the solution such as smoothness, sparsity or piece-wise constant structures. minimisation is done iteratively via gradient descent, where the differentiation with respect to λ can be implemented using backpropagation with respect to the input but with fixed weights Θ . We exemplify the procedure for the model reduction concept PCANN in Algorithm 6. A similar idea can be applied to the other solution operators mentioned in Sections 5.2 and 5.3.

3 Theoretical Results of Deep Learning for PDEs

One reason for the success of finite element methods is that the functions in Sobolev space can be approximated by piece-wise polynomials with a certain convergence rate depending on the mesh size. However, classical methods require degrees of freedom of the order of ε^{-d} for a desired accuracy ε in d dimensional problems, which limits their applications to high-dimensional problems. The task of deep learning for PDEs is to employ neural networks to approximate the solution or parameter-to-state operator with a limited amount of data or physical information. A fundamental question is therefore whether the neural network can effectively approximate the solution/parametric operator of a PDE system, and if so, how to estimate the complexity of a neural network in terms of the dimensionality growth and accuracy requirements. In this section, we will briefly review some approximation theoretical aspects of deep learning for PDEs.

3.1 Approximation Results for Solution Learning in PDEs

Neural networks are universal approximators [28, 71] in the sense that continuous functions on compact domains can be uniformly approximated by neural networks with arbitrary accuracy, provided the number of neurons is sufficiently large. A lower bound on the size of the neural network for achieving a desired accuracy was not given in these papers. With some assumptions on the activation functions and the space of functions to be considered, more refined results on the relationship between the size and the approximation accuracy of neural networks have been reported in e.g., [7, 13, 118, 143, 112, 31, 50, 56, 57]. The universal approximation theorem has also been generalised to convolutional neural networks in [169] and complex-valued neural networks in [152]. These results concern general function approximations and do not refer to PDE solutions.

3.1.1 Neural Networks Approximation for High Dimensional PDEs

We now shortly discuss the theoretical foundations for approximating solutions of PDEs by neural networks. Recent years have witnessed great empirical success of various deep learning methods [165, 65, 73, 167] in particular for solving high-dimensional PDEs. To explain these successes, several mathematical results have been proven which show that neural networks have the ability to approximate solutions of some PDEs without the curse of dimensionality (CoD). In particular, in [52] it is shown that the solutions of linear Black-Scholes PDEs can be approximated by neural networks with the size increasing at most polynomially with respect both the reciprocal of the prescribed approximation accuracy and the PDE dimension d . A number of articles

have appeared that significantly extend the results in [52] to more classes of PDEs [10, 46, 72, 75, 80, 139]. In particular, in [75] it is proven that neural networks have the expressiveness to overcome the CoD for semilinear heat PDEs.

On the other hand, there are also some articles, e.g. [54, 133, 162, 51], which derive some lower bounds on the complexity of neural networks with ReLU activation function to achieve a certain accuracy and show that there are natural classes of functions for which deep neural networks with ReLU activation cannot escape the CoD.

3.1.2 Barron Spaces

Typical classical approximation results for PDE solutions use a setting in Sobolev or Besov spaces. These spaces can be defined by their approximation properties using piece-wise polynomials or wavelets. In the same sense, the Barron space [22, 37] is the analogue when we consider approximation by two-layer neural networks. Roughly speaking, the Barron space consists of the functions that can be approximated by two-layer neural networks, and the approximation error is governed by the norm of the Barron space. A nice property of Sobolev/Besov type spaces is that solutions to partial differential equations lie in these spaces. This is the core of regularity theory for PDEs. When introducing Barron spaces in PDEs, a natural corollary and fundamental question is whether the solutions of the dimensional partial differential equations (PDEs) we are interested in belong to a Barron space. We will briefly review the definition of the Barron space and its approximation theorem, as well as an example of its use in escaping CoD in high-dimensional PDEs.

Consider functions $g \subset \mathbb{R}^d : X \rightarrow \mathbb{R}$ which allow the below representation:

$$g(x; \Theta) = \int_{\Omega} a\sigma(w^T x + b)\rho(da, dw, db), \quad x \in \mathbb{R}^d, \quad (3)$$

where ρ is a probability distribution on $\Omega = \mathbb{R} \times \mathbb{R}^d \times \mathbb{R}$ and $\sigma : \mathbb{R} \rightarrow \mathbb{R}$ is some activation function. This representation can be thought of as a continuum realisation of two-layer neural networks, which are given as

$$g_n(x, \Theta) = \frac{1}{n} \sum_{k=1}^n a_k \sigma(w_k^T x + b_k), \quad x \in \mathbb{R}^d. \quad (4)$$

We present the following definition from [22] for Barron functions defined in a domain $\Omega \subset \mathbb{R}^d$. This definition is an adaptation of the definition given in [37], with some crucial modifications, for the purpose of analysing PDEs.

Definition 3.1. *For a domain $\Omega \subset \mathbb{R}^d$ and a fixed radius $R \in [0, +\infty]$, the corresponding Barron space with index p is defined as*

$$\mathcal{B}_R^p(\Omega) = \{f : \|f\|_{\mathcal{B}_R^p(\Omega)} < \infty\}, \quad (5)$$

where

$$\|f\|_{\mathcal{B}_R^p(\Omega)} := \inf_{\rho \in \mathcal{P}_R} \left\{ \left(\int |a|^p \rho(da, dw, db) \right)^{1/p} : f = \int_{\Omega} a\sigma(w^T x + b)\rho(da, dw, db) \right\} \quad (6)$$

and $\mathcal{P}_R := \left\{ \rho : \rho \text{ is supported on } \mathbb{R} \times \{x \in \mathbb{R}^d : \|x\| \leq R\} \times \mathbb{R} \right\}$.

The most essential feature that distinguishes Barron function spaces from Sobolev or Besov spaces is that elements of the former can be approximated by a two-layer neural network with an approximation rate that is independent of the dimension, as shown in the next theorem [22]:

Theorem 1. *Suppose that the activation function σ is smooth with $C_0 := \sup_{z \in \mathbb{R}} |\sigma(z)| \leq \infty, C_1 := \sup_{z \in \mathbb{R}} |\sigma'(z)| \leq \infty$ and $\sup_{z \in \mathbb{R}} |\sigma''(z)| \leq \infty$, and that $g \in \mathcal{B}_R^1(\Omega)$. Then for any open bounded subset $\Omega_0 \subset \Omega$ and any $n \in \mathbb{N}_+$, there exists $\{(a_k, w_k, b_k)\}_{k=1}^n$ satisfying*

$$\left\| \frac{1}{n} \sum_{k=1}^n a_k \sigma(w_k^T x + b_k) - f \right\|_{H^1(\Omega_0)} \leq \frac{2(C_0^2 + R^2 C_1^2) m(\Omega_0) \|g\|_{\mathcal{B}_R^p(\Omega)}}{n}, \quad (7)$$

where $m(\Omega_0)$ is the Lebesgue measure of Ω_0 .

The above theorem gives an H^1 -approximation rate for the Barron space defined by its integral representation. Furthermore, for a family of second-order elliptic PDEs with some assumptions on the coefficients and the source term, it is proved in [22] that for any exact solution u and $\varepsilon \in (0, 1/2)$, there exists $u^* \in \mathcal{B}_R^1(\mathbb{R}^d)$ with $R \leq c_1(\frac{1}{\varepsilon})^{c_2}$ and $\|u^*\|_{\mathcal{B}_R^1(\mathbb{R}^d)} \leq c_3(\frac{d}{\varepsilon})^{c_4|\ln \varepsilon|}$ so that $\|u - u^*\|_{H^1(\mathbb{R}^d)} \leq \varepsilon$. Thus, it is easy to conclude that there is a two-layer neural network $u_m(x; \Theta)$ with $m \leq c_5(\frac{d}{\varepsilon})^{c_6|\ln \varepsilon|}$ such that $\|u_m - u\| \leq \varepsilon$, where c_1, c_2, c_3, c_4 are constants independent of u^*, ε and d . Therefore, these results prove that even a simple two-layer neural network with a single activation function has sufficient representational power to approximate the solution of an elliptic PDE without CoD.

In [23], the regularity theory of solutions to the static Schrödinger equation in spectral Barron spaces was studied. In [37] the flow-induced function space was introduced and analysed by considering the residual neural networks. And the analysis in [80] shows that the solutions of some linear parabolic PDEs belong to a close analogue of the flow-induced spaces.

3.1.3 The Monte Carlo Approach

The approximation power of neural networks is the basic requirement for escaping CoD in high dimensional PDEs, while the algorithms for finding the optimal parameters of the neural networks are also equivalently important when considering computational complexity. The approximation of high dimensional integrals plays an important role in such high dimensional problems. Let $f : D = [0, 1]^d \rightarrow \mathbb{R}$ be a function in $L^2(D)$ and let

$$I(f) = \int_D f(x) dx. \quad (8)$$

To approximate the integral (8), the Monte Carlo algorithm [36] randomly samples independent, continuous, uniformly distributed points $\{x_i\}_{i=1}^N$ from D and let

$$\mathcal{I}_N(f) = \frac{1}{N} \sum_i^N f(x_i). \quad (9)$$

Then by a simple calculation, we have

$$\mathbb{E}[|I(f) - \mathcal{I}_N(f)|^2] = \frac{\text{Var}(f)}{N} \quad \text{and} \quad \text{Var}(f) = \int_X |f(x)|^2 dx - \left[\int_X f(x) dx \right]^2. \quad (10)$$

Thus, the Monte Carlo algorithm, which approximates the integral in high-dimensional spaces, can escape the CoD in a probabilistic sense. The convergence rate of the Monte Carlo algorithm plays an important role in the theory of machine learning for high-dimensional PDEs. As we can see, the deep Ritz and WAN loss functions discussed later for PDEs all involve the evaluation of an integral over the domain of interest, and the PINN loss function can also be viewed as the integral of the squared residual of the PDE over its domain of definition. In addition, the paper [53] proved that if a function can be approximated by a proper discrete approximation algorithm without CoD, and if there are neural networks that satisfy certain regularity properties and approximate this discrete approximation algorithm without CoD, then the function itself can be approximated by neural networks without suffering the CoD. Full history recursive multilevel Picard approximation methods (MLP) [74, 36] are some recursive nonlinear extensions of the classical Monte-Carlo approximation methods, and it has been shown that such approximation schemes also escape the CoD in the numerical computation of semilinear PDEs with general time horizons.

In summary there exist a growing number of strict mathematical results which prove that deep neural networks have the expressive capacity to approximate the solutions of some specific PDEs without the CoD and that the Monte Carlo algorithm can provide an efficient method for computing the associated loss functions. Nevertheless, the conjecture that there is a deep learning-based approximation method that overcomes the CoD in terms of computational complexity in the numerical approximation of PDEs has not yet been fully analysed, for example, the convergence rate of the optimisation procedure to learn the solution is also required to overcome the CoD.

3.2 Neural Network Approximations for Parametric PDEs

Operator learning methods aim to approximate the parametric map connecting a parameter space with a solution state space (parameter-to-state map). In the literature, the proposed operator learning methods usually consider low-dimensional PDEs. However, the inputs and outputs of neural networks for operator learning are usually high dimensional vectors, which requires the neural networks to have sufficient expressiveness to approximate the parametric map. The first successful use of neural networks in the context of operator learning appeared in [20], where the authors designed a novel learning architecture based on neural networks and proved that these neural networks yield a surprising universal approximation property for infinite-dimensional nonlinear operators. This was later extended to deeper networks, see [134].

3.2.1 A Theoretical Analysis of Neural Networks for Parametric PDEs with Reduced Basis Assumption

In this subsection, we will briefly review a theoretical result [94] for parametric PDEs, which is based on the assumption of an inherent low dimensionality of the solution manifold. We will present a brief overview of the arguments that lead to the approximation theorem obtained in [94]. The lemmas in this paper and the arguments used for proving them are constructive and have important value in the analysis of neural networks.

In [94], the authors consider parameter-dependent equations in their variational form:

$$\mathcal{A}_\lambda(u_\lambda, v) = f_\lambda(v), \quad \text{for all } \lambda \in \mathcal{Y}, v \in \mathcal{H}, \quad (11)$$

where the parameter set \mathcal{Y} is a compact subset of \mathbb{R}^p with a fixed and potentially large p . \mathcal{H} is a Hilbert space and \mathcal{A}_λ is a symmetric, uniformly continuous and coercive bilinear form, $f_\lambda \in \mathcal{H}^*$ is bounded by a constant C for all $\lambda \in \mathcal{Y}$, $u_\lambda \in \mathcal{H}$ is the solution and the solution manifold is assumed to be compact in \mathcal{A} .

The following is a simplified outline of the arguments of [94], which derived upper bounds on the size of neural networks with activation ReLU approximating the solution operator of parametric partial differential equations under the assumption that the solution space is inherently lying in a low-dimensional space.

1. Firstly, it recalled the result shown in [162] that the scalar multiplication $f(x, y) = xy$ for $x, y \in [0, 1]$ can be constructed by a ReLU NN of size $\mathcal{O}(\log_2(1/\varepsilon))$ up to an error of $\varepsilon > 0$.
2. As a next step, the approximate scalar multiplication is used to show that a matrix multiplication of two matrices of size $d \times d$ with entries bounded by 1 can be performed by NN of size $\mathcal{O}(d^3 \log_2(1/\varepsilon))$ up to an error of $\varepsilon > 0$.
3. For $A \in \mathbb{R}^{d \times d}$ such that $\|A\|_2 \leq 1 - \delta$ for some $\delta \in (0, 1)$, the map $A \rightarrow \sum_{s=0}^n A^s$ can be approximated by a ReLU NN with an accuracy of $\varepsilon > 0$ and having a size of $\mathcal{O}(n \log_2^2(m) d^3 \cdot (\log_2(1/\varepsilon) + \log_2(n)))$. Furthermore, with the fact that the Neumann series $\sum_{s=0}^n A^s$ converges exponentially fast to $(\text{Id} - A)^{-1}$, a ReLU NN can be constructed that approximates the inversion operator $B \rightarrow B^{-1}$ to accuracy $\varepsilon > 0$ under suitable conditions on the matrix B . This NN has the size $\mathcal{O}(d^3 \log_2^q(1/\varepsilon))$ for a constant $q > 0$.
4. Next, two assumptions are required, which are satisfied in many applications. The first is that the map from the parameter space to the associated stiffness matrices of the Galerkin discretisation of the parametric PDE with respect to a reduced basis can be well approximated by neural networks. The second is that the map from the parameters to the right-hand side of the variational form of the parametric PDEs discretised with based on the reduced basis can be effectively approximated by neural networks. Then there exists a neural network that approximates the operator from parameters to the corresponding discretised solution with respect to the reduced basis. If the reduced basis is of size d and the implementations of the map obtaining the stiffness matrix and the right-hand side are adequately efficient, then the corresponding NN is of size $\mathcal{O}(d^3 \log_2^q(1/\varepsilon))$. Finally, if D is the size of the high-fidelity basis, then one can approximate a base change by applying a linear map $\mathbf{V} \in \mathbb{R}^{D \times d}$ to a vector with respect to the reduced basis. This procedure increases the size of the NN to $\mathcal{O}(d^3 \log_2^q(1/\varepsilon) + dD)$.

3.2.2 Approximation Results for Operator Learning Methods with State-to-the-Art Architectures

In contrast to neural networks aiming at function approximations, several operator learning methods for PDEs aiming at learning the full parameter-to-state map have been proposed in recent years. These operator learning methods have their own specific and somewhat complex architectures. For example, the networks of Fourier neural operators are mainly defined in Fourier space or the DeepONets consists of a branch network that approximates the map and a trunk network that approximates the solution basis. Thus, the network approximation result in (3.2.1) cannot be directly applied to these state-of-the-art operator learning methods. However, there are also some approximation results available for some operator learning methods.

In [89] it is shown that in the worst case, the network size of the Fourier neural operator can grow exponentially in terms of accuracy when approximating general operators. However, the author also proved that, under suitable hypotheses, the size of the network in FNOs for approximating the parametric map for a Darcy-type elliptic equation or for the incompressible Navier-Stokes equations of fluid dynamics scales only polynomially in the error bound.

For PCANN, under some assumptions on the probability measure of the parameter and solution spaces, in [12] it is proven that for any error level $\varepsilon > 0$ there exist dimensions for the reduced basis of the parameter and solution spaces, and a network with maximum layers and widths, such that the neural network can approximate the operator up to a certain error ε associated with the probability distribution.

In DeepONet [113], the basis functions of the solution space are represented by the trunk net. Thus, not only is the branch net required to have approximation capability to learn the map connecting the parameter functions and the coefficients of the solutions with respect to the basis of the trunk net, but also the trunk net should efficiently approximate the basis of the solutions. A first answer to this question lies in a remarkable universal approximation theorem for the operator network first proven in [20]. More refined results are given in [113, 96]. In particular, in [96] the authors extended the universal approximation theorem from continuous to measurable functions, while removing the compactness requirements. Upper and lower bounds on the DeepONet error are given in [96] with respect to the number of sensors, the number of branch and trunk networks p , and the sizes and depths of the networks.

Some approximation results for operator learning with convolutional neural networks have also been derived. In the paper [39], the authors have established and verified theoretical error bounds for the approximation of nonlinear operators using convolutional neural networks. The results shed light on the role of convolutional layers and their hyperparameters, such as input and output channels, depth and others.

4 DL concepts based on function approximation

In this section, we list the most common DL concepts based on function approximation for PDE forward solvers and their related inverse problems.

4.1 Deep Ritz Method

4.1.1 Motivation

The Deep Ritz method [165] is a function evaluation concept based on a combination of the classical Ritz method (variational method) and deep learning. The Deep Ritz method assumes that a variational formulation of a PDE as stated in Equation (1) exists, i.e. there exists a $\Psi : \mathbb{R} \rightarrow \mathbb{R}$ such that the unique solution u of the PDE is given by

$$u = \operatorname{argmin}_{v \in H} I(v) \quad (12)$$

where

$$I(u) = \int_{\Omega} \Psi(u(x)) dx \quad (13)$$

and H is the set of admissible functions. Hence, the Deep Ritz method is a physics-informed method.

The idea of the Deep Ritz method is to replace u with a neural network u_{Θ} which has a scalar or vectorial x as input. The network is trained by choosing suitable collocation points $\{x_i\}_{i=1}^N \subset \Omega$ and by replacing the

integral in the variational formulation by a finite sum

$$\min_{\Theta} \sum_{i=1}^N \Psi(u_{\Theta}(x_i)) . \quad (14)$$

After training, u_{Θ} can be evaluated efficiently at arbitrary points in the domain of definition.

4.1.2 Network architecture

For the numerical examples for our standard test problems, see Section 6, we used the network shown in Figure 3. The main building block of the Deep Ritz neural network consists of two stacked fully connected (FC) layers which are each followed by a non-linear somewhat "smooth" activation function. A residual connection, which can help to avoid the vanishing gradient, links the input of the first FC layer to the output of the second FC layer. Several blocks are then stacked to complete the architecture of the network.

Consider the i -th block of the neural net. Let $W_{i,1}, W_{i,2} \in \mathbb{R}^{m \times m}$ and $b_{i,1}, b_{i,2} \in \mathbb{R}^m$ be the respective weight and bias of the first and second FC layers. A block which receives an input s , performs the operation

$$B_i(s) = \sigma(W_{i,2} \cdot \sigma(W_{i,1}s + b_{i,1}) + b_{i,2}) + s, \quad (15)$$

where σ is the activation function. From experience,

$$\sigma(x) = \max\{x^3, 0\}, \quad (16)$$

provides a good balance between accuracy and simplicity. Its smoothness contributes to the accuracy of the Deep Ritz method. To match the input, resp. output, dimensions of the considered problem, an appropriate FC layer is used at the entrance (resp. exit) of the first (resp. last) layer of the first (resp. last) block of the neural network. Figure 3 shows the architecture of the Deep Ritz network.

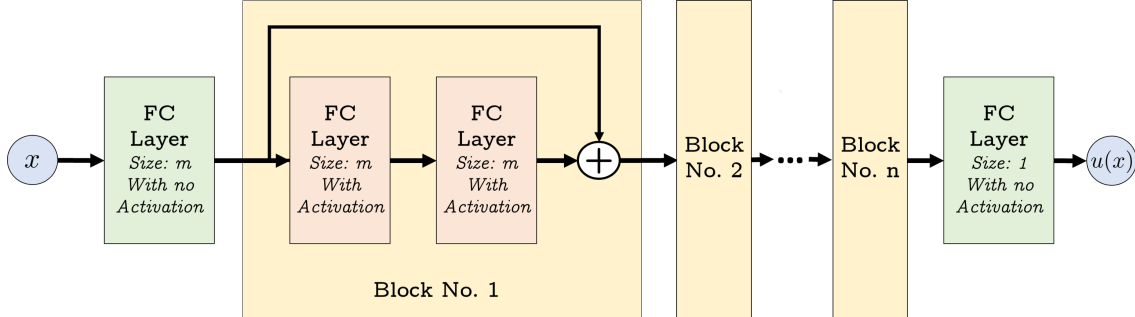


Figure 3: Deep Ritz network with n blocks and with appropriate input and output FC linear layers. The first FC linear layer can be replaced by zero padding

4.1.3 The algorithm

The training of the network does not need any information or data of the solution u , hence, with this respect, it is equivalent to classical numerical PDE solvers. It, however, needs the PDE in its variational formulation, hence, it is a physics-informed concept. The network architecture will be of the type 'function approximation', i.e. a rather small network with two or three nodes in the input level and a single value for output. This can be adjusted for higher-dimensional PDEs accordingly. The training of the network uses a loss function, which is simply a discretisation of the variational formulation. A second term is added for ensuring the boundary conditions. Hence, first of all, it requires sampling a suitable set of evaluation points $x_i, i = 1, \dots, N$ in the domain of definition and on the boundary. This can be done via stochastic sampling of a uniform distribution over the domain of definition (Monte Carlo integration) on a fixed grid. The training itself is

then done by classical stochastic gradient descent. The sampling points may be changed during training after a fixed number of epochs. We specify the approach for the classical Poisson problem

$$\begin{aligned}\Delta u &= \lambda \text{ on } \Omega \subset \mathbb{R}^2 \\ u &= g \text{ on } \partial\Omega\end{aligned}\tag{17}$$

This has the variational form: $I(u) = \int_{\Omega} (\frac{1}{2}|\nabla u(x)|^2 - \lambda(x)u(x)) dx$, see Algorithm 1.

Algorithm 1: Deep Ritz Method

Input:

- $N_{\mathcal{L}}/N_{\mathcal{B}}$: number of inner/boundary collocation points
- τ : learning rate

```

1 Initialise the network architecture  $u_{\Theta}$ 
2 while not converged do
3   Sample collocation points  $\{x_{\mathcal{L}}^i \in \Omega : i = 1, \dots, N_{\mathcal{L}}\}$  and  $\{x_{\mathcal{B}}^j \in \partial\Omega : j = 1, \dots, N_{\mathcal{B}}\}$ 
4   Compute  $E_{\mathcal{L}}(u_{\Theta}) = \frac{1}{N_{\mathcal{L}}} \sum_{i=1}^{N_{\mathcal{L}}} (\frac{1}{2}|\nabla u_{\Theta}(x_{\mathcal{L}}^i)|^2 - \lambda(x_{\mathcal{L}}^i)u_{\Theta}(x_{\mathcal{L}}^i))$ , via backpropagation
5   Compute  $E_{\mathcal{B}}(u_{\Theta}) = \frac{1}{N_{\mathcal{B}}} \sum_{j=1}^{N_{\mathcal{B}}} (u_{\Theta}(x_{\mathcal{B}}^j) - g(x_{\mathcal{B}}^j))^2$ 
6   Add loss values  $L = E_{\mathcal{L}}(u_{\Theta}) + E_{\mathcal{B}}(u_{\Theta})$ 
7   Optimise Loss, L using the appropriate optimisation algorithm.
8   Update  $\Theta \leftarrow \Theta - \tau \nabla_{\Theta} L$ 
9 end
```

It has been numerically shown that the Deep Ritz has the power to solve high-dimensional problems, this is mainly due to the use of the Monte Carlo algorithm for approximating the integral. In addition, Deep Ritz is potentially a naturally adaptive algorithm that can solve problems with corner singularities. One drawback of the Deep Ritz method is that the neural network parameterises the solution function instead of the parameter-solution operator. Hence, the Deep Ritz method is less suited for parametric studies, since it requires a new training of the full network for every new parameter. Note that the loss function of the Deep Ritz method can be negative and the minimal value is usually unknown, this also causes some challenges in the training process. In addition, the minimisation problem that results from Deep Ritz is usually not convex even when the original problem is. The treatment of the essential boundary condition is not as simple as for traditional methods.

4.1.4 Theoretical Background

The convergence properties of the Deep Ritz methods have been analysed intensively over the last years [33, 127, 35, 81]. The most far-reaching results - to the best of our knowledge - are described in [33]. This paper also contains a nicely written survey on the state of the art of other results concerning convergence properties. This paper use techniques from Γ -convergence for proving, that under rather mild assumptions on the network architectures, the loss function of the network training Γ -converges to the true variational formulation and also the minimisers converge weakly to the true solution of the PDE, see Theorem 7 [33].

4.2 Physics-informed Neural Network (PINN)

4.2.1 Motivation

The notion of 'physics-informed neural networks' is now used in more general terms. In this section, however, we discuss the baseline version of a PINN as introduced in the original paper [137]. Similar to the previously described Deep Ritz method, this original PINN concept parameterises the solution function as a neural network and requires knowledge of the underlying In contrast to the Deep Ritz method, PINNs use the strong form of the PDE, thus their application to general PDEs is straightforward. To describe the method, we split up the operator \mathcal{N} in equation (1) into a differential operator \mathcal{L} encoding the PDE and the initial/boundary

operator \mathcal{B} . The problem then reads

$$\begin{aligned}\mathcal{L}(u; \lambda) &= 0 \quad \text{in } \Omega \\ \mathcal{B}(u; \lambda) &= 0 \quad \text{on } \partial\Omega.\end{aligned}\tag{18}$$

The neural network u_Θ is again substituted into the PDE, where the differential operator \mathcal{L} can be applied to u_Θ via automatic differentiation (backpropagation). We note that $\mathcal{L}(u_\Theta; \cdot)$ and $\mathcal{B}(u_\Theta; \cdot)$ rely on the same set of parameters Θ as u_Θ , which is crucial for the optimisation of PINNs. To fit u_Θ to the PDE, we penalise the residuals of both operators by their mean squared error on previously sampled points. This leads to the training objective

$$\min_{\Theta} (MSE_{\mathcal{L}}(u_\Theta) + MSE_{\mathcal{B}}(u_\Theta)),\tag{19}$$

where

$$MSE_{\mathcal{L}}(u_\Theta) = \frac{1}{N_{\mathcal{L}}} \sum_{i=1}^{N_{\mathcal{L}}} |\mathcal{L}(u_\Theta; \lambda)(x_{\mathcal{L}}^i)|^2 \quad \text{and} \quad MSE_{\mathcal{B}}(u_\Theta) = \frac{1}{N_{\mathcal{B}}} \sum_{j=1}^{N_{\mathcal{B}}} |\mathcal{B}(u_\Theta; \lambda)(x_{\mathcal{B}}^j)|^2.\tag{20}$$

During optimisation, $MSE_{\mathcal{B}}$ enforces the initial or boundary conditions of a given problem and $MSE_{\mathcal{L}}$ checks the differential equation at the collocation points. A visual representation of the general idea is shown in Figure 4.

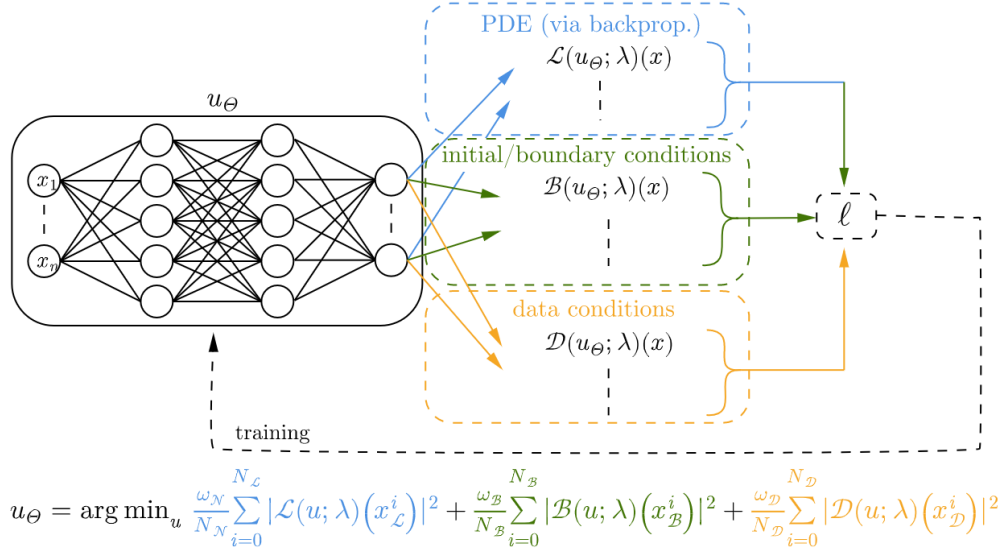


Figure 4: General training procedure of the PINN approach. As compared with the conditions in (20), in this figure we included a data condition that refers to observations of the solution on some points.

4.2.2 Network architecture

The architecture of the neural network u_Θ allows a lot of freedom, the original paper [137] uses a simple fully-connected architecture. Depending on the underlying differential equation, different network structures can lead to better approximation results. This promotes the existence of a great variety of extensions of the PINN approach, either focused on individual problems or designed for broader classes of equations. In Section 4.2.6 we will mention a few of these methods.

4.2.3 The algorithm

The general training procedure is comparable to the Deep Ritz algorithm 4.1.3. Again, the network itself is optimised to approximate the solution as a function, therefore the number of input nodes corresponds to

the dimensionality of Ω and the amount of output nodes denotes the dimensionality of the possibly vector-valued solution. The training requires the underlying PDE and some evaluation points $x_{\mathcal{L}}^i, x_{\mathcal{B}}^j, i = 1, \dots, N_{\mathcal{L}}, j = 1, \dots, N_{\mathcal{B}}$ to compute the residuals. The sampling strategy and therefore the distribution of these points can be chosen freely and may be changed throughout the training. Summarising the approach for the Poisson problem of Equation 17, the general algorithm is shown in 2.

Algorithm 2: Physics-Informed Neural Networks

Input: $N_{\mathcal{L}}/N_{\mathcal{B}}$: number of inner/boundary collocation points,
 τ : learning rate
1 Initialise the network architecture u_{Θ}
2 **while** not converged **do**
3 Sample collocation points $\{x_{\mathcal{L}}^i \in \Omega : i = 1, \dots, N_{\mathcal{L}}\}$ and $\{x_{\mathcal{B}}^j \in \partial\Omega : j = 1, \dots, N_{\mathcal{B}}\}$
4 Compute $MSE_{\mathcal{L}}(u_{\Theta}) = \frac{1}{N_{\mathcal{L}}} \sum_{i=1}^{N_{\mathcal{L}}} |\Delta u_{\Theta}(x_{\mathcal{L}}^i) - \lambda(x_{\mathcal{L}}^i)|^2$, via backpropagation
5 Compute $MSE_{\mathcal{B}}(u_{\Theta}) = \frac{1}{N_{\mathcal{B}}} \sum_{j=1}^{N_{\mathcal{B}}} |u_{\Theta}(x_{\mathcal{B}}^j) - g(x_{\mathcal{B}}^j)|^2$
6 Add loss values $L = MSE_{\mathcal{L}}(u_{\Theta}) + MSE_{\mathcal{B}}(u_{\Theta})$
7 Update $\Theta \leftarrow \Theta - \tau \nabla_{\Theta} L$
8 **end**

The generality of PINN allows the extension of the loss function to include several additional conditions. For example, if some observed data is available, it can be seamlessly incorporated into the loss function. In addition, PINN can be extended to solve integro-differential equations [114], fractional PDEs [132] and stochastic PDEs [168]. Furthermore, by using a discrete-time model (Runge-Kutta methods) to link two distinct temporal snapshots, the number of collocation points for time-dependent PDEs can be reduced significantly.

4.2.4 Application to parameter identification

Notably, PINNs are also suitable for the parameter identification of PDEs. Given a set of observed data points, the unknown parameters of the PDE can be optimised alongside the parameters of the solution network u_{Θ} . From an implementation point of view, PINNs can therefore be applied to parameter identification problems requiring minimal additional work, see [137, 21, 136, 115, 78, 166].

While the identification/learning of scalar parameters is quite straightforward, that of function-valued (e.g. space-dependent and/or time-dependent) parameters requires some additional effort. For function-valued parameters such as the right side, λ in equation 17 or the coefficient λ in 58 of a certain PDE, one usually introduces an additional neural network λ_{Θ} for the searched functions. The idea behind these networks is comparable to u_{Θ} which parameterises the PDE solution as described in 2, i.e. we input the space and/or time variables and the network should output an approximation of the searched function at these values. The training process then consists of a combination of physics-informed loss and data loss. Via the data loss, the network u_{Θ} learns an interpolation of the given (measured) data. A physics-informed loss, like the $MSE_{\mathcal{L}}$ term in 20, then enables us to learn the searched functions, by using the learned interpolation u_{Θ} . During the minimisation of the sum of both loss terms, the corresponding weights of all appearing networks then are optimised simultaneously via automatic differentiation. The resulting loss function which is optimised, e.g. in the case of the Poisson problem 17 is thus

$$L = \underbrace{\frac{1}{N_{\mathcal{P}}} \sum_{i=1}^{N_{\mathcal{P}}} |\Delta u_{\Theta}(x_{\mathcal{P}}^i) - \lambda_{\Theta}(x_{\mathcal{P}}^i)|^2}_{\text{Physics loss}} + \underbrace{\frac{1}{N_{\mathcal{D}}} \sum_{j=1}^{N_{\mathcal{D}}} |u_{\Theta}(x_{\mathcal{D}}^j) - u(x_{\mathcal{D}}^j)|^2}_{\text{Data loss}}, \quad (21)$$

where $N_{\mathcal{P}}$ is the number of collocation points, and $N_{\mathcal{D}}$ is the number of known data points, such that $\{x_{\mathcal{P}}^i \in \Omega : i = 1, \dots, N_{\mathcal{P}}\}$ and $\{x_{\mathcal{D}}^j \in \partial\Omega : j = 1, \dots, N_{\mathcal{D}}\}$.

In the case of noisy data, the physics can also act as a regularisation for the learned interpolation, since the loss also influences u_{Θ} . Even when only discrete data points of the solution are available, the physics loss

may be evaluated on arbitrary points, because of the interpolation properties of u_Θ . Moreover, the flexible framework of PINNs allows for further inclusion of a-priori knowledge on the solution or parameter functions, such as their regime or boundary values, by similar incorporation into the loss.

In the numerical experiments in Section 6, we will use simple fully connected neural networks (FCNNs), consisting of multiple FC layers. As an activation function, we will use $\phi(x) = \tanh(x)$.

4.2.5 Theoretical Background

In contrast to the large number of applications of PINNs, they still lack a rigorous theoretical background. First consistency results under additional assumptions for linear elliptic and parabolic PDEs, can be found in [163]. Some estimates on the generalisation error of PINNs approximating solutions for forward and inverse problems are proven in [122, 123]. The authors derive an error estimation in terms of training error and training points by exploiting the stability properties of the underlying equation. More general convergence results of the PINN approach still have to be found.

Some studies of the convergence rate were carried out in [155, 154]. There the Neural Tangent Kernel (NTK) theory [76] was applied to the PINN framework, which gave the first insight into the convergence behaviour of the different loss terms and spectral bias of PINNs. With the NTK theory special weights for the different terms can be found, to achieve more robust and accurate results. In [157], the same approach was also applied to the DeepONet architecture, which will be introduced in Section 5.3.

4.2.6 Generalisations and extensions of PINN

Lastly, we want to give a short overview of possible extensions and generalisations for PINNs. Since the literature in this regard is vast, we can not represent every approach.

- **Quadratic Residual Networks (QRES)** [16]: Extends PINNs by including quadratic terms in each layer. The used architecture consists of FC layers with additional weight matrices, see Figure 5. In each Layer, The output of the FC layer matrix and additional matrix are point-wise multiplied and added to the FC layer output, to create a quadratic term. This may lead to faster convergence and better parameter efficiency with respect to network width and depth.
- **Residual-based adaptive refinement** [114]: The idea of RAR is to add more residual points in the locations where the PDE residual is large during the training process, conceptually similar to FEM refinement methods.
- **Gradient-enhanced PINN (gPINN)** [166]: If the PDE residual $\mathcal{L}u$ is zero, then it is clear that the gradient of the PDE residual, i.e $\nabla \mathcal{L}u$, should also be zero. Thus, the gradient-enhanced PINN (gPINN) uses a new type of loss function by leveraging the gradient information of the PDE residual to improve the accuracy and training efficiency of PINNs.
- **XPINN and cPINN** [77, 78]: The XPINN and cPINN apply domain decomposition, and then different subdomains use independent neural networks to approximate the solutions. In addition to the loss function used in PINN, interface conditions are introduced to stitch the decomposed subdomains together in order to obtain a solution for the governing PDEs over the complete domain. These extensions efficiently lend themselves to paralleled computation and are able to solve more general PDEs, e.g. PDEs with jump parameter functions.

For further details on the PINN approach, we suggest the paper [27], which contains a comprehensive and nicely written survey for the current state of the art of the PINNs. Mentioning different applications, extensions, theories, general challenges and currently open questions.

4.3 Weak Adversarial Networks

4.3.1 Motivation

Similar to PINN and Deep Ritz, the method of weak adversarial networks [167] also parameterises the solution as a neural network and is a physics-informed method. However, the weak adversarial network is based on

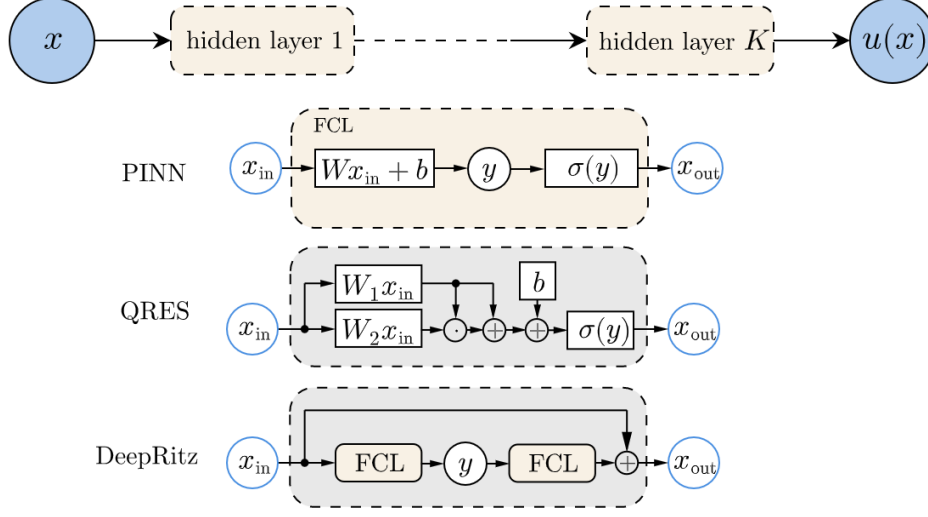


Figure 5: Overview and comparison of network architectures used in PINN, QRES and Deep Ritz. With weight matrix W , bias vector b and activation function σ .

the weak formulation of the PDE and the loss function is defined as an operator norm to be minimised. For simplicity, consider the following weak formulation of the Poisson problem with either Dirichlet or Neumann boundary conditions on an arbitrary domain $\Omega \subset \mathbb{R}^d$:

$$\langle \mathcal{L}[u, \lambda], \varphi \rangle := a(u, \varphi; \lambda) = \int_{\Omega} (\nabla u \cdot \nabla \varphi - \lambda \varphi) dx = 0, \quad \text{for all } \varphi \text{ in } H_0^1(\Omega), \quad (22)$$

$$\mathcal{B}(u, \lambda) = 0 \quad \text{on } \partial\Omega. \quad (23)$$

From the above formula, we see that for each $u \in H^1(\Omega)$, it defines a linear functional (operator) $\mathcal{L}[u, \lambda]$ such that $\mathcal{L}[u, \lambda](\varphi) = a(u, \varphi; \lambda)$. A function $u \in H^1(\Omega)$ satisfying the boundary condition is the weak solution of the equation if and only if the operator norm:

$$\|\mathcal{L}[u, \lambda]\|_{op} := \max\{|\langle \mathcal{L}[u, \lambda], \varphi \rangle| / \|\varphi\|_2 \mid \varphi \in H_0^1(\Omega), \varphi \neq 0\} \quad (24)$$

is equal to 0. Hence, the solution satisfies the boundary condition and solves the following minmax problem:

$$\min_u \max_{\varphi} |\langle \mathcal{L}[u, \lambda], \varphi \rangle|^2 / \|\varphi\|_2^2. \quad (25)$$

This weak formulation inspires an adversarial approach, where a network u_{Θ} with parameter Θ is used to parameterise the solution of the PDE and another network φ_{η} with parameter η approximates the test function.

4.3.2 Network architecture

As just stated, in weak adversarial networks, the solution is parameterised as a neural network u_{Θ} with parameter Θ , which is learned by minimising the operator norm $\|\mathcal{L}[u_{\Theta}]\|_{op}$. The test function, however, is parameterised by an adversarial network φ_{η} with parameter η and is trained by maximising $\langle \mathcal{L}[u_{\Theta}], \varphi_{\eta} \rangle / \|\varphi_{\eta}\|$, hence it approximates the operator norm $\|\mathcal{L}[u_{\Theta}, \lambda]\|_{op}$. Thus, it is an adversarial training in a way that the test function critics on the solution network where the PDE is violated, and the solution network corrects itself at those spots until the PDE system is satisfied (almost) everywhere in the domain. Thus the network version of (25) can be formulated as:

$$\min_{\Theta} \max_{\eta} |\langle \mathcal{L}[u_{\Theta}, \lambda], \varphi_{\eta} \rangle|^2 / \|\varphi_{\eta}\|_2^2. \quad (26)$$

Both networks u_Θ and φ_η can be general architectures, e.g., fully connected networks (FCN), residual neural networks (ResNet), convolutional neural networks (CNN), recurrent neural networks (RNN). However, the choice of neural networks can affect efficiency and accuracy. For example, using a ResNet for parameterising the trial and test function usually has better performance than using a fully connected network.

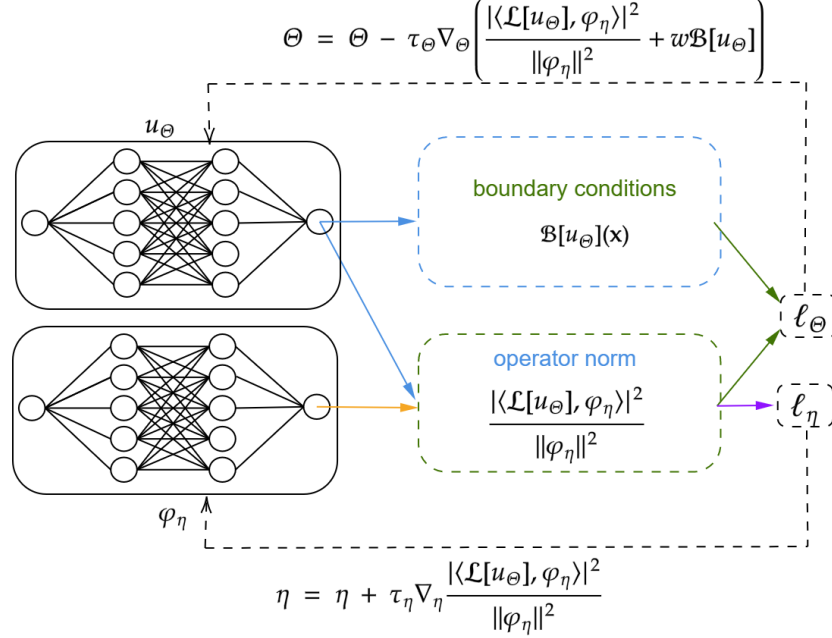


Figure 6: General training procedure of the WAN approach, where u_Θ and φ_η denote the neural network's approximations for the solution and the test function, respectively. ℓ_Θ and ℓ_η denote the loss functions for updating u_Θ and φ_η , respectively.

4.3.3 The algorithm

The main challenge of the WAN method is how to design an efficient algorithm for solving the minmax problem (26), or equivalently for

$$\min_{\Theta} \max_{\eta} L_{int}(\Theta, \eta) \quad \text{where} \quad L_{int}(\Theta, \eta) = \log |\langle \mathcal{L}[u_\Theta], \varphi_\eta \rangle|^2 - \log \|\varphi_\eta\|_2^2. \quad (27)$$

In addition, the weak solution u_Θ also needs to satisfy the boundary condition, which can be realised by minimising

$$L_{bdry}(\Theta) = \int_{\partial\Omega} |u_\Theta(x) - g(x)|^2 dx. \quad (28)$$

The total objective function is the weighted sum of the two objectives and we seek to compute a saddle point that solves the minmax problem:

$$\min_{\Theta} \max_{\eta} L(\Theta, \eta) = \min_{\Theta} \max_{\eta} L_{int}(\Theta, \eta) + \alpha L_{bdry}(\Theta). \quad (29)$$

where $\alpha > 0$ is a user-chosen balancing parameter. Typical algorithms use alternating updates, i.e. the objective function is alternatively minimised and maximised and the parameters Θ and η are alternately updated such that the primal network can approximate the solution gradually.

Given the objective function (8), the key components of the network training are the computation of $L(\Theta, \eta)$ and its gradients with respect to Θ and η , respectively. By denoting

$$I(x, \Theta, \eta) = \nabla u_\Theta(x) \cdot \nabla \varphi_\eta(x) - \lambda(x) \varphi_\eta(x), \quad (30)$$

Algorithm 3: Weak Adversarial Network (WAN) for Solving static PDEs.

Input: N_r/N_b : number of region/boundary collocation points;
 K_u/K_φ : number of solution/adversarial network parameter updates per iteration;
 τ_Θ/τ_η : learning rates for Θ and η ;
 α : balancing weight
1 Initialise the network architectures u_Θ, φ_η ;
2 **while** not converged **do**
3 Sample collocation points $\{x_r^j \in \Omega : j \in [N_r]\}$ and $\{x_b^j \in \partial\Omega : j \in [N_b]\}$
4 Update weak solution parameter
5 **for** $k = 1, \dots, K_u$ **do**
6 Update $\Theta \leftarrow \Theta - \tau_\Theta \nabla_\Theta L$ where $\nabla_\Theta L$ is approximated using $\{x_r^j\}$ and $\{x_b^j\}$.
7 **end**
8 **for** $k = 1, \dots, K_\varphi$ **do**
9 Update $\eta \leftarrow \eta + \tau_\eta \nabla_\eta L$ where $\nabla_\eta L$ is approximated using $\{x_r^j\}$.
10 **end**
11 **end**

we have

$$\nabla_\Theta I(x, \Theta, \eta) = \nabla(\nabla_\Theta u_\Theta(x)) \cdot \nabla \varphi_\eta(x), \quad (31)$$

$$\nabla_\eta I(x, \Theta, \eta) = \nabla u_\Theta(x) \cdot \nabla(\nabla_\eta \varphi_\eta(x)) - \lambda(x)(\nabla_\eta \varphi_\eta(x)), \quad (32)$$

and

$$\nabla_\Theta L_{int}(\Theta) = 2 \left(\int_\Omega I(x; \Theta, \eta) dx \right)^{-1} \left(\int_\Omega I(x; \Theta, \eta) dx \right). \quad (33)$$

Monte-Carlo (MC) approximations can be used to approximate the integrals, i.e., we randomly sample N_r collocation points $\{x_r^{(j)}\}_{j=1}^{N_r}$ uniformly in the interior of the region and approximate the gradient $\nabla_\Theta L_{int}(\Theta) \approx 2 \cdot (\sum_{j=1}^{N_r} I(x_r^{(j)}; \Theta, \eta))^{-1} (\sum_{j=1}^{N_r} \nabla_\Theta I(x_r^{(j)}; \Theta, \eta))$. The gradients $\nabla_\eta L_{int}$ and $\nabla_\Theta L_{bdry}$ can be approximated by the same procedure. Using these gradients of $\nabla_\Theta L$ and $\nabla_\eta L$, we can apply alternating updates to optimise the parameters Θ and η . The resulting algorithm is then summarised in Algorithm 3. Details on how to adapt weak adversarial networks for parabolic PDEs involving time can be found in the original paper.

4.3.4 Weak Adversarial Network for inverse problems

The weak adversarial network can be extended to solve inverse problems directly [6]. An inverse problem defined on an open and bounded domain in \mathbb{R}^d may be presented in a general form as

$$\mathcal{A}[u, \lambda] = 0, \quad \text{in } \Omega, \quad (34)$$

$$\mathcal{B}[u, \lambda] = 0, \quad \text{on } \partial\Omega, \quad (35)$$

where u is the solution and λ can be the coefficient in the inverse medium problem or the source function in the inverse source problem. $\mathcal{B}[u, \lambda] = 0$ are some observations on the boundary. Suppose that the variational form is given by

$$\langle \mathcal{L}[u, \lambda], \varphi \rangle := \int_\Omega \mathcal{L}[u, \lambda](x) \varphi(x) dx \quad \text{for all } \varphi \text{ in } H_0^1(\Omega). \quad (36)$$

Take the inverse conductivity problem as an example, we have

$$\langle \mathcal{L}[u, \lambda], \varphi \rangle = \int_\Omega (\lambda \nabla u \cdot \nabla \varphi - f \varphi) dx = 0. \quad (37)$$

By defining the norm of $\mathcal{A}[u, \lambda]$ as

$$\|\mathcal{L}[u, \lambda]\|_{op}^2 := \sup_{\varphi \in H_0^1, \varphi \neq 0} \frac{|\langle \mathcal{L}[u, \lambda], \varphi \rangle|^2}{\|\varphi\|^2}. \quad (38)$$

Then, the weak formulation and the boundary condition induce a minmax problem:

$$\min_{u, \lambda} \max_{\varphi} \frac{|\langle \mathcal{L}[u, \lambda], \varphi \rangle|^2}{\|\varphi\|^2} + \int_{\partial\Omega} |\mathcal{B}[u, \lambda]|^2 dx. \quad (39)$$

By parameterising u , λ , and φ as neural networks $u_{\theta_1, \lambda_{\theta_2}}$ and φ_{θ_3} , respectively, we have the network version of the minmax problem:

$$\min_{\theta_1, \theta_2} \max_{\theta_3} \frac{|\langle \mathcal{L}[u_{\theta_1}, \lambda_{\theta_2}], \varphi_{\theta_3} \rangle|^2}{\|\varphi_{\theta_3}\|^2} + \alpha \int_{\partial\Omega} |\mathcal{B}[u_{\theta_1}, \lambda_{\theta_2}]|^2 dx \quad (40)$$

The algorithm is then similar to that of the direct problems by updating $\theta = (\theta_1, \theta_2)$ and $\eta = \theta_3$ alternately.

5 DL concepts based on operator approximation

In this section, we introduce the basic concepts for DL approaches which aim at approximating the parameter-to-state operator. By construction, these methods are perfectly suited for parametric studies and can be adapted directly to inverse problems. The two basic concepts for adaptation to inverse problems have already been described in Section 2.3.

5.1 Model Reduction And Neural Networks For Parametric PDEs (PCANN)

5.1.1 Motivation

PCANN, as we call it in this paper, seeks to provide a meshless operator for the evaluation of the solution of a PDE by combining ideas of model order reduction with deep learning. For given training data (λ_i, u_i) one first obtains a model reduction by use of the principal component analysis (PCA) for both the input (parameter λ) and output (solution u) functions. Only the coefficients of a finite number of PCA components are retained. The PCA thus reduces the dimensions of both the input and output spaces to finite latent dimensional latent spaces. A neural network then maps the coefficients of the respective representations in these latent spaces as shown in Figure 2. The evaluation of this operator approximation for a novel parameter λ is then most efficient: one only needs to compute the scalar products with the specified finite number of PCA components, and the neural network then maps these coefficients to the latent coefficients of the output space and an expansion using these coefficients and the PCA on the output side gives a function approximation to the solution of the PDE.

The formulation of this approach is in a function space setting and hence mesh-free. For implementation purposes, however, one has to specify how to compute the scalar products with the PCA components. These functions are only given numerically, usually by their values on a specified grid. The red arrow in Figure 2 shows the flow during testing. The overall PCANN can be used to evaluate the solution of the PDE for any given grid size as illustrated in Algorithm 4. In line 2-3 of Algorithm 4, it is possible to use one of the numerous PCA algorithms available [160]. For the implementations in this work, we make use of randomised PCA proposed in [62, 63].

In a situation where the input-to-output operator is linear, like in the case of the Poisson problem considered, it might be beneficial to use a simple linear map for the mapping of the reduced/latent dimensions. Section 6, equally shows results for this case, PCALin, where a single linear layer with no activation functions is used to map the latent dimensions. PCALin is similar to the linear method proposed in [12], only, we use a neural network instead of the normal equations. The results in both cases are similar as we later show in 6. The combination of model order reduction with deep learning has recorded success in a number of application problems ranging from cardiac electrophysiology [42, 43], where the use of proper orthogonal decomposition (POD) further improves the results [41], to fluid flow [40] and non-linear models [25, 44]. Specifically, the PCANN operator has been used in [109, 91] in a multiscale plasticity problem to map strain to stress. Worth highlighting is an earlier work [70], which equally combines model order reduction with neural networks to solve PDEs.

5.1.2 Network Architecture

In our numerical examples, we followed the outline of the original paper [12] and used a fully connected feed-forward neural network for the mapping of the latent spaces. The number of nodes per layer is as follows $d_{\mathcal{X}}, 500, 1000, 2000, 1000, 500, d_{\mathcal{Y}}$. $d_{\mathcal{X}}$ and $d_{\mathcal{Y}}$ are considered to be hyperparameters, and for convenience, are chosen to be equal. As activation function we use the Scaled Exponential Linear Unit (SELU) activation function which that induce self-normalizing properties in feed-forward neural networks [86]. Figure 7 shows a simplified schematic of the overall architecture.

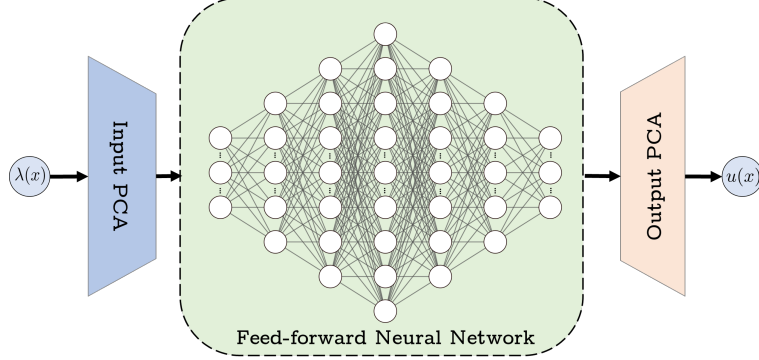


Figure 7: Architecture of the PCANN.

5.1.3 The Algorithm

As a purely data-driven method, no physics or PDE is needed in the training of the model. However, the data used for the training of the network is obtained from a classical FDM for solving the underlying By training the network with these input-output (numerically-given) function pairs, we obtain a neural operator which solves the PDE for various instances irrespective of the mesh size.

Once again, we specify the algorithm for the Poisson problem in Equation 17. The training data is the pair (λ_i, u_i) , with each $\lambda_i, u_i \in \mathbb{R}^{s^2}$. Originally, λ_i, u_i are functions given in a (square) grid of dimensions $s \times s$. By flattening these functions, we now have them in \mathbb{R}^{s^2} . Training then proceeds as in Algorithm 4, while testing/usage of the trained network proceeds as in Algorithm 5.

5.1.4 Theoretical Background

As the PCANN method combines both the PCA and Neural network (NN) to achieve the task of operator learning, the strength of its approximation, therefore, comes from that of both the PCA and NNs. For a good approximation, one thus needs not only a good neural network but also, appropriate PCA truncation parameters (resulting from choosing sufficient amounts of data). The existence of all these factors is shown in Theorem 3.1 of [12] which is a consequence of Theorem 3.5 of the same work. A recent work [95] further extends the approximation theory of PCANN. Notably, it derives novel approximation results, with minimal assumptions [95].

5.1.5 PCANN adaptation for inverse problems

Following the general concepts as discussed in Section 2.3 we have two principle options. We either train a PCANN network $\Psi_{\Theta}(u)$ with training data $(u_i^{\delta}, \lambda_i)$, where we reverse the input-output order. I.e. the (u_i^{δ}) are used as input and (λ_i) as output. After training we can directly use a new measurement (u^{δ}) and compute a corresponding parameter $\hat{\lambda} = \Psi_{\Theta}(u^{\delta})$.

The other option is to use a trained network for the forward problem Φ_{Θ} and include this into a Tikhonov functional. The resulting algorithm is summarized as follows:

Algorithm 4: PCANN

Input:

- (λ_i, u_i) : Training Data pair with $i = 0 \dots N_{\text{train}}$
- τ : learning rate

```
1 Initialise the network  $\Phi_{\Theta}$ 
2 Compute PCA of  $(\lambda_i)$ , store PCA  $(a_k), k = 1, \dots, d_{\mathcal{X}}$ 
3 Compute PCA of  $(u_i)$ , store PCA  $(b_{\ell}), \ell = 1, \dots, d_{\mathcal{Y}}$ 
4 for  $i \leftarrow 0, \dots, N_{\text{train}}$  do
5   | compute  $c_i^k = \langle \lambda_i, a_k \rangle \in R^{d_{\mathcal{X}}}$ 
6   | compute  $d_i^{\ell} = \langle u_i, b_{\ell} \rangle \in R^{d_{\mathcal{Y}}}$ 
7 end
8 while not converged do
9   | /* Train network */
10  | for  $i \leftarrow 0, \dots, N_{\text{train}}$  do
11  |   | Compute Loss,  $L_i = \sum_{\ell=1}^{d_{\mathcal{Y}}} \left\| \frac{\Phi_{\Theta}(c_i^k) - d_i^{\ell}}{d_i^{\ell}} \right\|_2$ 
12  | end
13  | Compute the Loss,  $L = \sum_{i=1}^{N_{\text{train}}} L_i$ 
14  | Optimise L using the appropriate/chosen optimisation algorithm.
15  | Update  $\Theta \leftarrow \Theta - \tau \nabla_{\Theta} L$ 
16 end
```

Algorithm 5: Using/Testing the PCANN

Input:

- Input parameter functions λ_i with $i = 0 \dots N_{\text{test}}$
- Input PCA basis $(a_k)_{k=1, \dots, d_{\mathcal{X}}}$
- Output PCA basis $(b_{\ell})_{\ell=1, \dots, d_{\mathcal{Y}}}$
- Trained network Φ_{Θ} .

Result: Output solution functions \tilde{u}_i , with $i = 0 \dots N_{\text{test}}$

```
1 for  $i \leftarrow 0, \dots, N_{\text{test}}$  do
2   |  $\tilde{u}_i = \sum_{\ell} \Phi_{\Theta}(\langle \lambda_i, a_k \rangle)_{\ell} b_{\ell}$ 
3 end
```

Algorithm 6: Using trained forward PCANN for Inverse Problem

Input:

- Solution function u^{δ}
- Input PCA basis $(a_k)_{k=1, \dots, d_{\mathcal{X}}}$
- Output PCA basis $(b_{\ell})_{\ell=1, \dots, d_{\mathcal{Y}}}$
- Trained network $\Phi_{\Theta} : c = (\langle \lambda, a_k \rangle) \mapsto d = (\langle u, b_{\ell} \rangle)$.

Result: Output parameter function $\hat{\lambda}$

```
1 Initialise  $c^0$ 
2 for  $m \leftarrow 0, \dots, N$  (large integer) do
3   | Compute  $J_{\alpha}(c) = \|\Phi_{\Theta}(c) - \langle u^{\delta}, b_{\ell} \rangle\|_2$ 
4   | Compute the loss  $J_{\alpha}(c) := J_{\alpha}(c) + \alpha R(c)$ .
5   | Optimise Loss  $J_{\alpha}(c)$  using gradient descent
6   | Update  $c^{m+1} \leftarrow (c^m - \sigma_m \partial J / \partial c(c^m))$ 
7 end
8 Compute  $\hat{\lambda} = \sum_k c_k^N a_k$ 
```

5.2 Fourier Neural Operator

5.2.1 Motivation

Fourier neural operators (FNO) [102] are designed as deep learning architectures for learning mappings between infinite-dimensional function spaces. The Fourier neural network is formulated as an iterative architecture, where each iteration (hidden layer), inspired by the convolution theorem, is a Fourier integral operator defined in Fourier space. The main network parameters are therefore defined and learned in Fourier space rather than in physical space, i.e., the coefficients of the Fourier series of the output function are learned from the data.

While standard feed-forward neural networks (FNN) and CNNs combine linear multiplications with non-linear activations in order to learn highly nonlinear functions, FNOs combine linear integral operators with non-linear activations in each layer to learn non-linear operators. The fast Fourier transform (FFT) makes the implementation even more efficient.

Different from DeepONet, and similar to the PCANN methods, FNO discretises both the input function $\lambda(x)$ and the output function $u(x)$ by using point-wise evaluations in an equispaced mesh. In addition, FNO requires that λ and u be defined on the same domain and are discretised by the same discretisation. The function space formulation of the approach allows training an FNO on a dataset with low resolution and applying it directly on a dataset with higher resolution, thus achieving the so-called zero-shot super-resolution.

5.2.2 Theoretical Background

The idea of FNO, stems from an earlier paper by the same team, see [103], which also seeks to approximate a neural operator by concatenating multiple hidden layers. While standard artificial neural networks (FCN, CNN) have affine functions (weights and biases) with scalar nonlinear activation as hidden layers, neural operators rather have affine operators (usually, in addition to affine functions with weights and biases [89] [116]) with scalar nonlinear activation functions. A hidden layer numbered $j + 1$ thus performs the update of input v_j as follows

$$v_{j+1}(x) := \sigma(Wv_j(x) + (\mathcal{K}(\lambda; \theta)v_j)(x)), \quad \forall x \in \Omega, \quad (41)$$

where W, b and \mathcal{K} are the respective weights, biases and neural operators. These neural operators are chosen to be integral operators of the form

$$(\mathcal{K}(\lambda; \theta)v)(x) = \int_{\Omega} \kappa_{\theta}(x, y; \lambda(x), \lambda(y))v(y)dy, \quad \forall x \in \Omega. \quad (42)$$

These operators can be realised by different concepts such as graph kernels [103], multipole expansions [104], non-local kernels [164], low-rank kernels [90], wavelet transforms [150], multiwavelet transforms [58], or Laplace transforms [18]. A recent work even uses some famous convolutional neural networks architectures [138]. In the special case where $\kappa_{\theta} = \kappa_{\theta}(x - y)$, Equation 42 becomes

$$\begin{aligned} (\mathcal{K}(\theta)v)(x) &= \int_{\Omega} \kappa_{\theta}(x - y)v(y)dy, \quad \forall x \in \Omega \\ &= (\kappa_{\theta} * v)(x), \quad \forall x \in \Omega \\ &= (\mathcal{F}^{-1}(\mathcal{F}(\kappa_{\theta}) \cdot \mathcal{F}(v)))(x), \quad \forall x \in \Omega \\ &= (\mathcal{F}^{-1}(K_{\theta} \cdot \mathcal{F}(v)))(x), \quad \forall x \in \Omega, \end{aligned}$$

by the use of the convolution theorem. This then leads to the parameterisation of the neural network given by κ_{θ} directly in the Fourier space K_{θ} . [89] provides a good theoretical background of FNOs and [90] offers a good overview of neural operators using different integral operators along with some theoretical justification.

It is worth mentioning the recent work in [97], which introduces the Nonlocal Neural Operator (NNO), that generalises over arbitrary geometries. FNO is a special case of the NNO, and this work highlights how increasing the number of channels in FNO as opposed to increasing the number of Fourier modes benefits the FNO. The same work also introduces the averaging neural operator which is a subclass of NNO but also happens to be at the core of many neural operator frameworks [97].

5.2.3 The algorithm

The classical FNO is only possible with a uniform grid (cartesian domain), but can be extended for any mesh. We note that, unlike the PCANN method, the input and output functions are inputted in their unflattened states. Once again, as an example, we consider the problem in Equation 17 and we seek to learn the operator

$$F : \Lambda(\Omega; \mathbb{R}^{d_\lambda}) \ni \lambda(x) \mapsto u(x) \in \mathcal{U}(\Omega; \mathbb{R}^{d_u}), \quad (43)$$

where d_λ and d_u depend on the discretisation used ($d_\lambda = d_u = 513^2$ if we use functions with a resolution of 513×513), Ω is a subset of \mathbb{R} while Λ and \mathcal{U} are Banach spaces of functions taking values in \mathbb{R} .

5.2.4 Network Architecture

The architecture of the FNO follows from the algorithm described in Section 5.2.3. For the special case in Equation 17, we consider a mesh of resolution $N \times M$. We denote each point in the domain Ω as x_k^l , with input $\lambda(x_k^l)$, and output $u(x_k^l)$, with $k \in \{1, \dots, N\}$ and $l \in \{1, \dots, M\}$. We equally denote $\lambda(x)$ and $u(x)$ as the input and output for the whole domain.

- The FCN P_θ takes each $\lambda(x_k^l) \in \mathbb{R}$ and maps it to a higher dimension d_{v_0} , i.e.

$$\begin{aligned} v_0(x_k^l) &= P_\theta(\lambda(x_k^l)) \in \mathbb{R}^{d_{v_0}}, \\ v_0(x) &= P_\theta(\lambda(x)) \in \mathbb{R}^{d_{v_0} \times N \times M}. \end{aligned}$$

$v_0(x)$ is thus an $N \times M$ ‘image’ with d_{v_0} channels.

- To obtain $v_1(x)$ from $v_0(x)$, the following operations are applied.
 - The (2D) Fourier transform \mathcal{F} is applied to each channel of $v_0(x)$, and the first $k = k_1 \cdot k_2$ modes are kept (k_1, k_2 , being the number of modes to be kept in the first and second dimensions respectively). As a result we obtain $\mathcal{F}(v_0(x)) \in \mathbb{C}^{d_{v_0} \times k}$.
 - The linear transform \mathcal{R}_ϕ , which is realised as a weight matrix in $\mathbb{C}^{k \times d_{v_0} \times d_{v_0}}$ is applied to $\mathcal{F}(v_0(x))$. The result is $\mathcal{R}_\phi \cdot \mathcal{F}(v_0(x)) \in \mathbb{R}^{d_{v_0} \times k}$.
 - Apply the inverse FFT to $\mathcal{R}_\phi \cdot \mathcal{F}(v_0(x))$, (appended with zeros to make up for the truncated/unselected modes). The outcome is $\mathcal{F}^{-1}(\mathcal{R}_\phi \cdot \mathcal{F}(v_0(x))) \in \mathbb{R}^{N \times M \times d_{v_0}}$.
 - Finally, $v_1(x)$ is obtained from the above together with a residual connection with a weight matrix $W_\Phi \in \mathbb{R}^{d_{v_0} \times d_{v_0}}$, as follows

$$v_1(x) = \sigma(W_\Phi \cdot v_0(x) + \mathcal{F}^{-1}(\mathcal{R}_\phi \cdot \mathcal{F}(v_0(x)))) \in \mathbb{R}^{N \times M \times d_{v_0}}$$

- v_2, v_3, \dots, v_T are obtained from v_1, v_2, \dots, v_{T-1} respectively in a similar manner as above. In this way, we have T Fourier layers.
- At the end of the last Fourier layer another FCN Q_ψ is applied, which projects $v_T(x)$ to the output dimension. We therefore obtain the output function

$$u(x) = Q_\psi(v_T(x)) \in \mathbb{R}^{N \times M}$$

In the FNO architecture, we use the Gaussian Error Linear Units (GELUs) [68, 67] as activation functions.

5.2.5 Generalisation and Extensions of FNOs

A detailed guide for implementation and an illustration of how to extend FNO to operators with inputs and outputs defined on different domains can be found in [116]. There, also two cases of generalisation are considered:

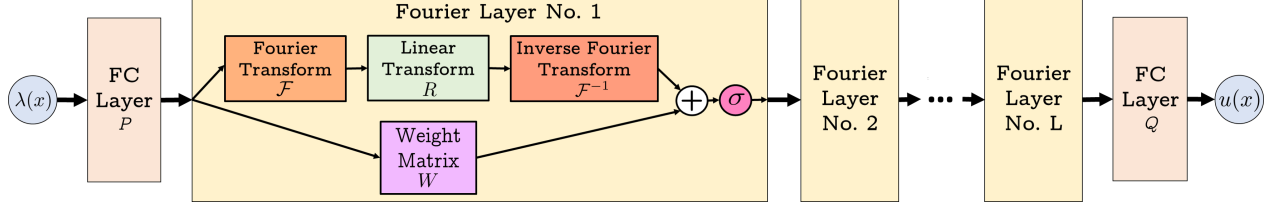


Figure 8: Architecture of the FNO.

Algorithm 7: FNO

Input:

- (λ_i, u_i) : Training data pair with $i = 0 \dots N_{\text{train}}$
- τ : learning rate

```

1 Initialise the fully connected networks (FCN)  $P_\theta$  and  $Q_\psi$ 
2 Initialise the linear transforms  $W_\Phi$  and  $R_\phi$ 
  /* Section 5.2.4 defines these FCN and linear transform networks */
3 Lift  $\lambda_i$  to a higher dimension by computing  $v_0 = P_\theta(\lambda_i)$ 
4 for  $j \leftarrow 0, \dots, T-1$  do
5    $v_{j+1} := \sigma(W_\Phi v_j + [\mathcal{F}^{-1}(R_\phi \cdot (\mathcal{F} v_j))])$ , output of Fourier layers
6 end
7 Obtain the target dimension by using  $Q_\psi$  to get  $\tilde{u}_i = Q_\psi(v_T)$ 
8 while not converged do
9   /* Train network */
10  for  $i \leftarrow 0, \dots, N_{\text{train}}$  do
11    Compute loss  $L_i = \left\| \frac{\tilde{u}_i - u_i}{u_i} \right\|_2$ 
12  end
13  Compute the Loss,  $L = \sum_{i=1}^{N_{\text{train}}} L_i$ 
14  Optimise L using the appropriate/chosen optimisation algorithm.
15  Update  $\Theta \leftarrow \Theta - \tau \nabla_\Theta L$  where  $\Theta = (\theta, \psi)$ .
16 end

```

C 1: As motivation, take a parabolic PDE, where the initial condition at time $t = 0$ is the input for the parameter-to-state operator. The output is the solution for all times $t \in [0, T]$. This leads to the general setting where the output space is that of functions defined on a product space, where the first component is the same as for the input space and the second component is arbitrary. i.e.

$$F : \Lambda(\Omega; \mathbb{R}^{d_\lambda}) \ni \lambda(x) = u(x, 0) \mapsto u(x, t) \in \mathcal{U}(\Omega \times [0, t]; \mathbb{R}^{d_u}),$$

where Ω is a subset of \mathbb{R} while Λ and \mathcal{U} are Banach spaces taking values in \mathbb{R}^{d_λ} and \mathbb{R}^{d_u} (with $d_\lambda = d_u$, depending on the discretisation of the functions) respectively. In order to match dimensions before applying an FNO, the output domain could be shrunk by use of a Recurrent Neural Network (RNN) or the input domain could be extended to incorporate the time, t as an extra coordinate.

C 2: The input space is a subset of the output space, like in the case of the operator F , mapping the boundary conditions of the domain to the solution of the PDE in the whole domain.

$$F : \mathcal{G}(\partial\Omega; \mathbb{R}^{d_g}) \ni g(x) = u|_{\partial\Omega} \mapsto u(x) \in \mathcal{U}(\Omega; \mathbb{R}^{d_u}),$$

where $\partial\Omega \subset \Omega \subset \mathbb{R}$, while \mathcal{G} and \mathcal{U} are Banach spaces taking values in \mathbb{R}^{d_g} and \mathbb{R}^{d_u} (defined in a similar way as above in the first case) respectively. For this situation, zero padding could be applied or better still, an appropriate transformation could be used to map the boundary condition to a lower dimension. This then brings us back to the previous case.

It is worth noting that the use of the FFT in the algorithm of the FNO restricts its applicability to situations where the input and output are defined on a cartesian domain (square, rectangle domain in 2D and cube, cuboid in 3D). This introduces a challenge when dealing with complex geometries. A practical workaround is as followed.

- W 1:** Define a new domain which is the minimum bounding box of the complex domain, and perform a zero padding for the area within this bounding box, but out of the complex domain. However, in practice, this makes the resulting function discontinuous in the ‘rectangle’ and usually yields larger errors.
- W 2:** Use the same minimum bounding of the complex domain, as previously described, but padding is done with the nearest function values within the complex domain, instead of zeros.

Though somewhat successful, the extensions provided in [116] do not seem to favour FNO. A better approach to complex domains is by transforming/deforming this complex domain to a cartesian domain by use of neural networks (NN), positioned before and after the FNO as proposed in [106]. These neural networks could either be fixed or learned together with the FNO parameters. The resulting NN-FNO-NN network is said to be ‘geometry aware’ and is called Geometry-Aware FNO (Geo-FNO).

Besides these structural considerations, the following generalisations have recently gained increasing attention:

5.2.5.1 From conv-FNO to U-FNO:

Possibly the most recent variant of the FNO, the U-FNO [159] introduces the famous U-Net to the architecture in the so-called U-Fourier layer. The U-FNO thus has both Fourier and U-net layers: it starts off with the former and ends with the latter. Essentially, a U-Fourier layer is similar to the Fourier layer, but has both a weight matrix and a two-step U-Net layer in the residual as illustrated in Figure 9. In contrast to the update performed by the Fourier layer in Equation 41, the U-Fourier layer performs the update in Equation 44, with U being the two-step U-Net.

$$v_{t+1}(x) := \sigma(Uv_t(x) + Wv_t(x) + (\mathcal{K}(a; \theta)v_t)(x)), \quad \forall x \in \Omega. \quad (44)$$

As compared with methods based on CNNs, the baseline FNO achieves a good accuracy for single-phase flow problems, but it doesn’t seem to do so well with multiphase flows [158]. On the other hand, conv-FNO does better than CNN-based methods, and the U-FNO even improves on that. conv-FNO is implemented by using a standard convolution in place of the U-Net.

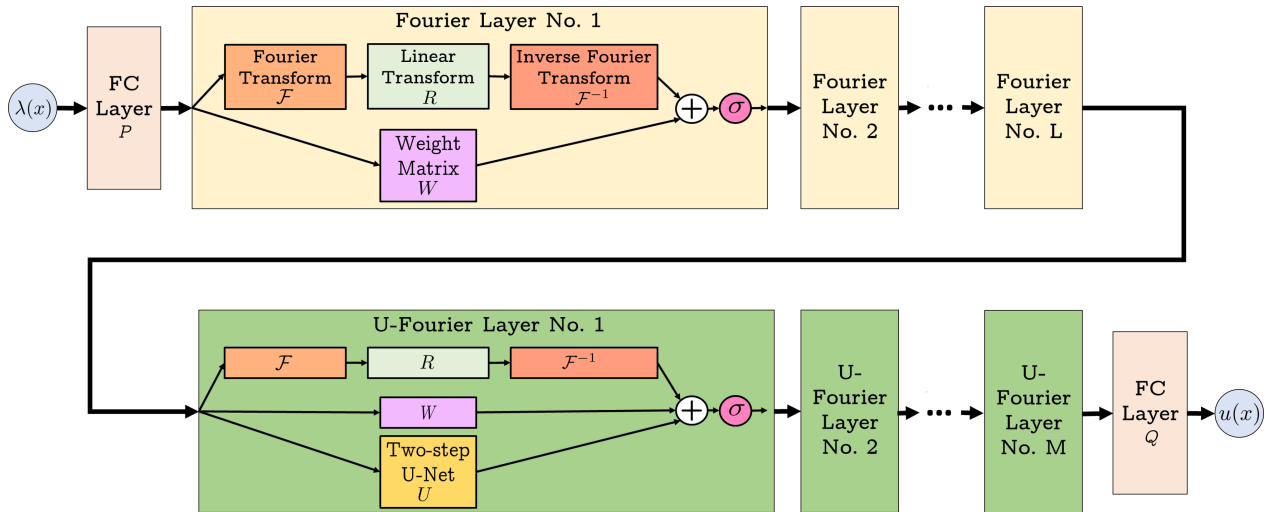


Figure 9: Architecture of the U-FNO.

5.2.5.2 Multiwavelet based operator (MWT):

In a more recent work [58], a neural operator which evaluates the kernel operator in (42) using a different approach is introduced. The idea here is to leverage the successes in signal processes of both orthogonal polynomials and wavelet basis (notably, vanishing moments and orthogonality). Multiwavelets, therefore, do not just project the function onto a single wavelet function as wavelets do, but rather, they project the function onto a subspace of degree-restricted polynomials.

For an understanding of the concept, the space of piece-wise polynomials of degree up to $k \in \mathbb{N}$ with $n \in \mathbb{Z} \cup \{0\}$ is defined on $[0, 1]$:

$$\mathbf{V}_n^k = \bigcup_{l=0}^{2^n-1} \{f \mid \deg(f) < k \text{ for } x \in (2^{-n}l, 2^{-n}(l+1)) \wedge 0, \text{ elsewhere}\}.$$

For each $k \in \mathbb{N}$ with $n \in \mathbb{Z} \cup \{0\}$, we have that $\dim(\mathbf{V}_n^k) = 2^n k$ and

$$\mathbf{V}_{n-1}^k \subset \mathbf{V}_n^k. \quad (45)$$

We note that, as n increases, so does l , and \mathbf{V}_n^k is defined from a lower(coarser) to a higher(finer) resolution; these resolutions being each time a power of 2. As a result, the method is restricted to discretisations which are a power of 2. Appropriate padding or interpolation could be applied to the function if its resolution is not a power of 2.

Given the basis $\phi_j, j = 0, 1, \dots, k-1$ w.r.t a measure μ_0 of \mathbf{V}_0^k , it is possible to obtain the basis of subsequent $\mathbf{V}_n^k, n > 0$ by appropriate shifts and scales of ϕ_j :

$$\phi_{jl}^n(x) = 2^{n/2} \phi_j(2^n x - l), \quad j = 0, 1, \dots, k-1, \quad l = 0, 1, \dots, 2^n - 1, \text{ w.r.t. } \mu_n \quad (46)$$

One then defines the multiwavelet subspace \mathbf{W}_n^k , which is related to the spaces of orthogonal polynomials as below:

$$\mathbf{V}_{n+1}^k = \mathbf{V}_n^k \oplus \mathbf{W}_n^k, \quad \mathbf{V}_n^k \perp \mathbf{W}_n^k. \quad (47)$$

Similarly, the basis of $\mathbf{W}_n^k, n > 0$ can be obtained by appropriate shifts and scales if the basis $\psi_j, j = 0, 1, \dots, k-1$ w.r.t a measure μ_0 of \mathbf{W}_0^k is known. A similar expression as in Equation 46 can thus be obtained.

Equations 45 and 47 inform us that the basis of \mathbf{V}_n^k and \mathbf{W}_n^k can be written as linear combinations of that of \mathbf{V}_{n+1}^k . As a result, for a given function it is possible to obtain a relationship between its coefficients in these bases. Specifically, the function $f \in \mathbb{R}^d$ has coefficients in the space of orthogonal polynomials (multiscale coefficients) $\mathbf{s}_l^n = [\langle f, \phi_{il}^n \rangle_{\mu_n}]_{i=0}^{k-1} \in \mathbb{R}^{k^d \times 2^n}$ and coefficients in the multiwavelet subspace (multiwavelet coefficients) $\mathbf{d}_l^n = [\langle f, \psi_{il}^n \rangle_{\mu_n}]_{i=0}^{k-1} \in \mathbb{R}^{k^d \times 2^n}$, which are related by the *decomposition* equations:

$$\mathbf{s}_l^n = H^{(0)} \mathbf{s}_{2l}^{n+1} + H^{(1)} \mathbf{s}_{2l+1}^{n+1}, \quad (48)$$

$$\mathbf{d}_l^n = G^{(0)} \mathbf{s}_{2l}^{n+1} + G^{(1)} \mathbf{s}_{2l+1}^{n+1}, \quad (49)$$

and *reconstruction* equations

$$\mathbf{s}_{2l}^{n+1} = \Sigma^{(0)} (H^{(0)T} \mathbf{s}_l^n + G^{(0)T} \mathbf{d}_l^n), \quad (50)$$

$$\mathbf{s}_{2l+1}^{n+1} = \Sigma^{(1)} (H^{(1)T} \mathbf{s}_l^n + G^{(1)T} \mathbf{d}_l^n). \quad (51)$$

$H^{(0)}, H^{(1)}, G^{(0)}, G^{(1)} \in \mathbb{R}^{k^d \times k^d}$ are the reconstruction filters while $\Sigma^{(0)}, \Sigma^{(1)}$ are the correction terms. The theory and derivation of these terms are well covered in [58], we only highlight it here for better explanation of the steps involved in the method. In Equations 48-49, $H^{(0)}$ and $G^{(0)}$ act on the even terms of the multiscale coefficient while $H^{(1)}$ and $G^{(1)}$ act on the odd terms. The result of these operations is visibly a down-sampling from the higher to a lower resolution (half the original resolution), thus the term decomposition. On the other hand, Equations 50-51 perform the reverse of this operation, leading to the recovery of the higher resolution.

So far, we walked through multiwavelet representation of a function $f \in \mathbb{R}^d$. This notion will be applied to the input and output functions of the neural network/operator. A different notion, known as the Non-Standard Form is used to obtain the multiwavelet representation of the kernel function. This method essentially reduces the operator kernel in Equation 42 $\mathcal{K}v = w$ to the set of equations.

$$\begin{aligned} U_{dl}^n &= A_n d_l^n + B_n s_l^n, \\ U_{sl}^n &= C_n d_l^n, \\ U_{sl}^L &= \bar{T} s_l^L, \end{aligned}$$

with U_{dl} and U_{sl} (respectively d_l^n and s_l^n) being the respective multiscale and multiwavelet coefficients of w (respectively v). L here is the index corresponding to the coefficients of the lowest resolution (output of the last decomposition). A_n, B_n, C_n and \bar{T} are then parameterised with a CNN (which could be done in Fourier space as in FNO or not) network followed by a ReLU activation then linear layer which we learn during training. In practice we use same neural networks for all n : thus $A_n = A_{\theta_A}, B_n := B_{\theta_B}, C_n := C_{\theta_C}$ and $\bar{T} := \bar{T}_{\theta_T}$. For a given input, the multiwavelet operator performs a series of operations as shown in Figure 10.

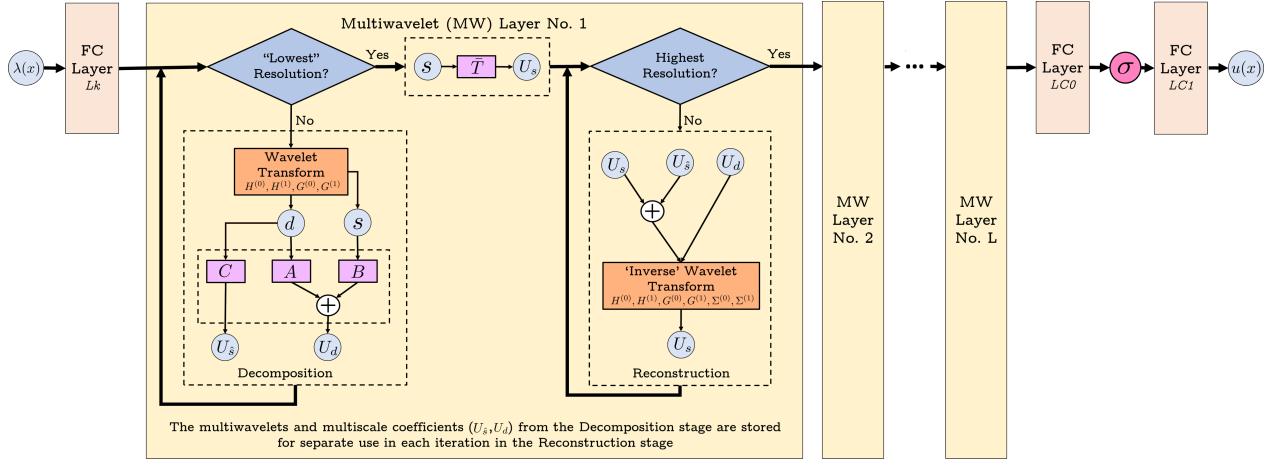


Figure 10: Architecture of the MWT Operator.

5.2.5.3 Physics Informed (Fourier) Neural Operator - PINO

This method combines the operator learning of FNOs and function learning PINNs, in a quest to alleviate the challenges faced in the individual cases [105]. While PINNs face a challenge in optimisation when dealing with complex problems as in multiscale dynamics, FNO needs a wealth of data which might not be readily available. PINO combines both concepts by introducing two stages in the learning process:

- Firstly, the operator is learned using either/both a **data loss** (same loss as in FNO) or/and a **PDE loss** (physics informed loss), in a phase termed Pre-training. This case reduces to the normal FNO method if no PDE loss is used. As an example, the PDE loss for Poisson's equation in 17 is given by Equation 52 where α is a hyperparameter.

$$L_{\text{PDE}} = \underbrace{\sum_{i=1}^{N_{\text{train}}} \|\Delta u_{i\Theta} - \lambda_{i\Theta}\|_{L^2(\Omega)}^2}_{\text{Domain } (\Omega) \text{ loss}} + \alpha \underbrace{\sum_{i=1}^{N_{\text{train}}} \|u_{i\Theta} - g_i\|_{L^2(\partial\Omega)}^2}_{\text{Boundary } (\partial\Omega) \text{ loss}}, \quad (52)$$

- Secondly, for a specific instance of the input (parameter, for forward problem), the learned operator from the first stage is further fine-tuned, using the **PDE loss** and an **operator loss**. The latter minimises the difference between the initial network, F_{Θ_0} resulting from the pre-training phase and the

further optimised networks $F_{\Theta_i}, i > 0$. This phase is the test-time optimisation stage. For a specific parameter instance λ , the operator Loss is thus given by

$$L_{OP} = \|F_{\Theta_i} - F_{\Theta_0}\|^2. \quad (53)$$

A strength of the PINO is in its ability to achieve competitive errors with fewer data as demonstrated in [105]. This is mainly due to the introduction of the PDE loss. Notably, this PDE loss is evaluated in a not-so-usual way as the input of the network is the function and not a set of collocation points. Automatic differentiation as we know it, is thus not possible. Three methods for gradient descent are outlined in [105]. One option is numerical differentiation, i.e. a finite difference method (FDM), which we use for our experiments in later sections.

5.2.6 FNO usage for inverse problems

FNO is an operator learning concept, hence both general concepts as outlined in Section 2.3 can be used for solving inverse problems. We will report on the achieved results in our section on numerical examples. FNO does remarkably well, despite its rather linear and Fourier-centric approach. However, it allows the incorporation of fine details related to high frequencies in a consistent way, nevertheless understanding the success of FNO methods for solving inverse problems should be an important direction for future research.

5.3 DeepONet

5.3.1 Motivation

It is widely known that deep neural networks are universal approximators, i.e., they can approximate any finite-dimensional function to arbitrary accuracy [28, 71]. This has been extended to a universal approximation theorem for operators [20], which states that a neural network with a single hidden layer can approximate accurately any nonlinear continuous operator. This theorem and its extension to multi-layer networks, see [113], provides the motivation for the concept of DeepONet.

5.3.2 Network architecture

The DeepONet [113] mirrors the structure of the universal approximation theorem of operators with a novel network architecture. Let us consider an operator \mathcal{F} that maps an input function λ to an output function u , i.e. $u = \mathcal{F}(\lambda)$. A DeepONet G_{Θ} takes an input function λ , which is sampled at fixed predefined collocation points, and provides an approximation for $u(x)$ at arbitrary points x by the combination of a trunk and branch net in the following way:

$$u(x) \approx G_{\Theta}(\lambda)(x) = \sum_{k=1}^p \underbrace{b_k(\lambda(s_1), \lambda(s_2), \dots, \lambda(s_m))}_{\text{branch}} \underbrace{t_k(x)}_{\text{trunk}} = \sum_{k=1}^p b_k(\lambda) t_k(x). \quad (54)$$

The trunk net $\mathbf{t} = \mathbf{T}(x; \theta_t)$ takes the continuous coordinates x as the input, and outputs a feature vector $\mathbf{t} = [t_1, \dots, t_p] \in \mathbb{R}^p$, which can be considered as p functions of x . The branch net $\mathbf{b} = \mathbf{B}(\lambda; \theta_b)$ takes $\lambda = [\lambda(s_1), \lambda(s_2), \dots, \lambda(s_m)]$, the discretisation of the input function, as input and returns a feature vector $\mathbf{b} = [b_1, \dots, b_p] \in \mathbb{R}^p$ as output. The branch and trunk nets are then combined by an inner product to approximate the underlying operator.

This DeepONet is named as "unstacked DeepONet", while it is called a "stacked DeepONet" if each $b_k(\lambda), k = 1, \dots, p$ is an individual neural network, i.e., $[b_1, \dots, b_m] = [\mathbf{B}(\lambda; \Theta_b^1), \dots, \mathbf{B}(\lambda; \Theta_b^m)]$. Several numerical results have shown that unstacked DeepONets typically have larger training errors as compared with stacked DeepONets, but the test error is smaller and unstacked DeepONets lead to smaller generalisation errors. Both branch net and trunk net can have general architectures, e.g., fully connected neural network (FCN), recurrent neural network (RNN), and convolutional neural network (CNN). However, as x is usually in low dimensional space, a standard FNN is commonly used as the trunk net. A bias can also be added to the last stage of the DeepONet to improve performance.

The novelty of the DeepONet is that its network architecture is composed of these two sub-networks, which treat the input λ and x differently, thus it is consistent with prior knowledge. In addition, there is

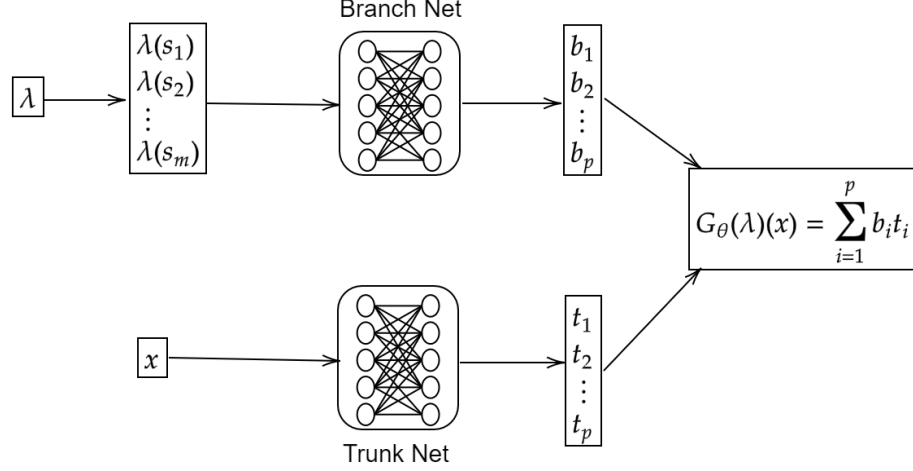


Figure 11: Architecture of the DeepONet

no need to discretize the domain to approximate the solution space, and the evaluated solution functions are defined in the whole domain. The only condition required is that the sensor locations $[s_1, s_2, \dots, s_m]$ should be consistent for the training dataset. There also are some generalisations which encode the input functions to the branch net by a feature vector, for example, we can use the coefficients of λ with respect to some chosen basis as input.

Once the DeepONet is trained, it is easy to see that the numerical solutions will lie in the linear space $\text{Span}\{t_1(x), \dots, t_p(x)\}$, i.e., $\{t_k(x)\}_{k=1}^p$ are actually the trained basis to approximate the solution space, and $\{b_k(\lambda)\}_{k=1}^p$ are the corresponding coefficients. Since usually, p is not large, e.g. around 100 for our 2 dimensional problems, the DeepONet can be regarded as a model reduction method in which the reduced basis is obtained by training.

5.3.3 The algorithm

Based on the architecture of the DeepONet, the parameters can be optimised by minimising the following mean square error loss:

$$L(\Theta) = \frac{1}{NM} \sum_{i=1}^N \sum_{j=1}^M |\mathcal{F}(\lambda_i)(x_{i,j}) - G_{\Theta}(\lambda_i)(x_{i,j})|^2 = \frac{1}{NM} \sum_{i=1}^N \sum_{j=1}^M |u_i(x_{i,j}) - \sum_{k=1}^p b_k(\lambda_i) t_k(x_{i,j})|^2. \quad (55)$$

There are two important hyper-parameters which should be determined before training: the positive integers m and p , i.e., the number of sensors for encoding the input functions and the number of the basis used to approximate solutions. Larger m and p means smaller encoding error and reconstruction error, respectively. However, increasing them usually does not necessarily reduce the total error due to the increased complexity of the optimisation problem. The locations of the sensors are not necessarily equispaced. However, they should be consistent with the training dataset.

Note that a pair of the training data in DeepONet is $\{\lambda_i, x_{i,j}, u_i(x_{i,j})\}$, thus it is slightly different from most neural operator methods, i.e. the full field observation of solutions is not necessary for the DeepONet and the DeepONet can work with only partially observed solutions. This is of particular importance for real applications where more often than not the available data is not complete. In addition, for different types of data sets, we can use different implementations for DeepONet to dramatically reduce the computational cost and memory usage by orders of magnitudes. For example, different branch input λ may share the same trunk net input x , and different input x may share the same input λ , see [116] for details. This computation technique can also be applied to the extension PI-DeepONet [156] when computing the derivatives of the output functions.

Algorithm 8: Fast implementation of DeepONet

Input: data: $\{(\lambda_i, x_j, u_i(x_j)) | i = 1, 2, \dots, N; j = 1, 2, \dots, M\}$
Number of sensors: m , and the locations of the sensors: $S = (s_1, \dots, s_m)$
Let $\lambda = [\lambda_1(S), \dots, \lambda_N(S)] \in \mathbb{R}^{N \times m}$; $X = [x_1, \dots, x_M] \in \mathbb{R}^M$, $U = [u_1, u_2, \dots, u_M] \in \mathbb{R}^{N \times M}$
 p : the number of basis to be learned.
 τ_b/τ_t : learning rates of the branch net and trunk net

```
1 Initialise the branch net  $B_{\Theta_b}$  and trunk net  $T_{\Theta_t}$ 
2 while not converged do
3    $B = B_{\Theta_b}(\lambda) \in \mathbb{R}^{N \times p}$  and  $T = T_{\Theta_t}(X) \in \mathbb{R}^{M \times p}$ 
4   Output  $= BT^T \in \mathbb{R}^{N \times M}$ 
5    $L(\Theta) = \frac{1}{MN} \|U - \text{Output}\|$ 
6   Update  $\Theta \leftarrow \Theta - \tau \nabla_{\Theta} L$ 
   /* The fast algorithm can be easily extended to the mini-batch case and the computation of the
   derivatives in PI-DeepONet. */
7 end
```

5.3.4 Generalisations of DeepONet

Several extensions of DeepONet have also been developed.

- In [116], a feature expansion for the trunk net input is proposed in order to satisfy some desirable properties of the output function, e.g., oscillating structures or decay properties. Feature expansion for the branch net can also be used to incorporate a feature which is a function of x . E.g. the POD-DeepONet as proposed in [116] precomputes a basis by performing proper orthogonal decomposition (POD) on the training data. Thus, POD-DeepONet shares the same idea with PCANN for the output space. Employing such feature vectors might be particularly advantageous for non-smooth parameters or solutions, i.e., discontinuous or highly oscillatory functions.
- The Bayesian B-DeepONet [108] uses the Bayesian framework of replica-exchange Langevin diffusion to enable DeepONets training with noisy data. The B-DeepONet and Prob-DeepONet as proposed in [125] were shown to have good predictive power along with uncertainty quantification. In [45], a further generalization 'Variational Bayes DeepONet' was introduced, in which the weights and biases of the neural network are treated as probability distributions instead of point estimates, and their prior distributions are updated by Bayesian inference.
- A universal approximation theorem of continuous multiple-input operators was proved and the corresponding MIONet was proposed to learn multiple-input operators in [82]. Similarly, The authors in [147] proposed a new enhanced DeepONet, in which multiple input functions are represented by multiple branch DNN sub-networks, which are then combined with an output trunk network via inner products to generate the output of the whole neural network.
- Several extensions for dealing with particular function properties were recently proposed. E.g., a multi-scale DeepONet [111] was proposed to approximate a nonlinear operator between Banach spaces of highly oscillatory continuous functions. The shift-DeepONets proposed in [61] extends Deep Operator Networks for discontinuous output functions by elevating the linear basis expansion of the classical DeepONet architecture to a non-linear combination. This can make the basis functions themselves dependent on the input function by exposing explicit shift and scale parameters. In the paper [146], the authors introduce the Deep Graph Operator Network, a combination of DeepONet and Graph neural networks, by using GNN-Branch Net to exploit spatially correlated graph information. The authors in [124] developed a framework named Fed-DeepONet to allow multiple clients to train DeepONets collaboratively under the coordination of a centralised server.
- The Variable-input Deep Operator Network (VIDON) [135], is peculiar in that it allows for sensor points to be queried from any point in the domain during training. In this way, no prior discretisation of the domain is needed.

5.3.5 Theoretical Background

In addition to the universal theorem, several analytic results have been published for DeepONet. In the original paper, a theoretical analysis was presented which allows estimation of the approximation properties for ODE operators with respect to an underlying probability distribution. The analysis depends on the number of sensors and the related approximation of the input functions.

In [96], the universal approximation property of DeepONets was extended to include measurable mappings in non-compact spaces. By decomposition of the error into encoding, approximation and reconstruction errors, both lower and upper bounds on the total error were derived, relating it to the spectral decay properties of the covariance operators associated with the underlying measures. For four prototypical examples of nonlinear operators, it was proved that DeepONets can break the curse of dimensionality.

In [30] the convergence rates of the DeepONet were considered for both linear and non-linear advection-diffusion equations with or without reaction. The conclusion is that the convergence rates depend on the architecture of the branch network as well as on the smoothness of the inputs and outputs of the operators. The paper [47] gives a bound on the Rademacher complexity for a large class of DeepONets.

6 Numerical experiments

The core of this paper is a numerical comparison of the described methods. The aim is to develop a guideline for scientists who want to start working with DL methods for PDE-based problems and face the problem of determining suitable methods.

We will perform numerical experiments on different levels. First of all, we will investigate the performance for solving the forward Poisson problem. This linear problem is most commonly used and -despite its limited value for generalisations to non-linear problems - already yields some insight into the performance of the chosen methods. We then perform tests for the inverse Poisson problem, where the source term is the sought-after parameter.

After that, we turn to analyse the behaviour of the chosen methods for forward and inverse Darcy flows. A particular emphasis is on evaluating and, comparing the respective numerical schemes in terms of accuracy but also computational time and storage needed for parametric studies.

After these basic numerical tests, we do report on how learned PDE solvers behave for two industrial projects.

We want to acknowledge that there already exists a growing list of publications devoted to testing DL concepts for the solution of PDEs, see e.g. [116, 49, 55]. However, these studies focus on PDE-based forward problems, in contrast, our experiments for comparing forward solvers is a preliminary step towards our main goal, namely a comparison of DL methods for PDE-based parameter identification problems.

We start this section with an outline of our data generation procedure, which follows [12, 103, 104]. In summary, this section is organised as follows

- Generating training and test data
- Poisson problem
 - Forward problem
 - Inverse problem trained with exact data
 - Inverse problem trained with noisy data
- Darcy flow
 - Forward problem
 - Inverse problem trained with exact data
 - Inverse problem trained with noisy data
- Industrial applications
 - A moving domain problem (Bosch)
 - Identification of material model parameters from stress tensor (Volkswagen)

6.1 Generating training and test data

The outline of our numerical experiments for the linear differential equations $\Delta u = \lambda$ on Ω , $u = g$ on $\partial\Omega$ (Poisson problem) as well as simulations for the Darcy flow follows the approach of [12]. Hence, we do a performance analysis in terms of accuracy as well as computational load and the parameter λ is randomly generated as a Gaussian random field. As a gold standard for comparison, we use a standard FDM code, which is tuned to high precision and also provides the ground truth data for training the networks.

Learning operators implies learning mappings between function spaces. For a supervised learning task, we need input-output data pairs for training, which in our case are the parameter and solution functions. We start with Gaussian Random Fields, commonly used in the stochastic modelling of physical phenomena as e.g. described in [12, 103, 104, 116]; more precisely we use as base measure the Gaussian distribution

$$\mu_G = \mathcal{N}(0, (-\Delta + 9I)^{-2}),$$

with a zero Neumann boundary condition on the operator Δ , which yields random but smooth test data for the Poisson problem. Other interesting measures are μ_L and μ_P which are the push-forwards of μ_G under the exponential and piece-wise constant maps respectively, so that $\mu_L = \exp_{\#} \mu_G$ and $\mu_P = T_{\#} \mu_G$, where $\exp_{\#}$ and $T_{\#}$ represent the respective push-forward functions, with

$$T(s) = \begin{cases} 12 & s \geq 0 \\ 3 & s < 0 \end{cases}$$

For our experiments with the Darcy flow, we used piece-wise constant parameters. We show some examples in Figure 12.

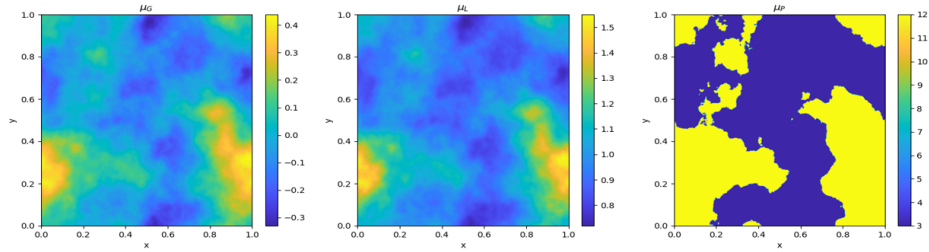


Figure 12: Example of samples from the GRF probability measures μ_G , μ_L and μ_P .

To complete the data pair, we use the generated samples as right-hand sides of the Poisson problem and use a finite difference method (FDM) to get the solution for the considered problem: As an example, we consider the Poisson problem given by

$$\begin{aligned} -\Delta u(s) &= \lambda(s) & s \in (0, 1)^2 \\ u(s) &= 0 & s \in \partial(0, 1)^2, \end{aligned} \tag{56}$$

where the forcing term $\lambda(s)$ is sampled from the GRF $\lambda \sim \mu_G$. Then, the domain $(0, 1)^2$ is discretised as shown in Figure 13, and a second-order FDM scheme is used to evaluate the Laplacian, reducing the Poisson equation to a system of linear equations given by Equation 57, where $i = 0, \dots, N_y$ and $j = 0, \dots, N_x$ for a resolution of $(N_x + 1) \times (N_y + 1)$

$$\frac{\Delta y}{\Delta x} (-u_{i,j-1} + 2u_{i,j} - u_{i,j+1}) + \frac{\Delta x}{\Delta y} (-u_{i-1,j} + 2u_{i,j} - u_{i+1,j}) = \Delta x \Delta y \lambda(x_j, y_i) \tag{57}$$

A similar discretisation scheme is used for the Darcy Flow equation 58 which is equally of interest to us in this work.

$$\begin{aligned} -\nabla \cdot (\lambda(s) \nabla u(s)) &= f(s) & s \in (0, 1)^2 \\ u(s) &= 0 & s \in \partial(0, 1)^2 \end{aligned} \tag{58}$$

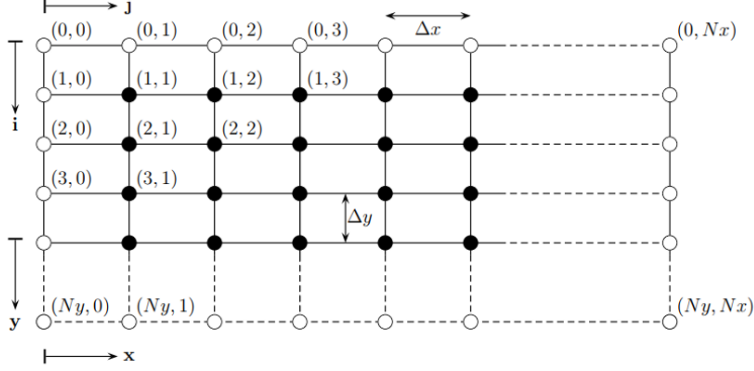


Figure 13: Computational grid showing interior grid points (black) and boundary grid points (white).

Our numerical tests are done using baseline implementations of the mentioned DL algorithms and we did some extensive hyperparameter search for every method. For details see the appendices. Nevertheless, hyperparameter search and fine-tuning the optimisation scheme in search of global minima is a never-ending story. Hence, the presented results should be understood as the best we could achieve within the given time and with the available computing capacity (specified in A.2). All methods were treated equally and we believe, that this leads to a fair basis for comparison.

In addition, we are well aware of the extensive body of literature dealing with sometimes rather refined extensions and improvements of these methods, e.g. there are several extensions of the PINN approach and a survey on different Physics-informed neural operator networks variants has been published recently, [49]. However, these extensions most often come with the necessity to fine-tune additional hyperparameters or they do apply only to special cases. Hence, as said before we focus on a comparison of the basic implementations in this section. To give proper credit to the different approaches, we assigned different co-authors to different concepts and everybody was doing his best to ‘defend’ the respective concepts.

So far we have addressed the general outline of our testing scenario and our data generation for the academic test examples. This is in line with procedures used by our collaborating industrial partners. Research and development departments in the industry also seem to rely mostly on simulated data for during the first development cycles for new products. In contrast to simulated data, real-life data for industrial applications typically is very scarce. Almost often this is only available in very limited numbers. This leads to the problem of data enrichment and data augmentation, which is outside the scope of the present paper. Hence, the two industrial examples included in this survey only use simulated data, which were obtained at least partially by the software of our collaboration partners.

Furthermore, let us clarify the criteria for our evaluation. There are several obvious categories such as achievable mean accuracy, training time, and time for solving the forward Poisson problem after training, but also degrees of freedom of the networks used, stability concerning hyperparameter tuning, etc. Nevertheless, in the following, we will mainly discuss two criteria, namely accuracy and the potential for parametric studies/inverse problems, i.e. the computational time needed to run the algorithm after training for novel sets of parameters.

6.2 Poisson problem

6.2.1 Forward problem

Testing different DL concepts for training a **forward solver** for the Poisson problem (56) is the most basic academic example which is used by almost all relevant publications in this context. This linear problem can be solved by all other methods considered and the errors are as reported in Table 2. These errors do not differ too much, they are below 1% relative error except for DRM, which has an error of approximately 2,5%. Still, there are some notable differences. The overall winner is PCALin both in terms of achievable accuracy as well as in terms of complexity of the network. However, none of the methods was able to achieve an accuracy comparable with fine-tuned FDM or FEM methods. The advantage of DL concepts, in this case, lies in the

potential for large-scale parametric studies, where the execution time for testing novel parameters has to be minimal.

However, not all DL concepts are suitable for parametric studies. In general DL concepts aiming for a function approximation do require expensive retraining of the network for every additional parameter and do have limited value for large-scale parameter variations. Hence, we focus on DL concepts for operator approximations, see Table 1. In our experiments, DeepONet and their physics-informed versions performed best in terms of efficiency (run time for testing). The differences in testing time for these methods are below the variance introduced by the random sampling of test data.

The comparison with respect to different resolutions of u does show the expected, but interesting result, that operator approximations, which are based on a functional analytic reasoning in function spaces rather than discrete settings, indeed show an independent accuracy across scales, see Table 3. This cannot be matched by function approximations where the error increases by several orders of magnitude for coarse discretisations.

These numerical findings for the linear Poisson problem in a standard domain do have little value for generalisations to other PDE problems. Nevertheless, as a punch line for simple linear PDE problems, we would stress the old saying ‘keep it simple’ and suggest applying ‘easy to use’ concepts such as PCALin with a suitable but comparatively small network.

PINNs do also offer an easily accessible concept, which is easy to adapt to other PDE, but it requires retraining, i.e. PINN in their original version are not suitable for parametric studies, and they did exhibit a slightly larger L_2 -error in our scenario.

As an alternative, MWT requires a more advanced implementation but seems to be more efficient for parametric studies, however, training times are rather high.

6.2.2 Inverse problem

The investigation of the performance of DL concepts for PDE-based inverse problems for parameter identification is the core of this survey. In this subsection, we summarise the results for the inverse Poisson problem, i.e. determining λ in Equation 17 from a measured version of u . Iterative methods for solving such inverse problems as well as parametric studies require multiple evaluations of the parameter-to-state map F . As already mentioned, DL concepts based on operator approximations are better suited in this context and we will focus on these methods. The only exception is the extension to inverse problems of PINNs and QRES as described in Section 4.2.4

Our tests for PDE-based inverse problems are organised in terms of how we attack the inverse problem and which data is used for training. First of all, there are two primary approaches for dealing with inverse problems, see Section 2.3, i.e. we can either train the inverse problem with a reversed input-output structure or we can integrate a learned forward solver in a Tikhonov approach. Secondly, we can train the network with either noiseless data or noisy data with different noise levels. Both tests are meant for applications depending on whether some clean data obtained in research labs or measured data from field experiments are available. As it is common for inverse problems, after training these networks will be evaluated for reconstruction problems with noisy data. The case of testing with noise-free data is included for reason of completeness.

Training is always done with 1000 training samples, where λ is computed as a smoothed random Gaussian field, see Section 6.1. The parameter-to-state map, $u = F(\lambda)$, is then computed with a high-precision finite difference scheme. The resulting solution u is then perturbed with normally distributed random noise of different levels, δ .

$$u^\delta(x) = u(x) + \delta \cdot \|u\| \cdot N(0, 1)$$

For the evaluation of the methods we use additional $N = 5000$ samples of u^δ , which are computed by the same procedure, i.e. drawing additional random samples for λ_{true} , computing the corresponding solution u and adding noise.

These perturbed solutions are the input for the inverse problem during evaluation. The resulting estimation of the parameter $\hat{\lambda}$ is then compared with the original, true parameter λ_{true} . As a standard measure of success we average over the different evaluation samples and take the mean L_2 -error, $E\left(\|\hat{\lambda} - \lambda_{true}\|\right)$.

For certain applications, i.e. control problems the output error is also of importance and for some experiments we also report the difference between the solution obtained with $\hat{\lambda}$ and the true, unperturbed solution u as shown in Tables 8b and 8c.

Let us comment on the different test scenarios (inverse learning or Tikhonov, noise-free or noisy data for training) in more detail.

The tests with unperturbed data, i.e. the case where the networks were trained and evaluated with perfect noise-free data are reported in Table 2 and Table 3 for different resolutions. For operator approximation methods the inverse problem in these tables is always solved by inverse learning (backward operator training). Also, PINN and QRES can be extended to parameter learning directly by a doubling of the network, see Section 4.2.4. This results in a doubling of the network parameters as shown in the second column of both tables. As a general observation, we remark that the achievable accuracy for the inverse problem is considerably below the accuracy of the forward problem, which reflects the ill-posedness of the inverse problem. Also, the baseline implementations of PCANN, PINN and DeepONet do perform less reliably as compared with their extensions such as PCALin, U-FNO, PINO or MWT. After training run times of the different methods are the same as for the forward problem.

Due to the linear nature of the problem and the missing noise in the data, one should not overestimate the value of these tests. In particular testing with noisy data is essential for inverse problems.

To this end, we have done experiments where the networks were trained with noiseless data but the evaluation was done with noisy data, see Table 6. We clearly see the networks trained with noise-free data do not generalise to the case of noisy data. The error exceeds 100% in most cases. The only notable exception is surprisingly DeepONet and PI-DeepONet. Even for high noise levels, this method still produces errors in the reconstructed parameter which are approx. 4 – times larger than the noise in the data, which is the range of errors one would expect for optimal regularisation schemes for ill-posed problems.

Tables 7 and 8 are the most meaningful ones for inverse problems. Here we report results on networks, which are trained and evaluated with noisy data. Table 7 reports results obtained by reversed/backward operator training, i.e. the network is trained to take u^δ as input and to return directly an estimate for the parameter λ . Table 8 reports results obtained by first training a forward network $\Phi_\Theta(\lambda)$ and then computing an approximation to the parameter by solving a Tikhonov minimisation problem

$$\min_{\lambda} \|\Phi_\Theta(\lambda) - u^\delta\|^2 + \alpha R(\lambda) .$$

In these experiments, R was always taken as a discretisation of the L_2 -norm and α was optimised by numerical experiments. Depending on the problem, one could add an additional regularisation term as shown in Equations 68 and 69.

Both approaches, i.e. inverse learning and embedding a learned forward operator into a Tikhonov scheme do give comparable results, see Tables 7 and 8. All errors in the reconstructions are naturally larger than the error in the input data, as is to be expected for ill-posed problems. Given the small differences achieved by the different methods, it is challenging to suggest a particular method. However, in our opinion, the range of errors 1% or 5% might be most important for applications and a closer look at the numbers reported in Table 7 for inverse training of the inverse Poisson problem shows that FNO and PINO seem to perform best, with PCALin and MWT as runner-ups. For Tikhonov-based training and giving higher importance to larger error rates of 1% or 5%, the best results are achieved by MWT with PINO as runner-up. Hence comparing the winners of either approach (FNO/PINO and MWT) for this range of errors yields a slight advantage for using the Tikhonov approach in connection with the MWT concept. However, we should remark that the Tikhonov approach requires solving a minimisation problem for each new data set and is computationally more expensive.

Finally, Tables 8b and 8c are based on experiments, where the reconstructed parameter $\hat{\lambda}$ was used to compute the corresponding solution $\hat{u} = F(\hat{\lambda})$. This is then compared with either the true solution u , see Table 8c), or the noisy data, which was used for training, see Table 8b). This is considered as a test for how well these parameter estimation problems can be used to solve control problems, which however is not the focus of this paper and this case is not investigated further.

Networks	# of Parameters	Forward Problem			Inverse Problem		
		Rel. L2 Error	Training (s/epoch)	Testing (s)	Rel. L2 Error	Training (s/epoch)	Testing (s)
DRM	6,721	0.0251	0.0514	~ 480	-	-	-
PINN	5,301 10,602	0.0075	0.1034	$\sim 1,315$	0.1650	0.2368	$\sim 3,370$
QRES	5,509 11,018	0.0076	0.1581	$\sim 2,150$	0.1549	0.4186	$\sim 5,730$
PCANN	5,155,150 5,205,200	0.0073	0.0142	0.6063	0.0981	0.0161	0.6179
PCALin	62,750	0.0013	0.0077	0.7453	0.0244	0.0090	0.7640
FNO	2,368,001	0.0066	42.6249	0.0168	0.0415	42.6245	0.0174
U-FNO	3,990,401	0.0053	97.6730	0.0346	0.0254	97.6434	0.0343
MWT	9,807,873	0.0036	114.2043	0.0488	0.0159	113.2655	0.0483
DeepONet	640,256 768,128	0.0042	0.1098	0.0002	0.1035	0.1201	0.0002
PINO	2,368,001	0.0031	42.6289	0.0166	0.0301	42.8172	0.0143
PI-DeepONet	640,256 739,712	0.0061	0.4637	0.0002	0.1068	0.4462	0.0002

Table 2: Performance of different methods for the Poisson Problem, using a 513×513 resolution. In the second column, for the forward and inverse problems, if the same amount of parameters is used, only one number is specified. If different amounts are used, two numbers are given. Where the left one corresponds to the forward problem and the right one to the inverse case. The networks were trained with noiseless data and backward operator training was used for solving the inverse problem.

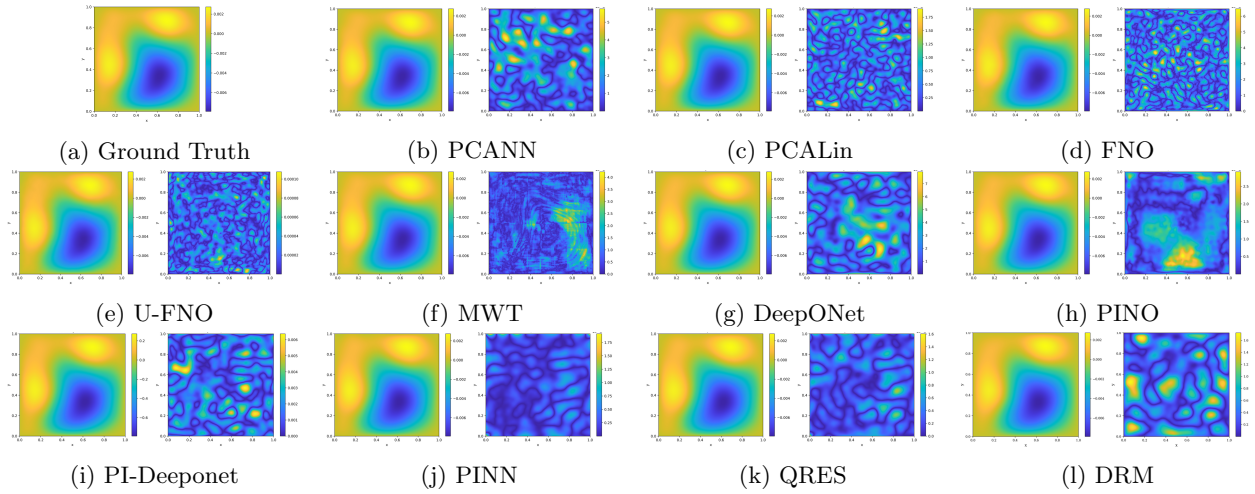


Figure 14: Test examples for Poisson forward problem using resolution of 513×513 . (b)-(l), shows the specified neural network’s approximation of the solution (left-hand side) and the absolute difference between the Ground truth in (a) with the approximation (right-hand side).

6.2.3 Summary Poisson problem

In summary, for the forward problem, the investigated DL concepts are less accurate as compared with finite difference methods on a fine grid. However, these DL concepts do produce competitive results for solving inverse problems with different noise levels. DL concepts for operator approximation perform best and offer a significant advantage in run time. Hence, either large-scale parametric studies or iterative solvers for parameter identification decisively benefit from well-trained DL concepts.

For the somewhat simple Poisson problem with vanishing boundary data, where both the forward as well as the inverse operator are linear, there is not much difference between the DL concepts. Overall, we propose to use PCALin, PCANN or PINN for first testing due to their ‘easy-to-use’ structure. They produce acceptable results for a wide range of hyper-parameters and are comparatively easy to train. For more accurate results, we propose to use MWT, which however is somewhat more involved, for implementation details see the respective appendices.

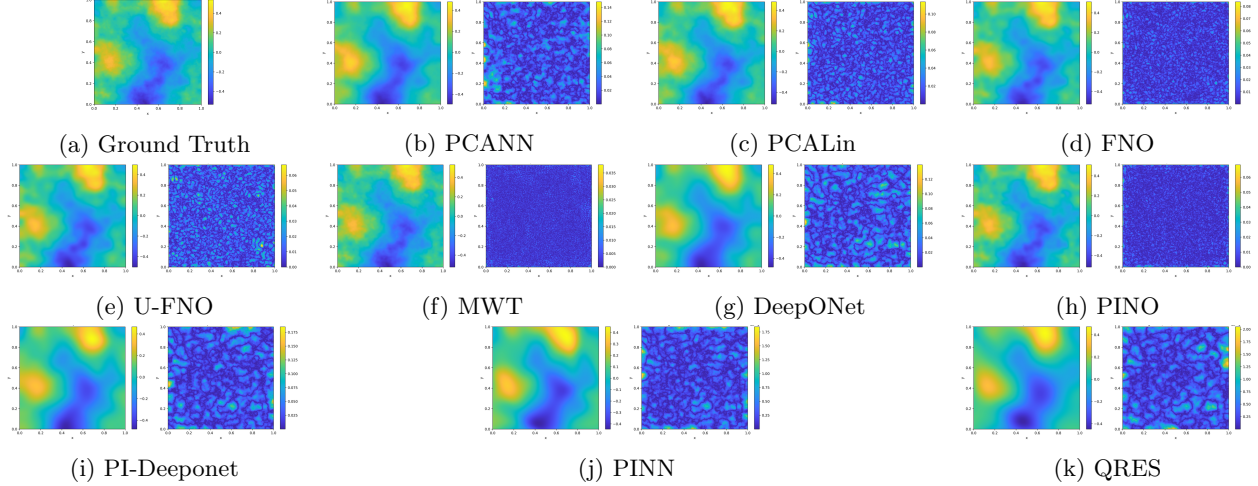


Figure 15: Test examples with backward operator training for inverse Poisson problem using a resolution of 513×513 . (b)-(k), shows the specified neural network's approximation of the solution (left-hand side) and the absolute difference between the Ground truth in (a) with the approximation (right-hand side). All examples are computed with noise free data. For reconstructions with noisy data see Figure 10.

Grid size, s	<i>Forward Problem Rel. Errors</i>				<i>Inverse Problem Rel Errors</i>			
	65	129	257	513	65	129	257	513
DRM	0.0397	0.0289	0.0244	0.0251	-	-	-	-
PINN	0.0245	0.0088	0.0084	0.0075	0.1715	0.1694	0.1653	0.1650
QRES	0.0288	0.0082	0.0088	0.0076	0.1598	0.1565	0.1542	0.1549
PCANN	0.0078	0.0075	0.0073	0.0073	0.0989	0.0979	0.0981	0.0981
PCALin	0.0016	0.0013	0.0013	0.0013	0.0303	0.0271	0.0253	0.0244
FNO	0.0066	0.0061	0.0067	0.0066	0.0299	0.0341	0.0366	0.0416
U-FNO	0.0063	0.0056	0.0062	0.0054	0.0292	0.0277	0.0288	0.0254
MWT	0.0047	0.0047	0.0048	0.0036	0.0357	0.0202	0.0198	0.0159
DeepONet	0.0047	0.0041	0.0041	0.0042	0.0983	0.0992	0.1041	0.1044
PINO	0.0031	0.0030	0.0034	0.0031	0.0263	0.0273	0.0319	0.0301
PI-DeepONet	0.0081	0.0057	0.0060	0.0061	0.1074	0.1068	0.1067	0.1068

Table 3: Error variation with the resolution for the Poisson problem. The networks were trained with noiseless data and backward operator training was used for solving the inverse problem.

6.3 Darcy flow

6.3.1 Forward problem

We now consider the steady-state of the 2-d Darcy Flow equation on the unit square which is the second order, linear, elliptic PDE

$$\begin{aligned} -\nabla \cdot (\lambda(s) \nabla u(s)) &= f(s) \quad s \in (0, 1)^2 \\ u(s) &= 0 \quad s \in \partial(0, 1)^2 \end{aligned} \quad (59)$$

with a Dirichlet boundary. In this equation $a \in L^\infty((0, 1)^2; \mathbb{R}_+)$ is the diffusion coefficient, $f = 1 \in L^2((0, 1)^2; \mathbb{R}_+)$ is the forcing function and $u \in H_0^1((0, 1)^2; \mathbb{R})$ is the unique solution of the

We start with a discussion of the forward problem, i.e. computing the solution u in Equation 58, for a given piece-wise constant diffusion coefficient λ . In all experiments, $\lambda(x) \in \{3, 12\}$, i.e. the domain of definition is segmented randomly into two regions with known values.

Surprisingly, the errors for PINN and QRES are relatively high, even if the network is trained and

evaluated with noise-free data, see Table 4. All other methods solve this non-linear forward problem reliably. MWT is the overall winner for solving the forward problem with noise-free data. This also holds for most levels of resolution.

Again, the comparison with respect to different resolutions of u does show the expected result that operator approximations based on functional analytic reasoning in function spaces indeed show an independent accuracy across scales, see Table 5.

6.3.2 Inverse problem

The investigation of the performance of DL concepts for inverse Darcy flows again either uses inverse training or embedding of a forward solver into a Tikhonov functional. The testing scenarios are similar to those of the Poisson problem, i.e. 1000 random samples were used for training and 5000 samples for evaluation.

In view of different applications we have either used no further assumption on λ , see Figure 17, or we have assumed that we know, that λ is a segmentation of the domain of definition into two components with a known value, see Table 11. This e.g. models the problem of mixing two liquids with known densities.

For a closer investigation, we start with a basic experiment for solving the Darcy inverse problems by inverse training with noise-free data. Results using a 513×513 resolution and without knowing the values of α a priori are shown in Figure 17. We notice the strength of the FNO, U-FNO, MWT, and PINO to identify the position of the discontinuities with backward operator training. PINO, however, computes a mismatch in the values of the densities. The network architecture seems to play a crucial role in these results. For e.g. DeepONet always provides a reconstruction, which is obtained by a linear combination of smooth functions (trunk nets), and in solution learning methods $u_\Theta(x)$ is naturally continuous, hence discontinuities are not in the range of these methods. Other methods based on discretisation, i.e. reconstructing the densities in the last layer of the networks at prescribed positions allow for sharper transitions of the densities.

As before, we have done experiments where the networks were trained with noiseless or noisy data. The results of inverse training with perfect data for training and evaluation are stated in Tables 4 and 5, they mimic the results of the forward training and do not yield additional insights. As for the Poisson problem, training with noise-free data does not generalise to noisy data, see Table 6, even only 1% error in the evaluation data yields reconstruction errors of 30% and larger. We should remark on the sub-optimal results obtained by DeepONet, which shows errors of about 25% for all noise levels tested. Here the error margins are considerably larger but almost constant over different noise levels. This might indicate, that the dominant error is not stemming from inversion and noise, but rather from a structural disadvantage of the network architecture or sub-optimal training. We have tested several larger DeepONet network architectures, which however did not cure the problem. A major reason for the large error of DeepONet for this inverse problem is that DeepONet has to learn the basis of the output space via the trunk net. Thus, the trunk net must have sufficient expressiveness to approximate the basis of the output space. In addition, even if the size of the trunk net is large enough, finding the optimal parameters of the trunk net is another challenge. Thus, if the number of reduced basis of the output space is large or the output functions are very complicated (e.g. highly oscillatory or discontinuous), it would be very difficult for the trunk net to learn the basis accurately. For both Poisson and Darcy problems, the parameter spaces are more complicated than the solution spaces, which explains the large error of DeepONet for inverse training.

Tables 7 and 9 state the results most important for inverse problems. They show some remarkable differences between the considered concepts. Most methods (PINN, QRES, PCANN, PCALin, DeepONet, PI-DeepONet) do show approximately the same errors for all noise levels. This indicates that a structural approximation error dominates the influence of the data noise. We have tested different hyperparameter settings for all of these methods, which, however, did not change the result. As a consequence, these methods do not yield competitive results for small levels of data noise. Nevertheless, PCANN exhibits about 10% error in the reconstructions even for 5% data error, which is remarkably good. In our test scenarios, there are clear winners: U-FNO and MWT for small noise levels and PCANN for larger noise levels. While the DeepONet, its physics-informed variant PI-DeepONet as well as PINO do not seem to be suitable for Darcy inverse problems. As mentioned earlier, PINO is capable of detecting the discontinuities but it fails to provide accurate density estimates.

When comparing the best methods for inverse training (MWT for small noise levels, PCANN for larger noise levels, see Table 7) with the best method for Tikhonov minimisation, see Table 9, we see an advantage

for inverse training, which generally yields better results. That errors are consistently larger for Tikhonov learning might be partially explainable by the difficulty of choosing a suitable regularisation parameter α . We have also included the accuracy metric which measures the segmentation error rather than the functional L_2 error. Here results again are similar for all methods, see Table 9a.

We finally estimated the output error by feeding the reconstructed $\hat{\lambda}$ into the respective neural networks and comparing the resulting \hat{u} with the exact data u and its noisy version u^δ , see Figures 9c and 9.

6.3.3 Summary Darcy flow

In summary, the investigated DL concepts do produce competitive results for solving inverse problems with different noise levels. DL concepts for operator approximation perform best and offer a significant advantage in run time. Hence, either large-scale parametric studies or iterative solvers for parameter identification decisively benefit from well-trained DL concepts. This training has to be done with the same noise level, training with noise-free data does not generalise to noisy data. As a general procedure, we would recommend favouring backward operator training over Tikhonov minimisation.

For choosing appropriate methods, we propose to use inverse training in combination with U-FNO and MWT for small noise levels and, the concept PCANN was best for solving the non-linear inverse Darcy flow problem with higher noise levels.

As extensive as our numerical tests have been, they only provide a snapshot of the diverse landscape of PDE problems and testing scenarios. In particular, it might be interesting e.g. to test Darcy inverse problems with continuous parameters and inverse Poisson problems with piece-wise constant functions. However, for the sake of an overview and the already somewhat lengthy list of tables presented, we decided to restrict ourselves to the tests presented in the paper.

Networks	# of Parameters	Forward Problem			Inverse Problem		
		Rel. L2 Error	Training (s/epoch)	Testing (s)	Rel. L2 Error	Training (s/epoch)	Testing (s)
DRM	22,201	0.0369	0.0859	$\sim 1,050$	-	-	-
PINN	6,291 7,972	0.1995	0.1164	$\sim 2,010$	0.1988	0.2528	$\sim 4,790$
QRES	6,562 8,895	0.2017	0.2108	$\sim 3,320$	0.1975	0.4221	$\sim 6,420$
PCANN	5,155,150 5,035,030	0.0253	0.0136	0.6108	0.0988	0.0487	0.1548
PCALin	10,100	0.0656	0.0075	0.3290	0.2203	0.0139	0.3108
FNO	2,368,001	0.0109	41.6857	0.0165	0.1490	42.0596	0.0163
U-FNO	3,990,401	0.0095	97.9580	0.0344	0.0085	98.8170	0.0345
MWT	9,807,873	0.0058	112.4575	0.0637	0.0156	112.8750	0.0403
DeepONet	568,320 1,047,644	0.0295	0.0606	0.0011	0.2220	0.0659	0.0011
PINO	2,368,001	0.0084	42.8685	0.0168	0.2345	42.7417	0.0142
PI-DeepONet	568,320 684,288	0.0384	0.2513	0.0011	0.2720	0.4905	0.0011

Table 4: Performance of different methods for the Darcy flow problem with piece-wise constant coefficients and using a 513×513 resolution. A similar convention is used for the second column as in Table 4.

6.4 Industrial Application Problems

6.4.1 A moving domain problem

Digital twins are ranked among the most influential technological developments of our decade, e.g. the Gartner report ranks digital twins or AI engineering amongst the Top 10 strategic development trends in all reports since 2018, [130, 131]. These digital twins combine data-driven concepts with domain-specific expert knowledge, most often in the form of DL solvers for PDE models.

One particular characteristic, which sets industrial applications apart from typical academic examples, is the domain of definition. In an industrial setting, these geometries tend to be complex, e.g. given by the shape of a production device or restricted measurement geometries.

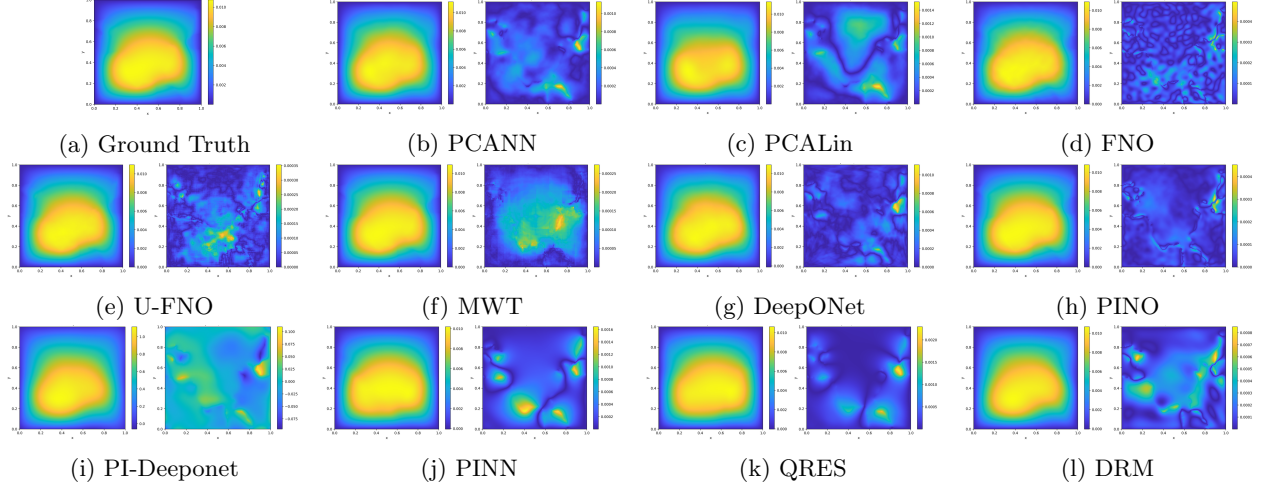


Figure 16: Test examples for forward Darcy problem using a resolution of 513×513 . (b)-(l), shows the specified neural network's approximation of the solution (left-hand side) and the absolute difference between the Ground truth in (a) with the approximation (right-hand side).

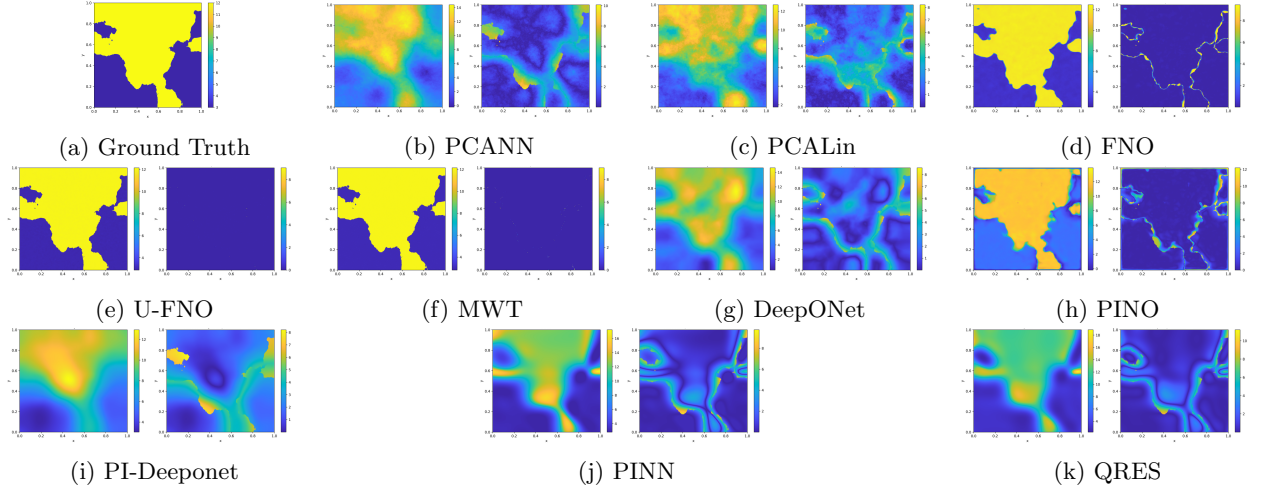


Figure 17: Test examples with backward operator training for inverse Darcy Flow problem using a resolution of 513×513 . (b)-(k), shows the specified neural network's approximation of the solution (left-hand side) and the absolute difference between the Ground truth in (a) with the approximation (right-hand side). All examples are computed with noise free data. For reconstructions with noisy data see Figure 11.

Particularly challenging are applications, where differential equations have to be solved on moving domains, e.g. the heat development inside a rotating electrical engine. The implementation of classical mesh-based methods is rather involved, e.g. computing the system matrix typically requires non-standard concepts, and they are expensive to solve. To tackle these problems, and other differential equations, with deep learning approaches, we developed, in collaboration with Bosch, the software package TORCHPHYSICS, cf. [149]. One characteristic feature of TorchPhysics is an easy-to-use generator for complex domains and geometries: Based on subtraction, addition and cross-product operations more and more complex geometries can be created from basic constituents. Another characteristic is the unbiased choice amongst several DL coders for solving forward or inverse problems.

In this Section, we give a small insight into a problem we are currently investigating in collaboration with Bosch.

As an example of a moving domain, we consider the two-dimensional geometry is shown in Fig. 18, which

Grid size, s	Forward Problem Rel. Errors				Inverse Problem Rel. Errors			
	65	129	257	513	65	129	257	513
DRM	0.0501	0.0375	0.0358	0.0369	-	-	-	-
PINN	0.2254	0.2043	0.2071	0.1995	0.2413	0.2014	0.2032	0.1988
QRES	0.2596	0.2077	0.1993	0.2017	0.2371	0.2117	0.2036	0.1975
PCANN	0.0256	0.0254	0.0253	0.0253	0.0983	0.0985	0.0987	0.0988
PCALin	0.0656	0.0656	0.0656	0.0656	0.2191	0.2198	0.2201	0.2203
FNO	0.0113	0.0106	0.0107	0.0109	0.1661	0.1536	0.1501	0.1490
U-FNO	0.0078	0.0071	0.0074	0.0095	0.0928	0.0640	0.0322	0.0085
MWT	0.0080	0.0060	0.0059	0.0058	0.1047	0.0800	0.0461	0.0156
DeepONet	0.0290	0.0292	0.0289	0.0295	0.2219	0.2261	0.2221	0.2220
PINO	0.0078	0.0066	0.0071	0.0084	0.1703	0.1997	0.2216	0.2345
PI-DeepONet	0.0390	0.0382	0.0381	0.0384	0.2706	0.2711	0.2682	0.2720

Table 5: Error variation with resolution for the Darcy Flow problem with piece-wise constant coefficients. The networks were trained with noiseless data and backward operator training was used for solving the inverse problem.

Noise level	Poisson					Darcy Flow PWC				
	0%	0.1%	1%	5%	10%	0%	0.1%	1%	5%	10%
PCANN	0.0988	0.0993	0.1171	0.3525	0.5645	0.0983	0.0983	0.0984	0.0998	0.1039
PCALin	0.0303	0.0379	0.0737	0.3134	0.6228	0.2191	0.2191	0.2192	0.2231	0.2348
FNO	0.0299	0.2966	2.6444	10.5499	19.9952	0.1341	0.1743	0.5100	3.3888	7.5197
U-FNO	0.0292	0.2102	1.1645	4.3941	8.3548	0.0896	0.1202	0.5896	1.4194	2.2052
MWT	0.0316	0.2201	1.2716	4.1969	7.6609	0.0865	0.1123	0.3668	0.6949	0.8620
DeepONet	0.0983	0.0985	0.1048	0.2059	0.3748	0.2219	0.2223	0.2224	0.2262	0.2375
PINO	0.0263	0.3457	3.3960	16.8352	33.8227	0.1703	0.1789	1.0438	6.1264	12.3570
PI-DeepONet	0.1074	0.1075	0.1120	0.1917	0.3352	0.2706	0.2706	0.2706	0.2714	0.2737

Table 6: Effects of noise on the solution for the inverse problems on a 65×65 resolution. The network is trained with noise-free data, but evaluated with noisy data. Backward operator training is used for solving the inverse problem.

Noise level	Poisson					Darcy Flow PWC				
	0%	0.1%	1%	5%	10%	0%	0.1%	1%	5%	10%
PINN	0.1715	0.1727	0.1734	0.2110	0.2378	0.2413	0.2407	0.2496	0.2564	0.2893
QRES	0.1598	0.1658	0.1714	0.2007	0.2256	0.2371	0.2421	0.2617	0.2789	0.2951
PCANN	0.0988	0.0991	0.1293	0.1876	0.2273	0.0983	0.0987	0.0990	0.1012	0.1093
PCALin	0.0303	0.0318	0.0840	0.1478	0.1846	0.2191	0.2191	0.2191	0.2217	0.2315
FNO	0.0299	0.0554	0.0957	0.1389	0.1678	0.1341	0.1344	0.1449	0.1770	0.2019
U-FNO	0.0292	0.0594	0.1036	0.1633	0.1839	0.0896	0.0902	0.1219	0.1649	0.1932
MWT	0.0316	0.0533	0.0966	0.1525	0.1867	0.0865	0.0893	0.1115	0.1634	0.1956
DeepONet	0.0983	0.1042	0.1084	0.1537	0.1870	0.2219	0.2283	0.2273	0.2379	0.2522
PINO	0.0263	0.0570	0.0957	0.1389	0.1678	0.1703	0.1737	0.2083	0.5147	0.9699
PI-DeepONet	0.1074	0.1086	0.1137	0.1516	0.1834	0.2706	0.2680	0.2703	0.2735	0.2742

Table 7: Effects of noise on backward operator inverse problems on a 65×65 resolution. The network is trained with noisy data and datasets with the same noise level are used for testing.

can be seen as a simplified sub-problem inside an electrical engine. The inside of the domain $\Omega(t, \omega) \subset \mathbb{R}^2$ is filled with fluid. We assume that the density of the incompressible fluid is $\rho = 1$ for simplicity. In the following, all physical values are in SI dimensions and they are not used. The blue outlined bar is rotating in time, inducing a circular motion onto the fluid. At the same time, the bar will heat up, and we also have to

	0%	0.1%	1%	5%	10%
PCANN	0.2128	0.2128	0.2137	0.2975	0.4468
PCALin	0.0803	0.0805	0.0918	0.1534	0.2132
FNO	0.0931	0.0936	0.1082	0.1450	0.1693
U-FNO	0.0687	0.0697	0.0909	0.1397	0.1802
MWT	0.0708	0.0714	0.0878	0.1368	0.1796
DeepONet	0.1341	0.1330	0.1350	0.1660	0.2088
PINO	0.0598	0.0623	0.0890	0.1441	0.1915
PI-DeepONet	0.1573	0.1580	0.1727	0.2040	0.2298

(a) λ_{err} , the relative error of the learned parameter

	0%	0.1%	1%	5%	10%
PCANN	0.0133	0.0128	0.0130	0.0123	0.0122
PCALin	0.0010	0.0010	0.0016	0.0074	0.0158
FNO	0.0022	0.0025	0.0097	0.0464	0.0924
U-FNO	0.0009	0.0013	0.0091	0.0457	0.0914
MWT	0.0014	0.0017	0.0093	0.0459	0.0917
DeepONet	0.0053	0.0054	0.0113	0.0497	0.0988
PINO	0.0006	0.0010	0.0088	0.0454	0.0911
PI-DeepONet	0.0045	0.0047	0.0135	0.0520	0.1013

(b) \tilde{u}_{err} , the relative error between the solution of the learned parameter and the noisy solution.

	0%	0.1%	1%	5%	10%
PCANN	0.0133	0.0128	0.0131	0.0150	0.0209
PCALin	0.0010	0.0010	0.0020	0.0074	0.0133
FNO	0.0022	0.0023	0.0040	0.0089	0.0133
U-FNO	0.0009	0.0010	0.0024	0.0072	0.0124
MWT	0.0014	0.0015	0.0025	0.0072	0.0124
DeepONet	0.0053	0.0053	0.0055	0.0085	0.0137
PINO	0.0006	0.0008	0.0023	0.0072	0.0126
PI-DeepONet	0.0045	0.0046	0.0058	0.0147	0.0152

(c) u_{err} , the relative error between the solution of the learned parameter and the noiseless solution.

Table 8: Effects of noise on Tikhonov-based inverse problems for the Poisson problem and using datasets with a resolution of 65×65 . The errors shown here are averaged over 100 test samples.

	0%	0.1%	1%	5%	10%
PCANN	77.74	77.70	77.83	76.79	74.19
PCALin	90.58	90.58	90.57	90.55	90.42
FNO	96.92	96.92	96.71	95.45	94.30
U-FNO	94.23	93.83	95.20	94.14	92.48
MWT	98.26	98.33	97.84	96.42	95.04
DeepONet	93.88	93.88	93.95	93.49	92.70
PINO	97.56	97.59	97.45	96.34	95.07
PI-DeepONet	92.03	91.93	91.84	91.80	91.60

(a) $\lambda_{\text{acc}}(\%)$, the accuracy of the learned parameter

	0%	0.1%	1%	5%	10%
PCANN	0.4684	0.4692	0.4680	0.4828	0.5148
PCALin	0.3157	0.3157	0.3159	0.3163	0.3183
FNO	0.1764	0.1764	0.1823	0.2143	0.2402
U-FNO	0.2140	0.2205	0.2017	0.2371	0.2734
MWT	0.1287	0.1250	0.1435	0.1880	0.2209
DeepONet	0.2484	0.2483	0.2469	0.2547	0.2691
PINO	0.1559	0.1549	0.1607	0.1932	0.2244
PI-DeepONet	0.2792	0.2801	0.2820	0.2822	0.2861

(b) λ_{err} , the relative error of the learned parameter

	0%	0.1%	1%	5%	10%
PCANN	0.1151	0.1152	0.1144	0.1211	0.1373
PCALin	0.0929	0.0929	0.0929	0.0931	0.0934
FNO	0.0104	0.0105	0.0174	0.0711	0.1362
U-FNO	0.0477	0.0517	0.0419	0.0698	0.1145
MWT	0.0129	0.0125	0.0177	0.0544	0.1032
DeepONet	0.0480	0.0484	0.0495	0.0773	0.1190
PINO	0.0167	0.0164	0.0211	0.0567	0.1065
PI-DeepONet	0.0586	0.0593	0.0604	0.0816	0.1244

(c) \tilde{u}_{err} , the relative error between the solution of the learned parameter and the noisy solution.

	0%	0.1%	1%	5%	10%
PCANN	0.1151	0.1152	0.1144	0.1207	0.1363
PCALin	0.0929	0.0929	0.0929	0.0928	0.0923
FNO	0.0210	0.0212	0.0223	0.0329	0.0421
U-FNO	0.0477	0.0517	0.0395	0.0437	0.0496
MWT	0.0129	0.0125	0.0142	0.0209	0.0276
DeepONet	0.0480	0.0484	0.0483	0.0561	0.0597
PINO	0.0167	0.0164	0.0181	0.0250	0.0349
PI-DeepONet	0.0586	0.0593	0.0593	0.0614	0.0677

(d) u_{err} , the relative error between the solution of the learned parameter and the noiseless solution.

Table 9: Effects of noise on Tikhonov-based Inverse Problems on the Darcy Flow problem with PWC coefficients, using a dataset of resolution of 65×65 . The errors shown here are averaged over 100 test samples.

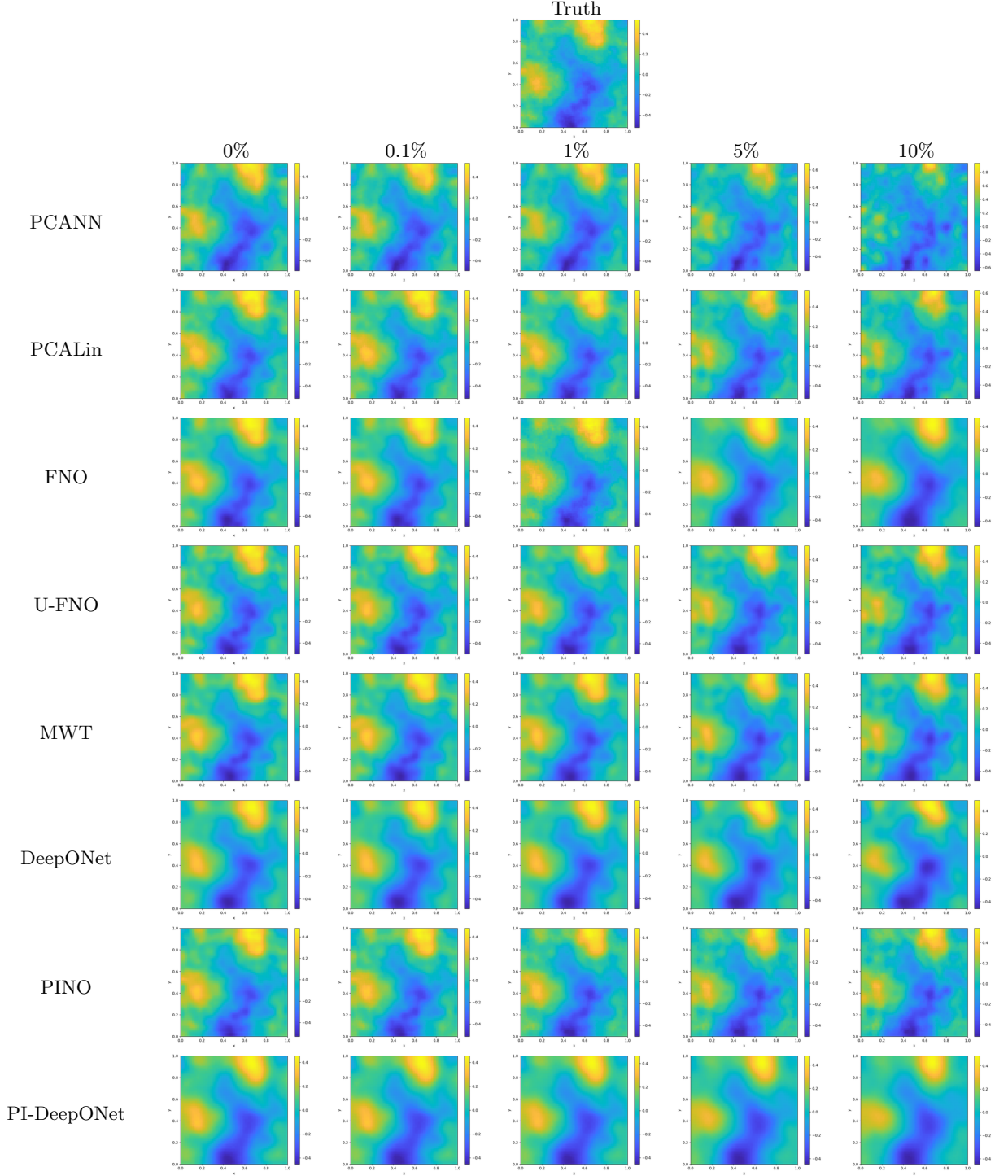


Table 10: Effects of noise on Tikhonov-based Inverse Problems on the Poisson problem, using a dataset of, resolution of 65×65 .

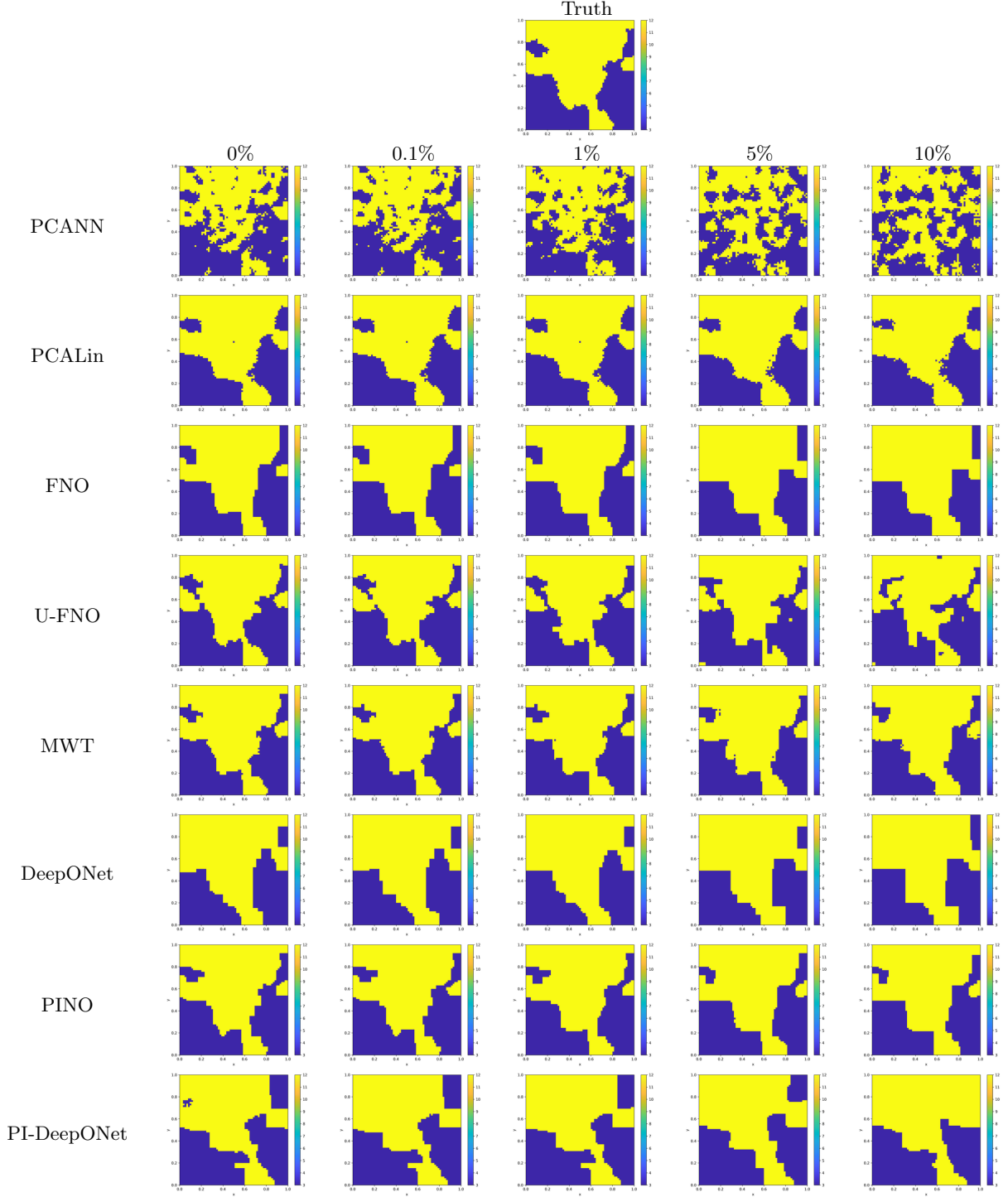


Table 11: Effects of noise on Tikhonov-based Inverse Problems on the Darcy Flow pwc problem, using dataset of, resolution of 65×65 .

compute the temperature profile. Additionally, we are not only interested in one solution for a fixed angular velocity ω . Instead, we aim to learn the solution operator, to approximate the system for different angular velocities, with one single neural network.

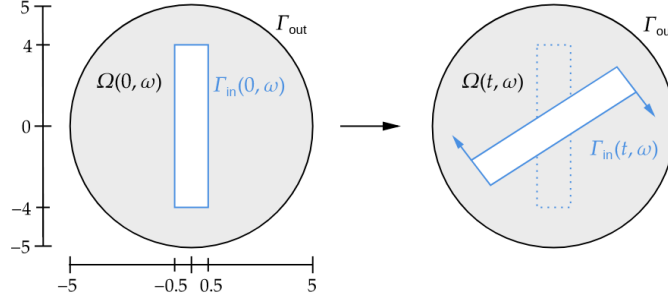


Figure 18: Time dependent rotating geometry in a circular housing

We consider the time interval $I_t := [0.0, 1.0]$ and interval for angular velocities $I_\omega := [\pi, 2\pi]$. To model the fluid inside the domain we use the incompressible Navier–Stokes equations in two dimensions, cf. [117]:

$$\begin{aligned} \partial_t u + (u \cdot \nabla)u &= \nu \Delta u - \nabla p \\ \nabla \cdot u &= 0. \end{aligned} \quad (60)$$

Here, $u = u(x, y, t; \omega) \in \mathbb{R}^2$ is the fluid velocity, $p = p(x, y, t; \omega) \in \mathbb{R}$ the pressure and $\nu \in \mathbb{R}^+$ the kinematic viscosity. For the modelling of the temperature $\theta = \theta(x, y, t; \omega) \in \mathbb{R}$ we consider a heat equation with forced convection due to rotating geometry, cf. [38]:

$$\partial_t \theta + u \cdot \nabla \theta = a \Delta \theta \quad (61)$$

with thermal diffusion coefficient $a \in \mathbb{R}^+$. Convection due to a temperature depending density is not considered due the assumption of incompressibility of the fluid. Initially, at $t = 0$, we set $u = (0, 0)$, $p = 0$ and assume a uniform temperature distribution $\theta = 270$ in the domain $\Omega(0, \omega)$. At the outer boundary Γ_{out} we set a no-slip condition for the fluid flow and a Dirichlet condition for the temperature θ :

$$\begin{aligned} u(x, y, t; \omega) &= (0, 0), \quad \text{for } (x, y, t, \omega) \in \Gamma_{\text{out}} \times I_t \times I_\omega \\ \theta(x, y, t; \omega) &= 270, \quad \text{for } (x, y, t, \omega) \in \Gamma_{\text{out}} \times I_t \times I_\omega \end{aligned}$$

The rotation of the rod is given by the matrix

$$A(t; \omega) := \begin{pmatrix} \cos(-\omega t(1 - e^{-\omega t})) & -\sin(-\omega t(1 - e^{-\omega t})) \\ \sin(-\omega t(1 - e^{-\omega t})) & \cos(-\omega t(1 - e^{-\omega t})) \end{pmatrix},$$

the factor $(1 - e^{-\omega t})$ is included to get a smooth start, which we scale with the rotation speed. Additionally $-\omega$ is used to get a clockwise rotation. As a heat source, a Dirichlet condition for the temperature on Γ_{in} is considered:

$$\theta(x, y, t; \omega) = 270 + 60(1 - e^{-\omega t}), \quad \text{for } (x, y, t, \omega) \in \Gamma_{\text{in}} \times I_t \times I_\omega \quad (62)$$

For the fluid on Γ_{in} we again apply a no-slip condition. Because of the moving boundary, this translates to

$$u(x, y, t; \omega) = \omega d(x, y, t; \omega) \begin{pmatrix} \cos(-\omega t(1 - e^{-\omega t})) \\ \sin(-\omega t(1 - e^{-\omega t})) \end{pmatrix} (1 - e^{-\omega t} + \omega t e^{-\omega t}), \quad (63)$$

for all $(x, y) \in \Gamma_{\text{in}}(t, \omega)$ and $(t, \omega) \in I_t \times I_\omega$. Here $d(x, y, t; \omega)$ corresponds to the signed distance of the point (x, y) to the line perpendicular to the bar, which is running through the origin. This distance is given by:

$$d(x, y, t; \omega) := \begin{pmatrix} x \\ y \end{pmatrix} \cdot \begin{pmatrix} -\sin(-\omega t(1 - e^{-\omega t})) \\ \cos(-\omega t(1 - e^{-\omega t})) \end{pmatrix}$$

The distance has to be included, since points further away from the center have a higher radial velocity.

This concludes the general description of the application problem. If classical PDE solvers such as FEM or FDM solvers are used, we have to compute a new solution for each velocity value ω , that leads to costly simulations for each new parameter value. Furthermore, the most challenging part would be the implementation of discretisation meshes for the moving domain. Especially, to correctly transfer the discrete solution data between different time steps to guarantee conservation of mass, momentum and energy.

By using a deep learning approach, we can try to learn the solutions for different values of ω in one single training process. Thus eliminating the need for new simulations for each ω .

This leads us to the crucial step of choosing a suitable DL method. In our case only the underlying differential equation is known, no data such as a solution for a particular parameter setting is available. Moreover, only scalar parameters appear, hence we can use the classical PINN to learn the solution operator. Additionally, since PINNs are mesh-free, the implementation of the domain is easier, compared to the classical methods. One only has to correctly sample points inside the domain $\Omega(t, \omega)$ and on the boundary $\Gamma_{\text{in}}(t, \omega)$, for each combination of $(t, \omega) \in I_t \times I_\omega$, to train the needed conditions.

The library TORCHPHYSICS was developed with this time (and parameter) dependent domains in mind. Therefore, the previously explained domain can be easily defined in TORCHPHYSICS and the needed points sampled. An example for sampled points on $\Gamma_{\text{in}}(t, \omega)$, for different ω , is shown in Fig. 19. These points can then be created and used in each training step. The same is possible inside $\Omega(t, \omega)$. However, the visualisation of inner points is more elaborate, so we do not show them here and refer any reader interested in more details to the TorchPhysics tutorial. To learn the problem's solution operators, we define three different neural

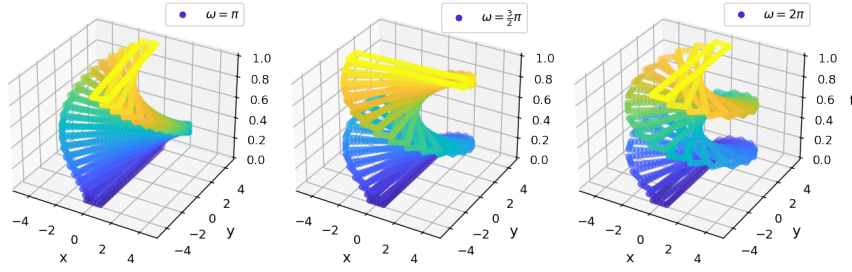


Figure 19: Example of sampled inner boundary points for the application problem. The points are only coloured for visual representation.

networks $u_\Theta, p_\Theta, \theta_\Theta$, for fluid velocity, pressure, and temperature respectively. Every network has space and time variables as input (x, y, t) and, since we want to train the solution for different ω , also the angular velocity ω . The network u_Θ has two output neurons, for the two velocity components.

Since the neural networks have to fulfil multiple conditions, this can lead to problems while training. I.e. different loss terms may have varying preferred minimisation directions. To somewhat simplify the optimisation process, we apply hard constraints to naturally fulfil some of the conditions and simplify the output range of our neural networks. These constrained networks are denoted by $\tilde{u}_\Theta, \tilde{p}_\Theta, \tilde{\theta}_\Theta$. For the temperature we consider:

$$\tilde{\theta}_\Theta(x, y, t; \omega) = 60(1 - e^{-\omega t}) \left(1 - \frac{\sqrt{x^2 + y^2}}{r} \right) \theta_\Theta(x, y, t; \omega) + 270.$$

In the following and the above equation, we omit the temperature unit. Our restricted network $\tilde{\theta}_\Theta$ fulfils the initial and outer boundary conditions. Here $r = 5$, describing the radius of the whole circle. The only constrain for the pressure is the time scale:

$$\tilde{p}_\Theta(x, y, t; \omega) = (1 - e^{-\omega t}) p_\Theta(x, y, t; \omega).$$

To somewhat implement the movement of the rotating bar into our velocity network, we choose the constraints:

$$\tilde{u}_\Theta(x, y, t; \omega) = r\omega(1 - e^{-\omega t} + \omega t e^{-\omega t}) \left(1 - \frac{\sqrt{x^2 + y^2}}{r} \right) \begin{pmatrix} \cos(-\omega t(1 - e^{-\omega t})) u_{\Theta,1}(x, y, t; \omega) \\ \sin(-\omega t(1 - e^{-\omega t})) u_{\Theta,2}(x, y, t; \omega) \end{pmatrix}.$$

Again, \tilde{u}_Θ naturally satisfies the initial and boundary conditions on Γ_{out} . All neural networks are FCNs, with hyperbolic tangent as activation. The networks u_Θ, θ_Θ consist of seven hidden layers with 100 neurons each and p_Θ use networks with 5 layers and 80 neurons.

The only conditions that have to be learned are the Eqs. (60)–(63). This is done via the classical PINN approach, as described in Sec. 4.2, and applied to the constrained networks. Since the temperature does not influence the fluid profile, we first train the solution of the Navier-Stokes equations. Then, the results are used in the training of the heat equation. For the optimisation process, Adam [85] is used and randomly distributed training points are resampled in each iteration, for both the inner part and the moving boundary.

ρ	ν	a
1.0	2.0	0.5

Table 12: Material and operation parameter

The results are presented in Figs. 20 and 21. Here two aspects have to be mentioned. Firstly, getting convergence of the training loss was rather challenging, and relatively large loss values for the divergence and heat term were obtained. Secondly, no reference solution is currently available. Therefore, we can not directly measure the accuracy of the learned approximation. Solely from a physical point of view, the results appear reasonable and would allow for a first step in a rapid prototyping cycle. However, this aspect has to be further investigated, in general, the research for this problem is, from our side, in a rather early stage. This example is shown primarily to present a new application area (moving domains) for the deep learning approaches, where they may be advantageous compared to classical methods, and to demonstrate the potential of TORCHPHYSICS.

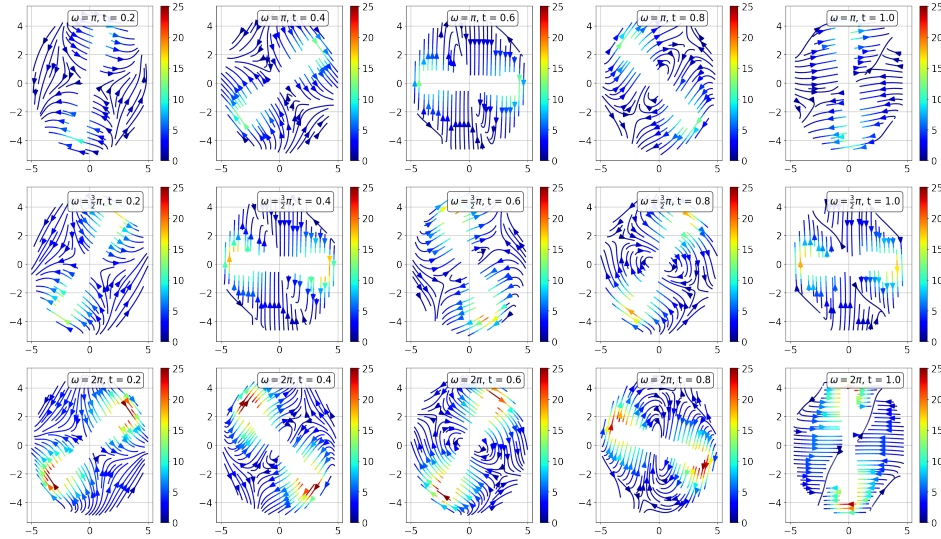


Figure 20: Learned velocity profile for different angular velocities ω , at some discrete time steps.

6.4.2 Identification of material model parameters from stress tensor (Volkswagen, Fraunhofer ITWM)

To shorten the design cycle of vehicles and to reduce the cost of development, automotive industries employ numerical simulation tools in the vehicle development process for testing and analysis. In this application example, we are interested in the interaction of vehicles with various roadbeds such as sand, snow, mud, etc. Vehicle stability depends largely on this interaction, and the safety of the passengers is thus a concern. To approach this problem, a full-body model of the vehicle dynamics is needed as well as proper modelling of the roadbed. Of interest to us, is the modelling of the roadbed consisting of granular material. This is a continuum mechanics problem that involves not only the well-known conservation equations of mass, momentum, and

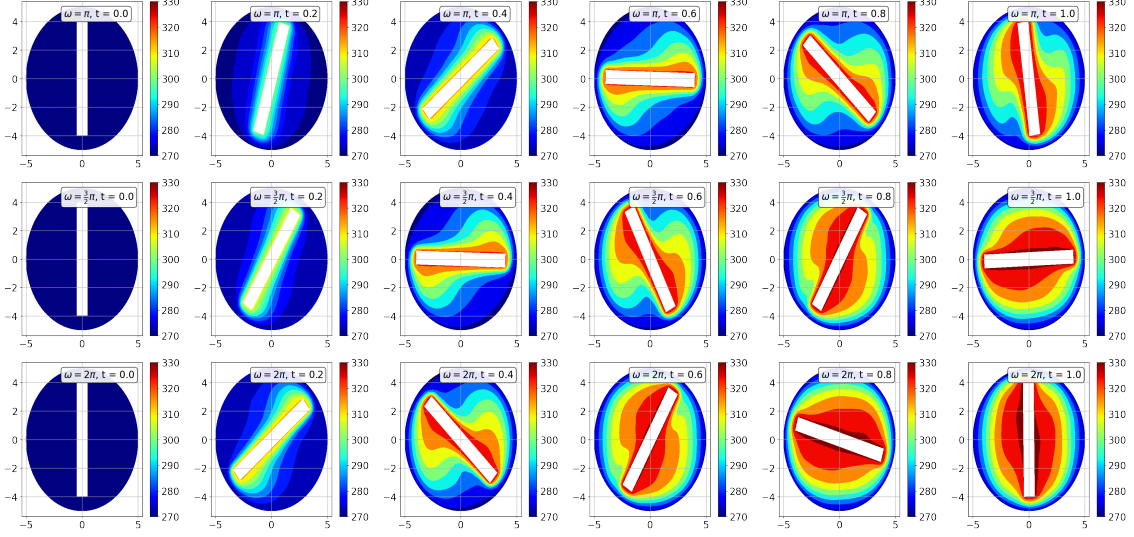


Figure 21: Learned temperature profile for different angular velocities ω , at some discrete time steps.

energy but also, supplementary phenomenological material models. While the former specifies the process conditions and is generally well understood, the latter relates the applied strain to the resulting stress and comes with uncertainties as well as non-linearities. Obviously, the overall goal is for the simulations to match the real-life experiments, thus the selected material model is of great importance.

Material models have parameters that are specific to the considered material as well as its reaction to external conditions, and these models range from simple to complex. By using single-parametric models for the granular material (roadbed), for example, one notices an increasing deviation between simulations and experiments as the simulation time progresses. Also, the simulations have long running times. As a result, complex material models with many more parameters are used. Such parameters are usually determined by a great wealth of expert knowledge, and costly experiments. The barodesy model [87, 88] is one of such complex material model which conforms to the basic mechanical properties of the material. It is formulated in tensorial form by Equations (64)–(65).

$$\frac{d\mathbf{S}}{dt} = \mathbf{W}\mathbf{S} - \mathbf{S}\mathbf{W} + \mathbf{H}(\mathbf{S}, \mathbf{D}, e) \quad (64)$$

$$\frac{de}{dt} = (1 + e) \cdot \text{tr}(\mathbf{D}), \quad (65)$$

with

$$\begin{aligned} \mathbf{D} &= \frac{1}{2} \left(\nabla \mathbf{v}^T + (\nabla \mathbf{v}^T)^T \right) & \mathbf{R} &= \text{tr}(\mathbf{D}^0) \cdot \mathbf{I} + c_1 \cdot \exp(c_2 \cdot \mathbf{D}^0) \\ \mathbf{W} &= \frac{1}{2} \left(\nabla \mathbf{v}^T - (\nabla \mathbf{v}^T)^T \right) & h_b &= \sigma^{c_3} \\ \mathbf{H}(\mathbf{S}, \mathbf{D}, e) &= h_b(\sigma) \cdot (f_b \mathbf{R}^0 + g_b \mathbf{S}^0) \cdot |\mathbf{D}| & f_b &= c_4 \cdot \text{tr}(\mathbf{D}^0) + c_5 \cdot (e - e_c) + c_6 \\ \sigma &= |\mathbf{S}| = \sqrt{\text{tr}(\mathbf{S}^2)} & g_b &= -c_6 \\ \mathbf{S}^0 &= \mathbf{S}/|\mathbf{S}|, \mathbf{D}^0 = \mathbf{D}/|\mathbf{D}|, \mathbf{R}^0 = \mathbf{R}/|\mathbf{R}| & e_c &= (1 + e_{c0}) \cdot \exp\left(\frac{\sigma^{1-c_3}}{c_4 \cdot (1 - c_3)}\right) - 1 \end{aligned}$$

where

- \mathbf{S} is the Cauchy stress tensor (with principal stresses $\sigma_1, \sigma_2, \sigma_3$ in axial and lateral directions),
- \mathbf{W} is the anti-symmetric part of the velocity (\mathbf{v}) gradient,
- \mathbf{D} is the stretching tensor (the symmetric part of the velocity gradient),

- $e = V_p/V_s$ is the void ratio, with a critical void ratio e_c , where V_p and V_s are the volumes of pores and solids (grains).
- t is the time.

The highly non-linear function \mathbf{H} introduces the material parameters $c_1, c_2, c_3, c_4, c_5, c_6$, and ec_0 , (as well as other constants defined above) which we will identify via deep learning in a supervised task.

Using the MESHFREE software [92] we generate parameters-stress pairs to train our neural network. MESHFREE employs a Generalised Finite Difference Method (GFDM): a meshless approach to numerically solve (coupled) PDEs based on their strong formulation on a sufficiently dense cloud of points carrying the physical information (such as velocity, pressure, etc.). A weighted moving least squares method is used to approximate the required spatial partial derivatives on a finite point set [129, 119]. MESHFREE has successfully been applied for the simulation of complex continuum mechanics problems in industry, like mining [120], flow inside a turbine [93], and vehicles travelling through water [79], just to name a few.

In our case, the simulation setting is that of the oedometric test: one of two benchmark problems usually considered in soil mechanics to, e.g., check and calibrate material models. It does so by simulating a one-dimensional compression; the soil (material) sample is loaded in the axial direction and rigid side walls prevent any lateral expansion as demonstrated in Figure 22a. Figure 22b shows the initial point cloud configuration for this test.

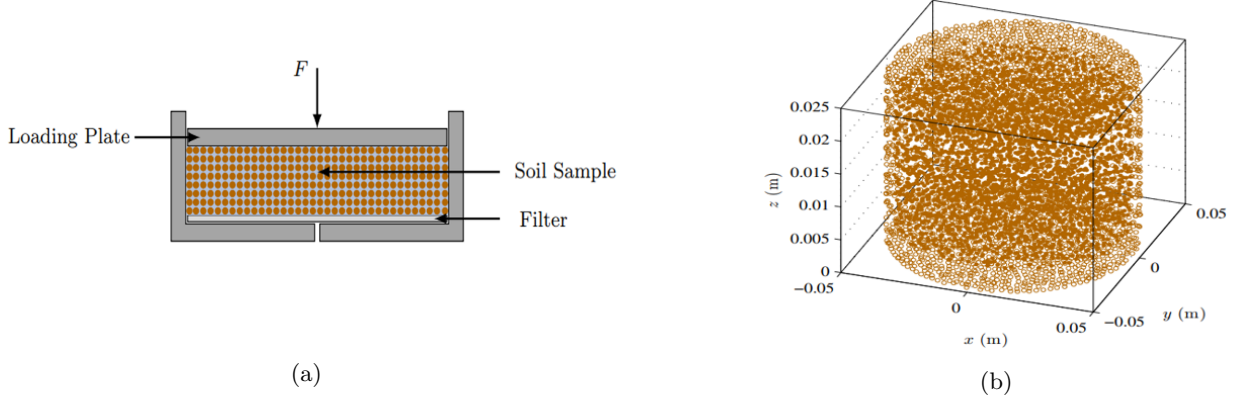


Figure 22: (a) Schematic illustration of the oedometric test. (b) Initial FPM point cloud configuration for the oedometric test (filled circles: interior points, non-filled circles: boundary points) using MESHFREE (see [129])

Randomised PCA as in Section 5.1 is used to reduce the dimensions of the principal stress component from 675 to 50. This reduced dimension is then used as input to the FCN (fully connected network) similar to that in Section 5.1. Since the parameter space is low enough, no PCA is used after the FCN. As a result, the output of the FCN yields the target parameters directly. Of the 6000 data pairs generated, 75% is used for training. During training, the relative L2 error of the individual parameters is calculated and their average is the loss function minimised for training the network. However, due to the nature of this loss function, the learning of the parameters of higher magnitude is favoured. As a remedy, the parameters of lower magnitude are scaled so that they are of the same order (of thousands) as the parameters of higher magnitude. In this way, learning of all the individual parameters is achieved. We obtained an average relative L2 test error of 2.63×10^{-3} on the test data set. Figure 23 shows the comparison of the ground truth (MESHFREE simulation in blue) and the learned parameters (PCANN in orange). A detailed discussion of this application is currently in preparation [128].

7 Conclusions

The presented survey aims at developing a guideline on whether and how to use deep learning concepts for PDE-based forward solvers and related inverse problems. To this end, we have implemented and tested the

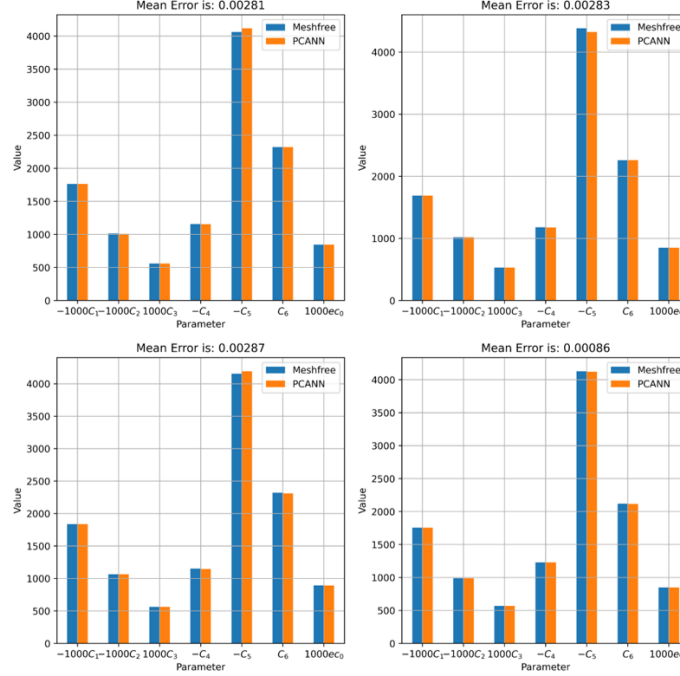


Figure 23: Comparison of ground truth(MESHFREE simulation in blue) and learned parameters (PCANN in orange) for four randomly chosen examples of the oedometric test

most widely used neural network concepts as well as several of their extensions for the two most common PDE problems (Poisson, Darcy flow). In addition, we have applied neural network concepts to two industrial projects.

Naturally, the present text tries to give a complete-as-possible snapshot of the situation at the time we started writing up the results of our test. We are well aware that several additional concepts have been proposed since and we apologise to those whose contributions are missing.

There is no unique criterion for determining the best method, this very much depends on the specific task at hand. Hence, we presented a survey of numerical values for each method, which should allow the user to evaluate the particular criterion relevant to its specific application and to determine a suitable method accordingly.

Nevertheless, we want to highlight some general findings. Within the restricted scope of our test environment, we have found the following conclusions. DL concepts for solely solving forward problems lack precision as compared with classical FEM methods. This finding has been confirmed by other authors as well, see e.g. a numerical study for PINNs in [55]. However, in general, they achieve reasonable accuracy and offer great potential for efficient parameter studies, e.g. for applications in rapid prototyping.

Our findings differ depending on whether the underlying PDE is linear or non-linear and whether training data, i.e. sufficiently many parameter-state pairs are known, is available. Several methods such as Ritz-method or PINN only use the PDE and do not use training data. Hence the comparison has to distinguish these cases

For a linear PDE and if only the PDE is known but no data is available, we propose to use PINN for solving the forward problem. If data, i.e. sufficiently many parameter-state pairs are known, then PCA or even better PCALin are an excellent starting point. As mentioned, this is only the first indication, our tests were restricted to the Poisson problem. Surprisingly, see Table 7, there is not much difference between different concepts for solving the inverse Poisson problem by backward operator training. All methods considered produce reliable results e.g. for 5% noise in the data. Hence, run times might be the criterion for the decision. Obviously, concepts for operator training are advantageous and DeepONet and PI-DeepONet are the overall winners in terms of run-time for testing.

The Poisson forward problem is a rather simple linear elliptic. Hence, the numerical test should be seen as some preliminary test giving some limited insight into the behaviour of DL concepts for forward linear PDEs. As we will see from the more evolved examples, the findings in this section have only a limited meaning for more general cases.

Concerning solvers for the Darcy problem, MWT is the overall winner for solving the forward problem with noise-free data, at least in our experiments. For solving the inverse Darcy problem we propose to use inverse training in combination with U-FNO and MWT for small noise levels and PCANN for solving the non-linear inverse Darcy flow problem with higher noise levels.

As a general remark, we observe that concepts which combine data-driven learning with mathematical concepts such as reduced order models or incorporating the PDE directly, e.g. PCANN/PCALin, PINO, FNO or MWT, have an advantage in terms of stability and performance. Again, we want to emphasise that it is premature to make this a general rule, this is rather an observation restricted to our numerical setting.

Naturally, there are many meaningful extensions of the chosen test scenario. E.g. inserting a classical FDM/FEM forward solver into a Tikhonov regularisation scheme or including H^1 - error measures for comparison would be most interesting. However, we prefer to stay with the present scope of focusing on comparing DL methods for inverse problems and restrict ourselves to the tests provided.

Concerning industrial applications, additional features gain influence. E.g. the simulation of heat inside a rotating engine requires working with a time-dependent domain of definition. Most codes will require substantial additional work when dealing with such complex domains. TorchPhysics offers an accessible concept for working with such domains, which in connection with a standard PINN concept did yield good performance for a parametric study in this context.

The other industrial problem of identifying parameters in a problem of mechanical engineering reduces to a rather low-dimensional task and can be solved by PCANN. Hence, choosing a method suitable for a given industrial problem requires problem-specific considerations, which have to be evaluated task by task.

We should remark, that the size of the network differs considerably. We have performed rather extensive hyper-parameter searches for each method. The reported network sizes did yield the best results. E.g. the DRM does not benefit from extending the network to larger sizes for the mentioned application.

In Table 1, we list the properties of classical methods, Deep Ritz method in [165], PINN in [137], model reduction and Neural Network in [12], DeepONets in [113] and Fourier Neural Operator [102]. We should mention that the properties only correspond to the methods in these mentioned papers, since by some modifications, they can have different properties. For example, the PINN may be used to model parameter-solution operators. In Figure 24, we schematically illustrate the properties of different deep learning methods for PDEs.

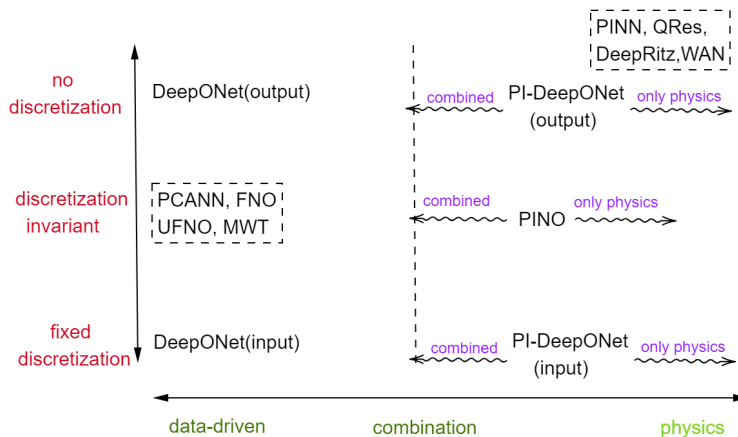


Figure 24: Properties of deep learning methods for PDEs.

The methods discussed above have shown their high potential for solving PDEs as well as their related parametric studies and inverse problems. Whenever efficiency is an issue, these methods perform most convincingly. However, there are still many open questions and problems that are common in the deep

learning community. Hyperparameter search can be very time-consuming and would benefit from a sound theoretical foundation. Also, the choice of activation functions and loss functions can be more refined.

References

- [1] C. Aarset, M. Holler, and T. T. N. Nguyen. Learning-informed parameter identification in nonlinear time-dependent PDEs. *arXiv preprint arXiv:2202.10915*, 2022.
- [2] J. Adler and O. Öktem. Learned primal-dual reconstruction. *IEEE transactions on medical imaging*, 37(6):1322–1332, 2018.
- [3] L. Ardizzone, J. Kruse, S. Wirkert, D. Rahner, E. W. Pellegrini, R. S. Klessen, L. Maier-Hein, C. Rother, and U. Köthe. Analyzing inverse problems with invertible neural networks. *arXiv preprint arXiv:1808.04730*, 2018.
- [4] S. Arridge and A. Hauptmann. Networks for nonlinear diffusion problems in imaging. *Journal of Mathematical Imaging and Vision*, 62(3):471–487, 2020.
- [5] S. Arridge, P. Maass, O. Öktem, and C.-B. Schönlieb. Solving inverse problems using data-driven models. *Acta Numerica*, 28:1–174, 2019.
- [6] G. Bao, X. Ye, Y. Zang, and H. Zhou. Numerical solution of inverse problems by weak adversarial networks. *Inverse Problems*, 36(11):115003, 2020.
- [7] A. R. Barron. Approximation and estimation bounds for artificial neural networks. *Machine learning*, 14:115–133, 1994.
- [8] A. G. Baydin, B. A. Pearlmutter, A. A. Radul, and J. M. Siskind. Automatic differentiation in machine learning: a survey. *Journal of Machine Learning Research*, 18:1–43, 2018.
- [9] C. Beck, S. Becker, P. Cheridito, A. Jentzen, and A. Neufeld. Deep splitting method for parabolic PDEs. *SIAM Journal on Scientific Computing*, 43(5):A3135–A3154, 2021.
- [10] P. Beneventano, P. Cheridito, A. Jentzen, and P. von Wurstemberger. High-dimensional approximation spaces of artificial neural networks and applications to partial differential equations. *arXiv preprint arXiv:2012.04326*, 2020.
- [11] P. Benner, W. Schilders, S. Grivet-Talocia, A. Quarteroni, G. Rozza, and L. Miguel Silveira. *Model Order Reduction: Volume 2: Snapshot-Based Methods and Algorithms*. De Gruyter, 2020.
- [12] K. Bhattacharya, B. Hosseini, N. B. Kovachki, and A. M. Stuart. Model reduction and neural networks for parametric PDEs. *arXiv preprint arXiv:2005.03180*, 2020.
- [13] H. Bolcskei, P. Grohs, G. Kutyniok, and P. Petersen. Optimal approximation with sparsely connected deep neural networks. *SIAM Journal on Mathematics of Data Science*, 1(1):8–45, 2019.
- [14] L. Bösel, M. Thürlmann, and S. Riniker. Machine learning in QM/MM molecular dynamics simulations of condensed-phase systems. *Journal of Chemical Theory and Computation*, 17(5):2641–2658, 2021.
- [15] S. C. Brenner and L. R. Scott. *The Mathematical Theory of Finite Element Methods*, volume 15 of *Texts in Applied Mathematics*. Springer, 2008.
- [16] J. Bu and A. Karpayne. Quadratic residual networks: A new class of neural networks for solving forward and inverse problems in physics involving PDEs. In *Proceedings of the 2021 SIAM International Conference on Data Mining (SDM)*, pages 675–683. SIAM, 2021.
- [17] M. Burger and A. Neubauer. Analysis of Tikhonov regularization for function approximation by neural networks. *Neural Networks*, 16(1):79–90, 2003.

- [18] G. Chen, X. Liu, Y. Li, Q. Meng, and L. Chen. Laplace neural operator for complex geometries. *arXiv preprint arXiv:2302.08166*, 2023.
- [19] J.-S. Chen, M. Hillman, and S.-W. Chi. Meshfree methods: Progress made after 20 years. *Journal of Engineering Mechanics*, 143(4):04017001, 2017.
- [20] T. Chen and H. Chen. Universal approximation to nonlinear operators by neural networks with arbitrary activation functions and its application to dynamical systems. *IEEE Transactions on Neural Networks*, 6(4):911–917, 1995.
- [21] Y. Chen, L. Lu, G. E. Karniadakis, and L. Dal Negro. Physics-informed neural networks for inverse problems in nano-optics and metamaterials. *Optics express*, 28(8):11618–11633, 2020.
- [22] Z. Chen, J. Lu, and Y. Lu. On the representation of solutions to elliptic PDEs in Barron spaces. *Advances in neural information processing systems*, 34:6454–6465, 2021.
- [23] Z. Chen, J. Lu, Y. Lu, and S. Zhou. A regularity theory for static schrödinger equations on \mathbb{R}^d in spectral Barron spaces. *SIAM Journal on Mathematical Analysis*, 55(1):557–570, 2023.
- [24] F. Chinesta, A. Huerta, G. Rozza, and K. Willcox. Model order reduction. *Encyclopedia of computational mechanics*, 2016.
- [25] L. Cicci, S. Fresca, and A. Manzoni. Deep-HyROMnet: A deep learning-based operator approximation for hyper-reduction of nonlinear parametrized PDEs. *arXiv preprint arXiv:2202.02658*, 2022.
- [26] D. Colombo, E. Turkoglu, W. Li, and D. Rovetta. Coupled physics-deep learning inversion. *Computers & Geosciences*, 157:104917, 2021.
- [27] S. Cuomo, V. S. Di Cola, F. Giampaolo, G. Rozza, M. Raissi, and F. Piccialli. Scientific machine learning through physics-informed neural networks: where we are and what’s next. *Journal of Scientific Computing*, 92(3):88, 2022.
- [28] G. Cybenko. Approximation by superpositions of a sigmoidal function. *Mathematics of control, signals and systems*, 2(4):303–314, 1989.
- [29] M. De Hoop, D. Z. Huang, E. Qian, and A. M. Stuart. The cost-accuracy trade-off in operator learning with neural networks. *arXiv preprint arXiv:2203.13181*, 2022.
- [30] B. Deng, Y. Shin, L. Lu, Z. Zhang, and G. E. Karniadakis. Convergence rate of DeepONets for learning operators arising from advection-diffusion equations. *arXiv preprint arXiv:2102.10621*, 2021.
- [31] R. DeVore, B. Hanin, and G. Petrova. Neural network approximation. *Acta Numerica*, 30:327–444, 2021.
- [32] S. Dittmer, T. Kluth, P. Maass, and D. O. Baguer. Regularization by architecture: A deep prior approach for inverse problems. *Journal of Mathematical Imaging and Vision*, 62(3):456–470, 2019.
- [33] P. Dondl, J. Müller, and M. Zeinhofer. Uniform convergence guarantees for the Deep Ritz method for nonlinear problems. *arXiv preprint arXiv:2111.05637*, 2021.
- [34] C. Drygala, B. Winhart, F. di Mare, and H. Gottschalk. Generative modeling of turbulence. *Physics of Fluids*, 34(3):035114, 2022.
- [35] C. Duan, Y. Jiao, Y. Lai, X. Lu, and Z. Yang. Convergence rate analysis for Deep Ritz. *arXiv preprint arXiv:2103.13330*, 2021.
- [36] W. E, J. Han, and A. Jentzen. Algorithms for solving high dimensional PDEs: From nonlinear Monte Carlo to machine learning. *Nonlinearity*, 35(1):278, 2021.
- [37] W. E, C. Ma, and L. Wu. The Barron space and the flow-induced function spaces for neural network models. *Constructive Approximation*, 55(1):369–406, 2022.

- [38] N. Elsner. *Grundlagen der technischen Thermodynamik*. Akademie-Verlag, 1988.
- [39] N. R. Franco, S. Fresca, A. Manzoni, and P. Zunino. Approximation bounds for convolutional neural networks in operator learning. *Neural Networks*, 161:129–141, 2023.
- [40] S. Fresca and A. Manzoni. Real-time simulation of parameter-dependent fluid flows through deep learning-based reduced order models. *Fluids*, 6(7):259, 2021.
- [41] S. Fresca and A. Manzoni. POD-DL-ROM: enhancing deep learning-based reduced order models for nonlinear parametrized PDEs by proper orthogonal decomposition. *Computer Methods in Applied Mechanics and Engineering*, 388:114181, 2022.
- [42] S. Fresca, A. Manzoni, L. Dedè, and A. Quarteroni. Deep learning-based reduced order models in cardiac electrophysiology. *PloS one*, 15(10):e0239416, 2020.
- [43] S. Fresca, L. Dede, and A. Manzoni. A comprehensive deep learning-based approach to reduced order modeling of nonlinear time-dependent parametrized PDEs. *Journal of Scientific Computing*, 87(2): 1–36, 2021.
- [44] S. Fresca, G. Gobat, P. Fedeli, A. Frangi, and A. Manzoni. Deep learning-based reduced order models for the real-time simulation of the nonlinear dynamics of microstructures. *International Journal for Numerical Methods in Engineering*, 123(20):4749–4777, 2022.
- [45] S. Garg and S. Chakraborty. Variational bayes deep operator network: A data-driven bayesian solver for parametric differential equations. *arXiv preprint arXiv:2206.05655*, 2022.
- [46] L. Gonon, P. Grohs, A. Jentzen, D. Kofler, and D. Šiška. Uniform error estimates for artificial neural network approximations for heat equations. *IMA Journal of Numerical Analysis*, 42(3):1991–2054, 2022.
- [47] P. Gopalani, S. Karmakar, and A. Mukherjee. Capacity bounds for the DeepONet method of solving differential equations. *arXiv preprint arXiv:2205.11359*, 2022.
- [48] S. Goswami, M. Yin, Y. Yu, and G. Karniadakis. A physics-informed variational DeepONet for predicting the crack path in brittle materials. *arXiv preprint arXiv:2108.06905*, 2021.
- [49] S. Goswami, A. Bora, Y. Yu, and G. E. Karniadakis. Physics-informed deep neural operator networks. *arXiv preprint arXiv:2207.05748*, 2022.
- [50] R. Gribonval, G. Kutyniok, M. Nielsen, and F. Voigtlaender. Approximation spaces of deep neural networks. *Constructive approximation*, 55(1):259–367, 2022.
- [51] P. Grohs and F. Voigtlaender. Proof of the theory-to-practice gap in deep learning via sampling complexity bounds for neural network approximation spaces. *arXiv preprint arXiv:2104.02746*, 2021.
- [52] P. Grohs, F. Hornung, A. Jentzen, and P. von Wurstemberger. A proof that artificial neural networks overcome the curse of dimensionality in the numerical approximation of black-scholes partial differential equations. *arXiv preprint arXiv:1809.02362*, 2018.
- [53] P. Grohs, A. Jentzen, and D. Salimova. Deep neural network approximations for solutions of PDEs based on Monte Carlo algorithms. *Partial Differential Equations and Applications*, 3(4):45, 2022.
- [54] P. Grohs, S. Ibragimov, A. Jentzen, and S. Koppensteiner. Lower bounds for artificial neural network approximations: A proof that shallow neural networks fail to overcome the curse of dimensionality. *Journal of Complexity*, page 101746, 2023.
- [55] T. G. Grossmann, U. J. Komorowska, J. Latz, and C.-B. Schönlieb. Can physics-informed neural networks beat the finite element method? *arXiv preprint arXiv:2302.04107*, 2023.
- [56] I. Gühring, G. Kutyniok, and P. Petersen. Error bounds for approximations with deep ReLU neural networks in $W^{s,p}$ norms. *Analysis and Applications*, 18(05):803–859, 2020.

- [57] I. Gühring, M. Raslan, and G. Kutyniok. Expressivity of deep neural networks. *arXiv preprint arXiv:2007.04759*, 2020.
- [58] G. Gupta, X. Xiao, and P. Bogdan. Multiwavelet-based operator learning for differential equations. *Advances in Neural Information Processing Systems*, 34:24048–24062, 2021.
- [59] J. Gwinner and E. P. Stephan. *Advanced boundary element methods*. Springer, 2018.
- [60] E. Haber and L. Ruthotto. Stable architectures for deep neural networks. *Inverse problems*, 34(1):014004, 2017.
- [61] P. S. Hadorn. Shift-DeepONet: Extending deep operator networks for discontinuous output functions. In *Master thesis, ETH Computational Science and Engineering*. ETH Zurich, Seminar for Applied Mathematics, 2022.
- [62] N. Halko, P.-G. Martinsson, Y. Shkolnisky, and M. Tygert. An algorithm for the principal component analysis of large data sets. *SIAM Journal on Scientific computing*, 33(5):2580–2594, 2011.
- [63] N. Halko, P.-G. Martinsson, and J. A. Tropp. Finding structure with randomness: Probabilistic algorithms for constructing approximate matrix decompositions. *SIAM review*, 53(2):217–288, 2011.
- [64] S. J. Hamilton and A. Hauptmann. Deep D-bar: Real-time electrical impedance tomography imaging with deep neural networks. *IEEE transactions on medical imaging*, 37(10):2367–2377, 2018.
- [65] J. Han, A. Jentzen, and W. E. Solving high-dimensional partial differential equations using deep learning. *Proceedings of the National Academy of Sciences*, 115(34):8505–8510, 2018.
- [66] A. Hauptmann and B. T. Cox. Deep learning in photoacoustic tomography: current approaches and future directions. *Journal of Biomedical Optics*, 25(11):112903, 2020.
- [67] D. Hendrycks and K. Gimpel. Bridging nonlinearities and stochastic regularizers with gaussian error linear units. *CoRR*, abs/1606.08415, 3, 2016.
- [68] D. Hendrycks and K. Gimpel. Gaussian error linear units (gelus). *arXiv preprint arXiv:1606.08415*, 2016.
- [69] W. Herzberg, D. B. Rowe, A. Hauptmann, and S. J. Hamilton. Graph convolutional networks for model-based learning in nonlinear inverse problems. *IEEE transactions on computational imaging*, 7:1341–1353, 2021.
- [70] J. S. Hesthaven and S. Ubbiali. Non-intrusive reduced order modeling of nonlinear problems using neural networks. *Journal of Computational Physics*, 363:55–78, 2018.
- [71] K. Hornik, M. Stinchcombe, and H. White. Multilayer feedforward networks are universal approximators. *Neural networks*, 2(5):359–366, 1989.
- [72] F. Hornung, A. Jentzen, and D. Salimova. Space-time deep neural network approximations for high-dimensional partial differential equations. *arXiv preprint arXiv:2006.02199*, 2020.
- [73] C. Huré, H. Pham, and X. Warin. Deep backward schemes for high-dimensional nonlinear PDEs. *Mathematics of Computation*, 89(324):1547–1579, 2020.
- [74] M. Hutzenthaler, A. Jentzen, T. Kruse, et al. On multilevel picard numerical approximations for high-dimensional nonlinear parabolic partial differential equations and high-dimensional nonlinear backward stochastic differential equations. *Journal of Scientific Computing*, 79(3):1534–1571, 2019.
- [75] M. Hutzenthaler, A. Jentzen, T. Kruse, and T. A. Nguyen. A proof that rectified deep neural networks overcome the curse of dimensionality in the numerical approximation of semilinear heat equations. *SN partial differential equations and applications*, 1:1–34, 2020.

- [76] A. Jacot, F. Gabriel, and C. Hongler. Neural Tangent Kernel: Convergence and generalization in neural networks. In *NIPS'18*, page 8580–8589. Curran Associates Inc., 2018.
- [77] A. D. Jagtap and G. E. Karniadakis. Extended physics-informed neural networks (XPINNs): A generalized space-time domain decomposition based deep learning framework for nonlinear partial differential equations. *Communications in Computational Physics*, 28(5):2002–2041, 2020.
- [78] A. D. Jagtap, E. Kharazmi, and G. E. Karniadakis. Conservative physics-informed neural networks on discrete domains for conservation laws: Applications to forward and inverse problems. *Computer Methods in Applied Mechanics and Engineering*, 365:113028, 2020.
- [79] A. Jefferies, J. Kuhnert, L. Aschenbrenner, and U. Giffhorn. Finite pointset method for the simulation of a vehicle travelling through a body of water. In *Meshfree methods for partial differential equations VII*, pages 205–221. Springer, 2015.
- [80] A. Jentzen, D. Salimova, and T. Welti. A proof that deep artificial neural networks overcome the curse of dimensionality in the numerical approximation of kolmogorov partial differential equations with constant diffusion and nonlinear drift coefficients. *arXiv preprint arXiv:1809.07321*, 2018.
- [81] Y. Jiao, Y. Lai, Y. Lo, Y. Wang, and Y. Yang. Error analysis of Deep Ritz methods for elliptic equations. *arXiv preprint arXiv:2107.14478*, 2021.
- [82] P. Jin, S. Meng, and L. Lu. Mionet: Learning multiple-input operators via tensor product. *arXiv preprint arXiv:2202.06137*, 2022.
- [83] J. Jumper, R. Evans, A. Pritzel, T. Green, M. Figurnov, O. Ronneberger, K. Tunyasuvunakool, R. Bates, A. Židek, A. Potapenko, et al. Highly accurate protein structure prediction with alphafold. *Nature*, 596(7873):583–589, 2021.
- [84] G. E. Karniadakis, I. G. Kevrekidis, L. Lu, P. Perdikaris, S. Wang, and L. Yang. Physics-informed machine learning. *Nature Reviews Physics*, 3(6):422–440, 2021.
- [85] D. P. Kingma and J. Ba. Adam: A method for stochastic optimization. *arXiv preprint arXiv:1412.6980*, 2014.
- [86] G. Klambauer, T. Unterthiner, A. Mayr, and S. Hochreiter. Self-normalizing neural networks. *Advances in neural information processing systems*, 30, 2017.
- [87] D. Kolymbas. Barodesy: a new hypoplastic approach. *International Journal for Numerical and Analytical Methods in Geomechanics*, 36(9):1220–1240, 2012.
- [88] D. Kolymbas. Barodesy: a new constitutive frame for soils. *Géotechnique Letters*, 2(2):17–23, 2012.
- [89] N. Kovachki, S. Lanthaler, and S. Mishra. On universal approximation and error bounds for fourier neural operators. *Journal of Machine Learning Research*, 22:Art–No, 2021.
- [90] N. Kovachki, Z. Li, B. Liu, K. Azizzadenesheli, K. Bhattacharya, A. Stuart, and A. Anandkumar. Neural operator: Learning maps between function spaces. *arXiv preprint arXiv:2108.08481*, 2021.
- [91] N. Kovachki, B. Liu, X. Sun, H. Zhou, K. Bhattacharya, M. Ortiz, and A. Stuart. Multiscale modeling of materials: Computing, data science, uncertainty and goal-oriented optimization. *Mechanics of Materials*, 165:104156, 2022.
- [92] J. Kuhnert. Meshfree simulations in car design: closing the gaps of classical simulation tools. *German Success Stories in Industrial Mathematics*, 35:130, 2021.
- [93] J. Kuhnert, I. Michel, and R. Mack. Fluid structure interaction (FSI) in the meshfree finite pointset method (FPM): Theory and applications. In *International workshop on meshfree methods for partial differential equations*, pages 73–92. Springer, 2017.

- [94] G. Kutyniok, P. Petersen, M. Raslan, and R. Schneider. A theoretical analysis of deep neural networks and parametric PDEs. *Constructive Approximation*, 55(1):73–125, 2022.
- [95] S. Lanthaler. Operator learning with PCA-Net: upper and lower complexity bounds. *arXiv preprint arXiv:2303.16317*, 2023.
- [96] S. Lanthaler, S. Mishra, and G. E. Karniadakis. Error estimates for DeepONets: A deep learning framework in infinite dimensions. *Transactions of Mathematics and Its Applications*, 6(1):tnac001, 2022.
- [97] S. Lanthaler, Z. Li, and A. M. Stuart. The nonlocal neural operator: Universal approximation. *arXiv preprint arXiv:2304.13221*, 2023.
- [98] J. Leuschner, M. Schmidt, D. O. Baguer, and P. Maass. LoDoPaB-CT, a benchmark dataset for low-dose computed tomography reconstruction. *Scientific Data*, 8(1):109, 2021.
- [99] J. Leuschner, M. Schmidt, P. S. Ganguly, V. Andriashen, S. B. Coban, A. Denker, D. Bauer, A. Hadjifaradji, K. J. Batenburg, P. Maass, et al. Quantitative comparison of deep learning-based image reconstruction methods for low-dose and sparse-angle ct applications. *Journal of Imaging*, 7(3):44, 2021.
- [100] R. J. LeVeque. *Finite Volume Methods for Hyperbolic Problems*. Cambridge University Press, 2002.
- [101] H. Li, J. Schwab, S. Antholzer, and M. Haltmeier. NETT: Solving inverse problems with deep neural networks. *Inverse Problems*, 36(6):065005, 2020.
- [102] Z. Li, N. Kovachki, K. Azizzadenesheli, B. Liu, K. Bhattacharya, A. Stuart, and A. Anandkumar. Fourier neural operator for parametric partial differential equations. *arXiv preprint arXiv:2010.08895*, 2020.
- [103] Z. Li, N. Kovachki, K. Azizzadenesheli, B. Liu, K. Bhattacharya, A. Stuart, and A. Anandkumar. Neural operator: Graph kernel network for partial differential equations. *arXiv preprint arXiv:2003.03485*, 2020.
- [104] Z. Li, N. Kovachki, K. Azizzadenesheli, B. Liu, A. Stuart, K. Bhattacharya, and A. Anandkumar. Multipole graph neural operator for parametric partial differential equations. *Advances in Neural Information Processing Systems*, 33:6755–6766, 2020.
- [105] Z. Li, H. Zheng, N. Kovachki, D. Jin, H. Chen, B. Liu, K. Azizzadenesheli, and A. Anandkumar. Physics-informed neural operator for learning partial differential equations. *arXiv preprint arXiv:2111.03794*, 2021.
- [106] Z. Li, D. Z. Huang, B. Liu, and A. Anandkumar. Fourier neural operator with learned deformations for PDEs on general geometries. *arXiv preprint arXiv:2207.05209*, 2022.
- [107] Y. Liao and P. Ming. Deep Nitsche method: Deep Ritz method with essential boundary conditions. *arXiv preprint arXiv:1912.01309*, 2019.
- [108] G. Lin, C. Moya, and Z. Zhang. Accelerated replica exchange stochastic gradient langevin diffusion enhanced bayesian DeepONet for solving noisy parametric PDEs. *arXiv preprint arXiv:2111.02484*, 2021.
- [109] B. Liu, N. Kovachki, Z. Li, K. Azizzadenesheli, A. Anandkumar, A. M. Stuart, and K. Bhattacharya. A learning-based multiscale method and its application to inelastic impact problems. *Journal of the Mechanics and Physics of Solids*, 158:104668, 2022.
- [110] D. C. Liu and J. Nocedal. On the limited memory BFGS method for large scale optimization. *Mathematical programming*, 45(1-3):503–528, 1989.
- [111] L. Liu and W. Cai. Multiscale DeepONet for nonlinear operators in oscillatory function spaces for building seismic wave responses. *arXiv preprint arXiv:2111.04860*, 2021.

- [112] J. Lu, Z. Shen, H. Yang, and S. Zhang. Deep network approximation for smooth functions. *SIAM Journal on Mathematical Analysis*, 53(5):5465–5506, 2021.
- [113] L. Lu, P. Jin, and G. E. Karniadakis. DeepONet: Learning nonlinear operators for identifying differential equations based on the universal approximation theorem of operators. *arXiv preprint arXiv:1910.03193*, 2019.
- [114] L. Lu, X. Meng, Z. Mao, and G. E. Karniadakis. DeepXDE: A deep learning library for solving differential equations. *SIAM Review*, 63(1):208–228, 2021.
- [115] L. Lu, R. Pestourie, W. Yao, Z. Wang, F. Verdugo, and S. G. Johnson. Physics-informed neural networks with hard constraints for inverse design. *SIAM Journal on Scientific Computing*, 43(6):B1105–B1132, 2021.
- [116] L. Lu, X. Meng, S. Cai, Z. Mao, S. Goswami, Z. Zhang, and G. E. Karniadakis. A comprehensive and fair comparison of two neural operators (with practical extensions) based on fair data. *Computer Methods in Applied Mechanics and Engineering*, 393:114778, 2022.
- [117] G. Łukaszewicz and P. Kalita. Navier–stokes equations. *Advances in Mechanics and Mathematics*, 34, 2016.
- [118] H. N. Mhaskar. Neural networks for optimal approximation of smooth and analytic functions. *Neural computation*, 8(1):164–177, 1996.
- [119] I. Michel, I. Bathaeian, J. Kuhnert, D. Kolymbas, C.-H. Chen, I. Polymerou, C. Vrettos, and A. Becker. Meshfree generalized finite difference methods in soil mechanics—part ii: numerical results. *GEM-International Journal on Geomathematics*, 8(2):191–217, 2017.
- [120] I. Michel, T. Seifarth, J. Kuhnert, and P. Suchde. A meshfree generalized finite difference method for solution mining processes. *Computational Particle Mechanics*, 8(3):561–574, 2021.
- [121] P. M. Milani, J. Ling, and J. K. Eaton. Generalization of machine-learned turbulent heat flux models applied to film cooling flows. *Journal of Turbomachinery*, 142(1), 2020.
- [122] S. Mishra and R. Molinaro. Estimates on the generalization error of physics informed neural networks (PINNs) for approximating PDEs. *arXiv preprint arXiv:2006.16144*, 2020.
- [123] S. Mishra and R. Molinaro. Estimates on the generalization error of physics informed neural networks (PINNs) for approximating a class of inverse problems for PDEs. *arXiv preprint arXiv:2007.01138*, 2020.
- [124] C. Moya and G. Lin. Fed-DeepONet: Stochastic gradient-based federated training of deep operator networks. *Algorithms*, 15(9):325, 2022.
- [125] C. Moya, S. Zhang, M. Yue, and G. Lin. DeepONet-Grid-UQ: A trustworthy deep operator framework for predicting the power grid’s post-fault trajectories. *arXiv preprint arXiv:2202.07176*, 2022.
- [126] M. Mozumder, A. Hauptmann, I. Nissilä, S. R. Arridge, and T. Tarvainen. A model-based iterative learning approach for diffuse optical tomography. *IEEE Transactions on Medical Imaging*, 41(5):1289–1299, 2021.
- [127] J. Müller and M. Zeinhofer. Deep Ritz revisited. *arXiv preprint arXiv:1912.03937*, 2019.
- [128] D. Nganyu Tanyu, I. Michel, A. Rademacher, P. Maass, and J. Kuhnert. Parameter identification by deep learning of a material model for granular media. *In preparation*, 2022.
- [129] I. Ostermann, J. Kuhnert, D. Kolymbas, C.-H. Chen, I. Polymerou, V. Šmilauer, C. Vrettos, and D. Chen. Meshfree generalized finite difference methods in soil mechanics—part i: theory. *GEM-International Journal on Geomathematics*, 4(2):167–184, 2013.

- [130] K. Panetta. Gartner top 10 strategic technology trends for 2019. <https://www.gartner.com/smarterwithgartner/gartner-top-10-strategic-technology-trends-for-2018>, 2018. Accessed: May 17, 2023.
- [131] K. Panetta. Gartner top 10 strategic technology trends for 2020. <https://www.gartner.com/smarterwithgartner/gartner-top-10-strategic-technology-trends-for-2019>, 2019. Accessed: May 17, 2023.
- [132] G. Pang, L. Lu, and G. E. Karniadakis. fPINNs: Fractional physics-informed neural networks. *SIAM Journal on Scientific Computing*, 41(4):A2603–A2626, 2019.
- [133] P. Petersen and F. Voigtlaender. Optimal approximation of piecewise smooth functions using deep ReLU neural networks. *Neural Networks*, 108:296–330, 2018.
- [134] A. Pinkus. Approximation theory of the MLP model in neural networks. *Acta numerica*, 8:143–195, 1999.
- [135] M. Prasthofer, T. De Ryck, and S. Mishra. Variable-input deep operator networks. *arXiv preprint arXiv:2205.11404*, 2022.
- [136] M. Raissi. Deep hidden physics models: Deep learning of nonlinear partial differential equations. *The Journal of Machine Learning Research*, 19(1):932–955, 2018.
- [137] M. Raissi, P. Perdikaris, and G. E. Karniadakis. Physics-informed neural networks: A deep learning framework for solving forward and inverse problems involving nonlinear partial differential equations. *Journal of Computational Physics*, 378:686–707, 2019.
- [138] B. Raonić, R. Molinaro, T. Rohner, S. Mishra, and E. de Bezenac. Convolutional neural operators. *arXiv preprint arXiv:2302.01178*, 2023.
- [139] C. Reisinger and Y. Zhang. Rectified deep neural networks overcome the curse of dimensionality for nonsmooth value functions in zero-sum games of nonlinear stiff systems. *Analysis and Applications*, 18(06):951–999, 2020.
- [140] L. Ruthotto and E. Haber. Deep neural networks motivated by partial differential equations. *Journal of Mathematical Imaging and Vision*, 62(3):352–364, 2020.
- [141] W. Schilders. Introduction to model order reduction. *Model order reduction: theory, research aspects and applications*, pages 3–32, 2008.
- [142] W. Schilders. MSODE: Modelling, simulation and optimization in a data-rich environment. In *Mathematics: Key Enabling Technology for Scientific Machine Learning*, pages 24–30, 2021.
- [143] U. Shaham, A. Cloninger, and R. R. Coifman. Provable approximation properties for deep neural networks. *Applied and Computational Harmonic Analysis*, 44(3):537–557, 2018.
- [144] J. Sirignano and K. Spiliopoulos. DGM: A deep learning algorithm for solving partial differential equations. *Journal of computational physics*, 375:1339–1364, 2018.
- [145] J. C. Strikwerda. *Finite Difference Schemes and Partial Differential Equations*. Society for Industrial and Applied Mathematics, second edition, 2004.
- [146] Y. Sun, C. Moya, G. Lin, and M. Yue. DeepGraphONet: A deep graph operator network to learn and zero-shot transfer the dynamic response of networked systems. *arXiv preprint arXiv:2209.10622*, 2022.
- [147] L. Tan and L. Chen. Enhanced DeepONet for modeling partial differential operators considering multiple input functions. *arXiv preprint arXiv:2202.08942*, 2022.
- [148] N. Thuerey, P. Holl, M. Mueller, P. Schnell, F. Trost, and K. Um. Physics-based deep learning. *arXiv preprint arXiv:2109.05237*, 2021.

- [149] TorchPhysics. TORCHPHYSICS: A deep learning library to solve differential equations. <https://github.com/boschresearch/torchphysics>, 2022. Accessed: May 17, 2023.
- [150] T. Tripura and S. Chakraborty. Wavelet neural operator: a neural operator for parametric partial differential equations. *arXiv preprint arXiv:2205.02191*, 2022.
- [151] F. Tröltzsch. *Optimal Control of Partial Differential Equations*, volume 112 of *Graduate Studies in Mathematics*. American Mathematical Society, Providence, 2010.
- [152] F. Voigtlaender. The universal approximation theorem for complex-valued neural networks. *Applied and Computational Harmonic Analysis*, 64:33–61, 2023.
- [153] R. Wang, K. Kashinath, M. Mustafa, A. Albert, and R. Yu. Towards physics-informed deep learning for turbulent flow prediction. In *Proceedings of the 26th ACM SIGKDD International Conference on Knowledge Discovery & Data Mining*, pages 1457–1466, 2020.
- [154] S. Wang, X. Yu, and P. Perdikaris. When and why PINNs fail to train: A Neural Tangent Kernel perspective. *arXiv preprint arXiv:2007.14527*, 2020.
- [155] S. Wang, H. Wang, and P. Perdikaris. On the eigenvector bias of Fourier feature networks: From regression to solving multi-scale PDEs with physics-informed neural networks. *Computer Methods in Applied Mechanics and Engineering*, 384:113938, 2021.
- [156] S. Wang, H. Wang, and P. Perdikaris. Learning the solution operator of parametric partial differential equations with physics-informed DeepOnets. *arXiv preprint arXiv:2103.10974*, 2021.
- [157] S. Wang, H. Wang, and P. Perdikaris. Improved architectures and training algorithms for deep operator networks. *Journal of Scientific Computing*, 92(2):35, 2022.
- [158] G. Wen, C. Hay, and S. M. Benson. CCSNet: A deep learning modeling suite for CO₂ storage. *Advances in Water Resources*, 155:104009, 2021.
- [159] G. Wen, Z. Li, K. Azizzadenesheli, A. Anandkumar, and S. M. Benson. U-FNO—An enhanced fourier neural operator-based deep-learning model for multiphase flow. *Advances in Water Resources*, 163: 104180, 2022.
- [160] S. Wold, K. Esbensen, and P. Geladi. Principal component analysis. *Chemometrics and intelligent laboratory systems*, 2(1-3):37–52, 1987.
- [161] H. Xie, C. Zhai, L. Liu, and H. Yong. A weighted first-order formulation for solving anisotropic diffusion equations with deep neural networks. *arXiv preprint arXiv:2205.06658*, 2022.
- [162] D. Yarotsky. Error bounds for approximations with deep ReLU networks. *Neural Networks*, 94:103–114, 2017.
- [163] S. Yeonjong, J. Darbon, and G. E. Karniadakis. On the convergence of physics informed neural networks for linear second-order elliptic and parabolic type PDEs. *Communications in Computational Physics*, 28(5):2042–2074, 2020.
- [164] H. You, Y. Yu, M. D’Elia, T. Gao, and S. Silling. Nonlocal kernel network (NKN): A stable and resolution-independent deep neural network. *arXiv preprint arXiv:2201.02217*, 2022.
- [165] B. Yu and W. E. The Deep Ritz method: A deep learning-based numerical algorithm for solving variational problems. *arXiv preprint arXiv:1710.00211*, 2017.
- [166] J. Yu, L. Lu, X. Meng, and G. E. Karniadakis. Gradient-enhanced physics-informed neural networks for forward and inverse PDE problems. *Computer Methods in Applied Mechanics and Engineering*, 393: 114823, 2022.
- [167] Y. Zang, G. Bao, X. Ye, and H. Zhou. Weak adversarial networks for high-dimensional partial differential equations. *Journal of Computational Physics*, 411:109409, 2020.

- [168] D. Zhang, L. Lu, L. Guo, and G. E. Karniadakis. Quantifying total uncertainty in physics-informed neural networks for solving forward and inverse stochastic problems. *Journal of Computational Physics*, 397:108850, 2019.
- [169] D.-X. Zhou. Universality of deep convolutional neural networks. *Applied and computational harmonic analysis*, 48(2):787–794, 2020.
- [170] Y. Zhu and N. Zabaras. Bayesian deep convolutional encoder–decoder networks for surrogate modeling and uncertainty quantification. *Journal of Computational Physics*, 366:415–447, 2018.

A Appendix

A.1 Application Problems

A.1.1 Darcy Flow

For this problem, we consider the steady state of the 2-d Darcy Flow equation on the unit box which is the second order, linear, elliptic PDE

$$\begin{aligned} -\nabla \cdot (\lambda(s) \nabla u(s)) &= f(s) & s \in (0, 1)^2 \\ u(s) &= 0 & s \in \partial(0, 1)^2 \end{aligned} \tag{66}$$

with a Dirichlet boundary where $a \in L^\infty((0, 1)^2; \mathbb{R}_+)$ is the diffusion coefficient, $f = 1 \in L^2((0, 1)^2; \mathbb{R}_+)$ is the forcing function and $u \in H_0^1((0, 1)^2; \mathbb{R})$ is the unique solution of the PDE. Some few applications of this PDE are seen in the domains of modelling the pressure of the subsurface flow, the deformation of linearly elastic materials, and the electric potential in conductive materials.

A.1.2 Poisson Equation

We are interested in the PDE

$$\begin{aligned} -\Delta u(s) &= \lambda(s) & s \in (0, 1)^2 \\ u(s) &= 0 & s \in \partial(0, 1)^2 \end{aligned} \tag{67}$$

which is a special case of Equation 58 where the diffusion coefficient is constant and equals to 1 everywhere in the domain $\Omega = (0, 1)^2$.

A.2 Setting of Numerical Implementations

The details of the experiments are provided in Section 6. The computing environment is described below:

- GPU: 8x nVidia GeForce GTX 2080 Ti
- CPU: Intel Xeon Gold 6234 (8 cores, 32 threads)
- RAM: 1500 GB of system RAM
- OS: Ubuntu 16.04.7 LTS

While the parameters for the Poisson problem are sampled from the distribution μ_G , those for the Darcy Flow are sampled on μ_P (piece-wise constant). These distributions are described in Section 6.

For the operator learning scenarios (PCANN, FNO, UFNO, DeepONet), for both forward and inverse problems of the Poisson and Darcy Flow problems, we train the neural operator on 1000 training data-set pairs we evaluate on 5000 test pairs. This also holds for the pre-training phase of the PINO.

The experiments for DRM, PINN, QRES, DeepONet and PI-DeepONet were all done in the deep learning library TORCHPHYSICS [149]

All codes will be available online at https://github.com/dericknganyu/dl_for_pdes.

		PINNs & QRES				DRM	
		<i>Forward</i>		<i>Inverse</i>		<i>Forward</i>	
		ADAM	LBFGS	ADAM	LBFGS	ADAM	LBFGS
Poisson	Hyperparameter						
	Learning rate	0.001	0.2	0.001	0.5	0.001	0.2
	Iterations	5,000	8,000	5,000	10,000	5,000	5,000
	Scale factor s $(\omega_{\mathcal{L}}, \omega_{\mathcal{B}}, \omega_{\mathcal{D}})$	100 (1, 10,000, 0)		100 (1, 0, 10,000)		100 (1, 10,000, 0)	
Darcy Flow	Learning rate	0.001	0.25	0.005	0.5	0.002	0.25
	Iterations	5,000	12,000	5,000	15,000	5,000	8,000
	Scale factor s $(\omega_{\mathcal{L}}, \omega_{\mathcal{B}}, \omega_{\mathcal{D}})$	0.01 (1, 100, 0)		100 (1, 0, 100)		0.01 (1, 100, 0)	

Table 13: Used parameters for the DRM, PINNs and QRES in the simulations.

A.2.1 DRM, PINNs and QRES

Since the general training procedures of DRM, PINNs and QRES are closely related, we explain the implementation of all 3 approaches at the same time.

The accuracy of the results mainly depends on the size of the network, the number of training points and the range of the solution. To get a fair comparison between PINN and QRES, we choose the networks in such a way that they have roughly the same number of trainable parameters. We considered both accuracy and training time while choosing the network architecture. All other Hyperparameters for PINNs and QRES are the same. In the inverse problem, we use two networks (u_{Θ}, f_{Θ}) . Where u_{Θ} interpolates the given data and f_{Θ} approximates the searched data function.

In the Poisson problem for PINNs, we use a FCN with 3 hidden layers and 50 neurons. For QRES the architecture 5 with 3 layers and 36 neurons is utilised. In the inverse problem, (u_{Θ}, f_{Θ}) have both the same structure as in the forward problem. The used neural network in the Deep Ritz method consists of 2 residual blocks and the initial and last FC layer. Where each layer has 40 neurons.

For the Darcy equation, deeper neural networks were in general more advantageous. Therefore, the Deep Ritz network consisted of 3 residual blocks with 60 neurons. For the forward problems with PINNs, we applied an architecture with 4 layers, where the number of neurons of layer k was the k -th entry in $(50, 50, 50, 20)$. Analogue, for QRES a network with the structure $(36, 36, 36, 15)$ was used. For the inverse problem, the PINN u_{Θ} was given by $(50, 50, 20)$ and for QRES by $(36, 36, 15)$. For the network of the data function f_{Θ} , we choose for PINNs $(30, 40, 40, 20, 20)$ and for QRES $(25, 35, 25, 15, 15)$.

The strong formulation of the Darcy equation (58) with a piece wise constant coefficient λ is ill-posed at the points where the jump occurs. This leads to an additional challenge for the training of the forward problem with PINNs and QRES. When the derivatives of λ become large, so does the loss function, and the optimisation is mainly focused on reducing the influence of the derivatives. Which leads overall to a worse approximation of the real solution. To avoid this problem, in [161] a special weight function is introduced. The function is constructed in such a way, that the weight is zero at the interfaces where the discontinuities are and $\mathcal{O}(1)$ away from the interfaces. If we apply this idea to our problem, we have to remove all points where the discrete jumps occur and the equation reduces everywhere else to $\lambda \Delta u = f$, since our parameter is piece-wise constant. For the DRM we can use the original PDE (58). This is also possible in the inverse case, since there the unknown parameter λ is approximated by a smooth neural network.

Additionally, neural networks can best work with values in the range of $[-1, 1]$, because of this we scale our data by a factor s . The used values are listed in table 13. For the forward problem the given data function is scaled, for the inverse problem, the known solution u is multiplied by s .

Training is done with a combination of Adam [85] and LBFSGS [110]. We start with a fixed number of iterations of Adam and then switch over to LBFSGS, like usually done in the literature. Since two different optimisation algorithms are used, the needed time per iteration (epoch) in table 2 is an average over both algorithms. For LBFSGS we use the PyTorch implementation and set the *max_iteration* variable to 2. In the inverse case, both data fitting and the minimisation of the PDE loss are trained at the same time. For LBFSGS all available points have to be used in each training step, this leads to a rather slow training process for higher resolutions. Using lower resolutions leads to roughly the same accuracy, but speeds up the training considerably.

To control the influence of each condition we add additional weights $(\omega_{\mathcal{L}}, \omega_{\mathcal{B}}, \omega_{\mathcal{D}})$. The used values are presented in table 13. Since the magnitude of the loss of the PDE condition is much larger than the loss of the other conditions, we use a large weight for the boundary and data conditions. If the weight is zero, in table 13, this means the condition did not appear in the training. E.g. no additional boundary condition in the inverse case and data of the solution in the forward problem. Lastly, we want to mention, that if the boundary condition is built into the network architecture better results can be achieved.

A.2.2 PCANN, PCALin

The obtained error for the PCANN depends largely on the reduced/latent dimension used for the PCA. For each reduced dimension $d_{\mathcal{X}} = d_{\mathcal{Y}} \in [30, 50, 70, 100, 150, 200, 250]$, the hyperparameters were grid searched. The choice of this range was based on [12], which showed how larger dimensions do not necessarily guarantee better approximations for the PCANN. However, larger dimensions could lead to better results for the PCALin. The results shown in Tables 2 and 5 are for the best-performing cases. We present the hyperparameter setting for each separate case in Table 14. ADAM was used in PCALin while SGD is was used in PCANN.

Hyperparameter	Poisson				Darcy Flow			
	PCANN		PCALin		PCANN		PCALin	
	<i>Forward</i>	<i>Inverse</i>	<i>Forward</i>	<i>Inverse</i>	<i>Forward</i>	<i>Inverse</i>	<i>Forward</i>	<i>Inverse</i>
Latent dimension	150	200	250	250	150	30	100	100
Weight decay	0.1	0.1	0.015	0.1	0.5	0.1	0.1	0.15
Batch size	500	500	1000	1000	500	100	1000	200
Learning rate	5×10^{-7}	1×10^{-5}	0.01, 0.001, 0.0025		1×10^{-6}	1×10^{-4}	1×10^{-3}	1×10^{-3}
Step size	2000	2500	2500, 5000		7500	2500	-	2500
Gamma	0.5	0.1	0.01, 0.1		0.5	0.01	-	0.01
Epochs	20000	10000	6000		20000	5000	2000	1000
Dropout	0	0.001	0		0	0.01	0	0
Weight Initialisation	kaiming normal		xavier		kaiming normal		xavier	

Table 14: Best performing hyperparameters for the PCANN method and its linear version-PCALin

A.2.3 FNO, UFNO, MWT, PINO

We use the same hyperparameters for the 2D FNO/MWT problem as in the paper, and the code made available. Notably, training is done for 500 *epochs*, with a *batch-size* of 10. The ADAM algorithm is used for optimisation, with a *learning rate* of 0.001 which is reduced by a factor of 0.5 (a.k.a. *gamma*) after every 100 (a.k.a. *step size*) epochs. An L-2 regularisation is added to the loss function with a *weight decay* of 1×10^{-4} . Specific to the FNO, UFNO and PINO methods are the Fourier modes and width, we truncate 12 *Fourier modes* and use a *width* size of 32.

On the other hand, in the MWT, Convolutional Neural Networks (CNNs) are used to parameterise the networks A, B, C and T is a single $k \times k$ linear layer with $k = 4$. The Legendre orthogonal polynomial basis is used as it produces better results as reported in [58].

For the PINO, we optimise the loss function L , given by:

$$L = L_{\text{data}} + 0.2 \cdot L_{\text{pde}}$$

A.2.4 DeepONet

For the poisson problem, we use a linear model for the branch net, while the trunk net is a neural network with a width of 128 and 6 hidden layers and Tanh as the activation function. For Darcy-flow with piece-wise constant coefficients, we use the convolutional neural network for the branch net, while the trunk net is a neural network with a width of 128 and 4 hidden layers, and ReLU is the activation function. However, for the inverse training of the Darcy-flow problem, we use sin as the activation for the trunk net, which can achieve better results than using general activation functions. We use the fast implementation to train the neural network as described in the algorithm. The training is done for 50000 epochs, with a batch size of

125. The Adam algorithm is used for optimisation with a learning rate of 0.002 which is reduced by a factor of 0.9 after every 1250 epoch.

We need to note that the resolution size will affect the size of the branch net of DeepONet. For example, for 513×513 resolution case, the number of parameters in the branch net would be $513 \times 513 \times 128 \approx 3.0 \times 10^7$ and the server we use will face the memory limitation problem. Thus, for high-resolution cases, an adaptive average pooling is first used in the branch net to reduce the size of the data, which can reduce the number of parameters and training time.

A.2.5 PI-DeepONet

In our experiments on PI-DeepONet, we add an additional physics loss to the optimisation of a data-driven DeepONet described above. Therefore, we use architectures that are similar to the experiments done on DeepONet. In the case of inverse operator training for the Darcy-flow problem, we increase the size of the convolutional branch net and its adaptive average pooling.

In all cases, we re-scale the input and output data such that the values are roughly in the range of $[-1, 1]$ to improve the training performance. All terms in the physics loss are scaled accordingly.

The construction of a physics-based loss in the inverse operator training requires the derivatives of the discrete PDE solution. To obtain these, we come up with a concept that is inspired by the solution of inverse problems in PINN: We introduce a second trunk net that is optimised to interpolate the solution via mean squared error and shares the same branch network. The derivatives of the solution can then be computed via gradient descent and be included in the physics-based loss to reconstruct the parameter. As a result, in addition to the data- and physics-based loss, we have to minimise an interpolation loss $MSE_{\mathcal{I}}$. Both trunk nets are optimised simultaneously.

One has to choose the weights $\omega_{\mathcal{L}}, \omega_{\mathcal{B}}, \omega_{\mathcal{D}}$ (and $\omega_{\mathcal{I}}$) of the physics-informed, boundary condition, data-based (and interpolation) parts of the loss function. In most cases, we choose all weights to have the value 1. Only in the Darcy-flow inverse operator learning, we scale the interpolation loss by $\omega_{\mathcal{I}} = 5$ to improve the influence of the learned derivatives.

Hyperparameter	Poisson		Darcy Flow	
	α_1	α_2	α_1	α_2
PCANN	0.0005	0.05	0.0001	0.005
PCALin	0.00001	0.025	0.001	0.001
FNO	0	0.25	0	0.025
UFNO	0	0.05	0	0.005
MWT	0	0.05	0	0.005
PINO	0	0.05	0	0.005
DeepONet	0	0.05	0	0.025
PI-DeepONet	0	0.05	0	0.025

Table 15: Hyperparameter configurations for Tikhnov-based methods for Inverse Problems.

In all settings, we train for 1,650,000 iterations that consist of 128 branch inputs and 100 randomly sampled trunk input points. We reduce the learning rate in an iterative scheme for every 50,000 steps. For the Poisson forward problem, we use an initial learning rate of $5e - 4$ and reduce it iteratively by a factor of 0.8. For the inverse operator training, we end up using an initial learning rate of $1.5e - 4$ (Poisson) respectively $2.5e - 4$ (Darcy) and a factor of 0.85.

During training, we use the full dataset, to ensure comparability to the other used methods. The advantages of a physics-informed approach might however come better into play in a setting in which only partial data is available, therefore, this might not be the optimal use case for PI-DeepONets.

A.2.6 Tikhonov-based methods for Inverse Problems

For learning the parameter, we used a learning rate of 0.1 and trained for 10000 epochs, decreasing the learning rate by a factor of 0.5 every 2000 epochs. The below loss functions are used.

$$Loss(\lambda)_{\text{poisson}} = \|G_\theta \lambda - u_\delta\|_2 + \alpha_1 \|\lambda\|_2 + \alpha_2 \|D(\lambda)\|_2 \quad (68)$$

$$Loss(\lambda)_{\text{darcy}} = \|G_\theta \lambda - u_\delta\|_2 + \alpha_1 \|\lambda\|_2 + \alpha_2 \text{Var}(\lambda), \quad (69)$$

where G_θ is the forward operator, $D(\lambda)$ is the first difference quotient of λ , and Var is the Total Variation loss. Using same hyperparameter configuration, testing was done on 100 test examples and the results were reported in Tables 8 and 9. For a visual appreciation of the results, we also show in Tables 10 and 11 the learned parameter for both Poisson and Darcy Flow with piece-wise constant parameter problems.